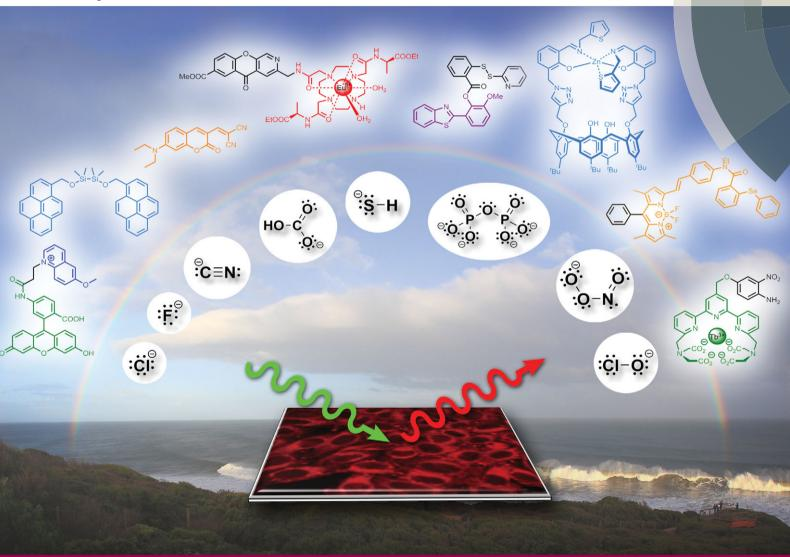
Chem Soc Rev

Chemical Society Reviews

www.rsc.org/chemsocrev



Themed issue: Imaging agents

ISSN 0306-0012



REVIEW ARTICLE

Chem Soc Rev



REVIEW ARTICLE

View Article Online



Cite this: Chem. Soc. Rev., 2015, **44**, 4547

Received 3rd November 2014 DOI: 10.1039/c4cs00372a

www.rsc.org/csr

Luminescent probes for the bioimaging of small anionic species in vitro and in vivo

Trent D. Ashton, a Katrina A. Jolliffe and Frederick M. Pfeffer*

The ability to spatiotemporally identify the formation of specific anionic species, or track changes in their concentration inside living systems, is of critical importance in deciphering their exact biological roles and effects. The development of probes (also called bioimaging agents and intracellular sensors) to achieve this goal has become a rapidly growing branch of supramolecular chemistry. In this critical review the challenges specific to the task are identified and for a select range of small anions of environmental and biological relevance (fluoride, chloride, iodide, cyanide, pyrophosphate, bicarbonate, hydrosulphide, peroxynitrite, hypochlorite and hypobromite) a comprehensive overview of the currently available in vitro and in vivo probes is provided.

1. Introduction

1.1 Overview

The study of anion *recognition* is now a relatively mature science in line with the closely related field of cation recognition. ^{1–5} Over the last 10-15 years sustained effort from the supramolecular chemistry community has refined the fundamental principles relating to how a host interacts with a negatively charged guest. 1-17

Similarly anion sensing has matured and an array of effective molecular detectors, operating by means of well understood principles, are now available. 11,18-32 An excellent recent tutorial review by Gale (see also other articles in this special issue) neatly highlights the strategies that are now widely employed in the detection and/or quantification of anionic species. 33 While the field has matured, challenges still exist for the detection of anions in water; the heavily hydrated nature of these species in aqueous environments makes strong binding difficult and also hinders their reactivity.7,12,26,34

As the study of anion recognition and sensing has advanced supramolecular chemists have applied their fundamental knowledge to the detection of anions of biological significance. 14,21,35-46 Indeed the rise of anion recognition as a field of study was in no



Trent D. Ashton

Trent Ashton received his PhD in organic chemistry from Monash University's Victorian College of Pharmacy campus (now Monash Pharmaceutical Institute of Sciences) in 2008. After a year working for Prof. Michael Pollastri at Boston University he returned to Monash to work for Peter Scammells. He originally joined the Pfeffer lab at Deakin University in 2010 to work on small molecule agents for the treatment of type II diabetes in

conjunction with Verva Pharmaceuticals. In addition to supramolecular anion recognition chemistry his current research interests include the development of class selective HDAC inhibitors to target metabolic disorders.



Katrina A. Jolliffe

Katrina (Kate) Jolliffe received her BSc (Hons 1) in 1993 and PhD in 1997 from the University of New South Wales. She then positions at Twente University, The Netherlands; the University of Nottingham, UK and the Australian National University before taking up an ARC QEII research fellowship at The University of Sydney in 2002. In 2007 she became a Senior lecturer at the same institution and was promoted to Associate

Professor in 2008 and to full Professor in 2009. She is currently Head of the School of Chemistry at The University of Sydney. Kate's research interests encompass elements of synthetic organic chemistry, supramolecular chemistry and peptide chemistry.

^a Centre for Chemistry and Biotechnology, School of Life and Environmental Sciences, Deakin University, Pigdons Rd, Waurn Ponds, Victoria, Australia. E-mail: fred.pfeffer@deakin.edu.au

^b School of Chemistry, School of Chemistry (F11), The University of Sydney, Sydney, New South Wales, Australia

Table 1 Design criteria for anion sensors versus anion probes in vitro and in vivo

For recognition/sensing in water

Selective for the target in water Strong binding/signalling and low detection limit Water soluble

"Switch on" or ratiometric Large extinction coefficient, quantum yield and Stokes shift. For recognition/sensing in vitro and in vivo

Selective for target in cells/small organisms

Sensitive at relevant biological concentrations (e.g. Cl vs. ONOO)

Water soluble yet amphiphilic for cell permeability.

Localise in relevant compartment

Non-toxic

"Switch on" or ratiometric

Large extinction coefficient, quantum yield and Stokes shift.

Red or NIR emissive

Photostable and metabolically stable

small part due to the fact that the majority of intracellular operations involve anionic species. 47 A natural extension of such efforts is the detection or sensing of biologically relevant anions in a biologically relevant setting such as inside living cells or in living organisms. 30,35,43,45,48-60 Thus the field of anion imaging has emerged and supramolecular chemists now find themselves planning and executing the synthesis of reporters to selectively detect and indicate the presence of anions inside living cells and organisms. Probes capable of achieving this feat are amongst the most powerful resources available for elucidating the exact biological role of the target anion. While the number of probes capable of efficiently communicating an anion recognition event from such a venue is growing, it is still small when compared to the large number of intracellular sensors/probes for cationic species⁶¹ (see also other articles in this special issue). As such the field provides fertile ground for both emerging and established researchers alike.

1.2 Challenges

The ideal anion sensor functioning in vitro or in vivo must satisfy a demanding set of criteria (outlined in brief in Table 1)⁶²⁻⁶⁴ and it is clear from this list that an imaging agent must 'do more' than a sensor. Key challenges include (i) selecting a suitable



Frederick M. Pfeffer

Fred Pfeffer received his BSc (Hons 1) in 1996 and PhD in 2001 from Deakin University. He then worked for three years at Trinity College Dublin, first as a lecturer then as postdoctoral fellow in the group of Prof Thorfinnur Gunnlaugsson. In 2004 returned to Australia as lecturer and in 2010 was appointed Senior lecturer. Research interests include many aspects of supramolecular chemistry including anion recognition and sensing. A

research focus is the synthesis and use of fused [n]polynorbornane scaffolds as preorganising elements for further applications including host: guest chemistry and the construction of metallosupramolecular cages.

fluorophore, (ii) choosing an effective switching mechanism and (iii) catering for the biological environment in which the probe must function (see additional discussion for these three points below). Few, if any, of the currently available probes satisfy all of these criteria and given that sensors that are truly selective for specific anions in water have only emerged in the last 10-15 years it is no surprise that the development of selective anion sensors for bioimaging applications is currently at the forefront of applied supramolecular chemistry.

1.2.1 The fluorophore. An extensive range of fluorophores are now available, however, for in vivo work those that are not just bright ($\varepsilon \times \Phi$) but have NIR emission are of considerable benefit. 54,65-67 A "window" of increased optical transparency exists in the range 650 to 950 nm and at these wavelengths tissue autofluorescence is minimised and the major interferents (haemoglobin, lipids and water) absorb to a less significant extent.66 The use of NIR emission also minimises light scattering and is far less likely to damage the living system. The use of multiphoton excitation (or inverse Stokes) techniques is also of particular relevance for in vivo studies^{68,69} and several multiphoton probes for anions are described herein. For in vitro studies which require little photon penetration the requirements are slightly more forgiving and probes with emission wavelengths ranging to 350 nm have been successfully used. In all cases a large Stokes shift is desirable to minimise light scattering. Emission wavelengths (and in turn Stokes shift) are known to be influenced by a number of factors including the structure of the excited state and solvent reorganisation upon excitation. 70-72 Recently, quantum chemical calculations have been employed in the design of fluorophores with ca. 200 nm Stokes shift.⁷³

While well-known fluorophores (such as rhodamine, fluorescein, BODIPY and cyanine)48,64,74-77 are common in anion imaging studies, several unconventional fluorophores (e.g. Si, Se, Ge and Te rhodamines^{78,79} and squaraine-rotaxanes⁵⁴) have successfully been used in recent years. An increasing number of effective probes also employ lanthanide based luminescence for signal transductance. 45,56,80-83

1.2.2 The switch. The ideal probe must either "switch on" in the presence of the target analyte or if quantitation is required the probe should arrive with an "internal standard" present i.e. the active signalling luminophore should be coupled to a fluorophore that has a constant unwavering response in the biological environment. Such ratiometric sensing84,85 allows exact quantification of

the target as the response from the active signalling moiety can be measured against that of the "constant" fluorophore. Such requirements can also be met if both the unbound and bound probe are fluorescent at measurably distinct wavelengths. A recent article by Sessler highlights the use of ratiometric probes for bioimaging applications. 43 Unfortunately, for many anions (such as Cl⁻, I⁻, HCO₃⁻ and BrO⁻) the current list of selective "switch on" and ratiometric probes is limited.

A probe can also be classified according to the *electronic* event by which fluorescence is "switched" or modulated (for example ICT/PET modulation, FRET, heavy ion effect, and excimer formation). Many sensors-known as chemodosimeters-have been designed such that a chemical reaction controls this modulation 30,33,35,49,86 and it is logical that these strategies have been adopted by those pursuing the goal of in vitro and in vivo imaging. While the chemodosimeter approach is by far the most popular (and is excellent for the selective detection of a specific species) the chemodosimeter is, in most instances, irreversibly transformed to the signalling moiety and as such true spatiotemporal information cannot be gleaned. Continued effort from the research community is required to achieve the goal of tracking rather than trapping the anionic species of interest. Another very popular approach to modulating fluorescence is the displacement approach. 27,46,87 The luminophore is quenched by a species that is non-covalently attached and the luminophore-quencher combination is chosen such that the target anion interacts with the quencher more strongly than it does with the luminophore. Hence the quencher is displaced, the luminophore is released and fluorescence is "switched on".

1.2.3 The biological environment. The solvent for life is water, hence the probe must possess a degree of water solubility and many hydrophobic probes have been made more biocompatible by attaching either a PEG⁸⁸ or a sugar.⁸⁹ Nevertheless, a hydrophilic/hydrophobic (amphipathic) balance must be struck such that the sensor can passively diffuse through cell membranes. In the wider field of cellular imaging a commonly employed manoeuvre to ensure uptake is to mask polar hydroxy groups and carboxylates as esters (especially acetoxymethyl (AM) esters⁹⁰) that are subsequently hydrolysed by one of the myriad of intracellular esterases to release the desired probe. This approach has been adopted in the field of anion imaging agents and three peroxynitrite probes are shown in Fig. 1 as examples. The early (1997) dichlorodihydrofluorescein was used as the diacetate diester DA-DCHF91 and the more recent (2010) HKGreen3 employed a single acetate. 92 The tetraacetoxymethyl ester AM-DTTA passively diffused into cells whereupon the tetracarboxylate ligand (DTTA) was liberated and in the presence of terbium and europium the desired lanthanide probes assembled in cellulo.93 An added benefit of this approach is that the unmasked probe is typically retained inside the cell, nevertheless, even probes containing carboxylates can be expelled from the cell by active anion transport mechanisms.94

Ideally once the probe is inside the living entity it should localise in the most relevant sub-cellular compartment. Guidelines to predict the likely compartmentalisation of new probes

Fig. 1 Examples of peroxynitrite probes DA-DCHF, HKGreen3 and AM-DTTA in which intracellular uptake and subsequent trapping was performed using a lipophilic ester (highlighted in red) that was cleaved in vivo by intracellular esterases

Fig. 2 Examples of probes that localise in the mitochondria (Rh-TPP, Rh-Py) and lysosome (Lyso-NHS).

are not unequivocally established^{63,95} and colocalisation studies with well-established dyes are generally required. Nevertheless some general trends exist: (i) cationic probes gravitate to the mitochondria^{96,97} as the mitochondrial membrane is negatively polarised and (ii) weakly basic probes accumulate within the more acidic lysosomes.98 These general guidelines have also been adopted in the field of anion bioimaging, for example, the recently described probes for hypochlorite Rh-TPP and Rh-Py (Fig. 2)99 employ a triphenylphosphonium and pyridinium appendage respectively for mitochondrial localisation. The intracellular sensor for hydrosulfide Lyso-NHS used a morpholine substituent for lysosomal localisation. 100

Structure of this review

In conjunction with a comprehensive listing of recent examples (the majority of examples are from the last 5 years) the broad concept of this review is to provide both a "why" and "how to" target the specific anion of interest. For each of the anions covered herein a justification of the cellular relevance is first provided—even anions of obvious environmental importance (such as cyanide and fluoride) have considerable relevance and interest for intracellular studies (see Section 2). Also covered are

a number of anions that are of relevance primarily at a cellular level (see Section 3), for example bicarbonate plays a critical role in living systems as a measure of CO₂ uptake/respiration (hypercapnia/hypercapnia = CO₂/HCO₃⁻ poisoning respiratory acidosis). Similarly, reactive oxygen and nitrogen species (such as hypochlorite ClO and peroxynitrite ONOO have critical in vivo roles and elevated levels of these species are associated with many disease states (see Section 4). Where possible, examples have been grouped by the means (mechanism) by which sensing is achieved and also whether the probes are: intensity modulated ("switch off" or "switch on") or ratiometric (wavelength modulation). The terms fluorescent probe, anion imaging agent and intracellular sensor are all used interchangeably.

2. Anions of environmental and biological relevance

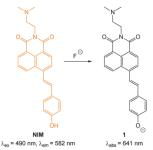
There now exists a number of excellent sensors for anions such as fluoride and cyanide; 35,37,39,101 widely recognised as anions of environmental concern. While not commonly appreciated, these anions also have significant relevance in a biological setting and a number of intracellular probes have been developed for their detection. Chloride has a more passive, nonetheless important, role in the environment and, like iodide, plays an important physiological role. 102 Anions covered in this section are fluoride, chloride, iodide and cyanide.

2.1 Fluoride

Fluoride is a very well-known anion due to its use in drinking water and toothpaste to prevent dental caries and osteoporosis. 103 Nevertheless excess fluoride is responsible for a number of deleterious conditions including dental and skeletal fluorosis and is now linked to cancer and neurotoxicity. 104-106 Probes capable of selectively indicating fluoride in vitro and in vivo may assist in clarifying the exact biological roles of this anion.

Given its "Janus" behaviour the recognition and sensing of fluoride has been a focus of supramolecular chemists. 37,39,101,107,108 Two approaches that have been widely used in the design of both sensors and bioimaging agents are (i) deprotonation (Section 2.1.1) and (ii) desilylation (Section 2.1.2). Deprotonation, mediated by the strongly basic fluoride anion, leading to enhanced ICT of a luminophore, was one of the first means by which this anion was detected, 18,109-112 and while the approach has been used for imaging, this design is prone to interference from other basic anions (such as acetates). By far the most common approach employs the fluoride mediated desilylation reaction of chemodosimeters that have been designed with a silyl ether.

2.1.1 Fluoride mediated deprotonation. The phenolic naphthalimide probe NIM (Fig. 3) was reported in 2014. 113 The probe was both colourimetric (strong absorption band emerging at 641 nm in the presence of F⁻) and fluorescence "switch off" (λ_{ex} = 490 nm, $\lambda_{\rm em}$ = 582 nm decreases). In solution, a similar, yet less pronounced, change was also recorded with acetate-a common interferent for probes operating by means of deprotonation.



Structure, and deprotonation, of NIM with fluoride

HO
$$\lambda_{\text{ex}} = 388 \text{ nm}, \lambda_{\text{em}} = 490 \text{ nm}$$

$$\lambda_{\text{ex}} = 388 \text{ nm}, \lambda_{\text{em}} = 450 \text{ nm}$$

$$\lambda_{\text{ex}} = 388 \text{ nm}, \lambda_{\text{em}} = 450 \text{ nm}$$

Fig. 4 Top: structure of hydroxynaphthalene 2. Bottom: PC3 cells incubated with 2 (10 μM) and nucleus stain propidium iodide (a) red channel image; (b) green channel image of (a); (c) overlay of (a) and (b). PC3 cells incubated with 2, NaF and propidium iodide (d) red channel image; (e) blue channel image of (d); (f) overlay of (d) and (e). Image reproduced with permission. 114

Of interest, and hinting at an additional role for this probe, the fluorescence of the unreacted probe was considerably enhanced in the lysosomes of cancer cells as opposed to healthy cells. Preliminary experiments indicate that both a protein-rich and an acidic environment (such as in cell lysosomes) were required for the enhancement.

The ratiometric hydroxynaphthalene probe 2 (Fig. 4) was reported by Liu and Ke in 2014. 114 A PEG cyanoacrylate was included to enhance ICT and also balance solubility. The probe was selective to fluoride (no significant fluorescent changes were elicited by AcO⁻) and the emission intensity ratio I_{490}/I_{450} nm could be used to quantitate fluoride up to 10 equivalents with a limit of detection (LOD) of 8.5 µM. The probe was cell permeable, non-toxic to prostate cancer (PC3) and epithelial cervical cancer (HeLa) cells and located in the cytoplasm of these cells (confirmed using the red nuclear stain propidium iodide-PI). In PC3 cells a clear change in emission colour was observed when cells pre-treated with 2 were exposed to fluoride.

A recent report by Mahapatra (2014) outlined the ratiometric BODIPY azaindole 4 (Fig. 5) which was synthesised in three steps. 115 In solution studies (7:3 CH3CN:H2O) the strong emission at 512 nm (λ_{ex} = 350 nm) decreased upon addition

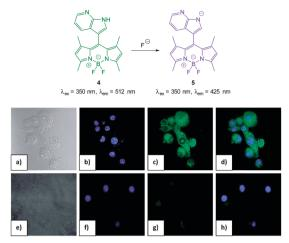


Fig. 5 Top: structure, and deprotonation, of probe 4 by F⁻. Bottom: images of RAW264.7 cells. (a) Bright field image; (b) nuclei stained with 4',6-diamidino-2-phenylindole (DAPI); (c) cells treated with probe 4; (d) overlay image of (b) and (c); (e) bright field image of probe 4 and F⁻; (f) probe 4 and F⁻ (g) nuclei with DAPI; (h) overlapping image of (f) and (g). Image reproduced with permission. 115

of fluoride (and to a similar extent acetate) as weak emission at 425 nm increased and the ratio F_{425}/F_{512} was used to determine F concentration (<200 equivalents). The N-H of indole has been used previously for the recognition and sensing of fluoride anions 116,117 and for probe 4 deprotonation significantly enhanced ICT and a clear change in fluorescence emission was recorded in murine macrophages (RAW264.7) upon addition of fluoride.

In 2013 Chellappa reported the rhodamine based probe RDF-1 (Fig. 6) that operates by means of deprotonation leading to spirocycle ring opening. 118 A strong "switch on" fluorescence response at 557 nm was observed in the presence of F⁻. In HeLa cells RDF-1

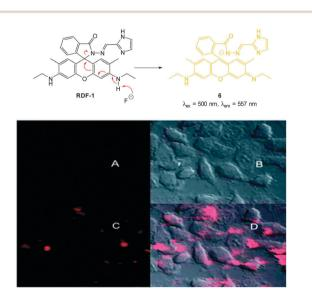


Fig. 6 Top: structure and reaction of rhodamine probe RDF-1 with F Bottom: (A) fluorescence image of HeLa cells incubated with RDF-1; (B) corresponding bright-field image; (C) fluorescence image of HeLa cells incubated with RDF-1 and NaF; (D) overlaid images of HeLa cells (B and C). Image reproduced with permission. 118

was non-toxic and within 10 minutes of NaF addition significant fluorescence enhancement was observed.

2.1.2 Fluoride mediated desilylation. Many chemodosimeter have been designed to use the selective reaction of fluoride with silicon (incorporated as a Si-O-C bond) to form the exceptionally strong Si-F bond (>800 kJ mol⁻¹). The approach is essentially identical to the fluoride mediated cleavage of silyl containing protecting groups. 119 For the probes shown herein the hydroxy fragment is released as a phenoxide anion which is a component of an ICT fluorophore; hence the desilvlation reaction leads to a dramatic fluorescence "switch on".

One of the earliest "switch on" probes functioning by means of desilylation, a TBDPSO-coumarin (TBPCA, Fig. 7), was published by Park and Hong in 2009. 120 The probe readily entered cells and was retained with no toxicity. Images in human epithelial lung carcinoma A549 cells show clear blue fluorescence upon exposure to NaF.

The "switch on", red emitting probe 8 (Fig. 8) was recently published by Zhu (2014).121 Synthesis of the masked ICT fluorophore involved aldol type reaction of the potential electron donor 4-OTBPS-benzaldehyde with the electron withdrawn 2-dicyanomethylene-3-cyano-4,5,5-trimethyl-2,5-dihydrofuran (TCF). For probe 8 a linear emission "switch on" at 612 nm was observed upon reaction with fluoride and a LOD = 0.07 mM was determined. The absorption spectra could be used to quantify

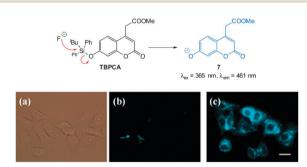


Fig. 7 Structure and reaction of coumarin TBPCA with fluoride. (a) Brightfield image of A549 cells with TBPCA (b) fluorescence image with TBPCA without NaF (c) fluorescence image with **TBPCA** and NaF. Scale = $20 \mu m$. Reproduced with permission. 120

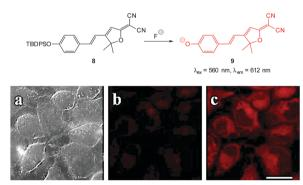


Fig. 8 Top: structure and reaction of "switch on" fluoride probe 8. Bottom: fluorescence images of HeLa cells incubated with probe 8 (a) bright-field transmission (b) red channel with no NaF (c) red channel with NaF. Scale = 20 μ m. Image reproduced with permission. ¹²¹

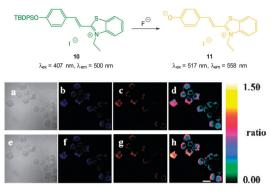


Fig. 9 Top: structure and reaction of benzothiazolium hemicyanine 10 with F⁻. Bottom: images of RAW264.7 macrophages incubated with 10 and no added F^- (a) bright-field, (b) blue channel at 490 \pm 20 nm, (c) orange channel at 560 \pm 20 nm, and (d) ratio image from (c) and (b). Images of RAW264.7 macrophages incubated with 6 after addition of NaF (e) bright-field, (f) blue channel at 490 \pm 20 nm, (g) orange channel at 560 \pm 20 nm, and (h) ratio image from (g) and (f). Scale = 20 μ m. Image reproduced with permission. 122

the amount of fluoride present in solution due to the linear relationship between the increase at 596 nm and the decrease at 438 nm. Imaging was performed in live HeLa cells and 10 µM NaF was readily visualised using fluorescence microscopy.

The highly selective, ratiometric, benzothiazolium hemicyanine 10 (Fig. 9) developed by Ma, Du and Zhang (2011)¹²² could monitor fluoride concentration using the ratio F_{500}/F_{558} . A limit of detection (0.08 nM) was identified and in live RAW264.7 macrophages a distinct ratiometric fluorescence response was observed upon addition of buffered NaF. The probe was also shown to penetrate rapidly (<5 minutes) and was non-toxic.

A variation on the desilylation probe was reported by Zhang in 2013. 123 In the presence of fluoride, desilylation of the functionalised naphthalimide chemodosimeter 12 (Fig. 10) was immediately followed by fragmentation to give the conjugate base of 4-hydroxynaphthalimide 13. In solution studies a linear fluorescence

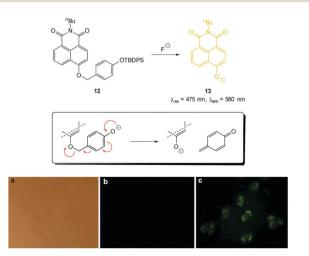


Fig. 10 Top: functionalised naphthalimide probe 12 and its reaction with F⁻; inset shows fragmentation mechanism. Bottom: (a) bright-field image of A549 cells incubated with 12 (20 μ M) for 24 h (a) bright field (b) without NaF (c) with NaF (50 mM). Image reproduced with permission. 123

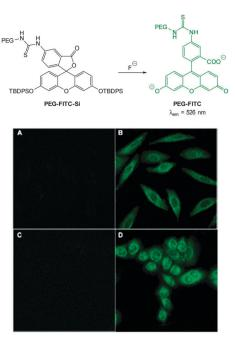


Fig. 11 Top: structure of fluoride chemodosimeter PEG-FITC-Si. Bottom: fluorescence imaging of L929 (top) and HeLa (bottom) cells incubated with the sensor before (A and C) and after (B and D) treatment with NaF. Image reproduced with permission.88

"switch on" (λ_{em} = 560 nm) was realised (20-fold increase in one hour with only 1.0 equivalent of F^- ; LOD = 0.35 µg L^{-1}). After incubation of probe 12 with human epithelial carcinoma cells (A549) addition of a solution of NaF elicited a distinct green fluorescent response.

With an eye to enhanced solubility the PEG-thioureafluorescein probe PEG-FITC-Si (Fig. 11) was synthesised by Zeng and Wu (2013)88 in two steps from the corresponding fluorescein isocyanate. Again in the presence of fluoride a dramatic increase in fluorescence (λ_{ex} = 490 nm, λ_{em} = 526 nm) was observed (LOD = 19 ppb). Imaging was successfully achieved in HeLa and murine fibroblasts (L929) only 15 minutes following addition of fluoride (100 μM) with perinuclear probe localisation.

The TBSO-benzothiazole BBTGA (Fig. 12), also deliberately designed for biocompatibility by conjugating glucosamine to improve solubility, was reported by Wang in 2013.89 A linear

Fig. 12 Structure of BBTGA and 15, showing reaction of BBTGA with F⁻.

30-fold fluorescence enhancement (λ_{em} = 508 nm) was noted 5 minutes after the addition of NaF in PBS buffer. The probe was water soluble, non-toxic and when a buffered solution of NaF (0.1 mM) was added to human nasopharyngeal epidermal carcinoma (KB) cells that had been pre-treated with a dilute solution of BBTGA strong fluorescence was observed.

Again with solubility and biocompatibility in mind the carbohydrate conjugate probe 15 (Fig. 12) was synthesised by Du (2011) using the well-known copper assisted azide alkyne cycloaddition (CuAAC).124 A very strong (160 fold), linear, fluorescence "switch on" response ($\lambda_{em} = 520 \text{ nm}$) was observed with increasing NaF (from 0 to 1.4 mM, probe concentration 50 μM) and a limit of detection of 10.5 μM was identified. A strong fluorescence response was observed upon addition of NaF solution to Hep2G cells that had been incubated with 15 (Fig. 13).

The pyrene dimer 16 (Fig. 14) containing a disilane (Si-Si) bond was designed and constructed by Li and Shen (2012). 125 Ratiometric measurement in solution (THF: H₂O) was possible as the well-known pyrene excimer fluorescence at 470 nm ceased upon reaction of the probe with fluoride and only monomer emission at 378 nm was present. Up to 6 equivalents of F could be measured using F_{378}/F_{470} . Loading of 16 into HeLa cells was performed using polylactic acid nanoparticles and upon exposure to fluoride a clear change in emission was detected.

In 2012 Lee, Kim and Ahn published an interesting variant on the desilylation probe. 126 Upon desilylation the carefully functionalised aminonaphthalene P1 (Fig. 15) reacts in an additional intramolecular process to give the extended aminocoumarin 20. A fluorescence "switch on" (λ_{em} = 595 nm) was observed in both murine metastatic melanoma (B16F10) cells and also in live zebrafish. Imaging was accomplished using two photon microscopy (TPM) and the lower excitation energy associated with this technique is perfect for in vivo research to understand how fluoride is distributed in a whole body context. In the zebrafish, increased concentrations of F in the tail and abdomen were observed at t = 2 h versus t = 30 min.

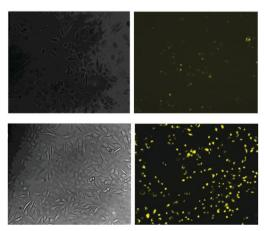


Fig. 13 Images of HepG2 cells (left) brightfield and (right) fluorescence with (above) only probe 15, (below) probe 15, and NaF. Image reproduced with permission.8

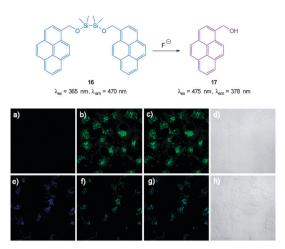


Fig. 14 Top: structure and reaction of pyrene dimer 16 with F⁻. Bottom: images of live HeLa cells incubated with probe 16; (a) emission 410-440 nm (blue channel) (b) emission 440-600 nm (green channel), (c) overlaid a and b, (d) bright-field transmission image. The above cells after addition of 100 μ M F $^-$ (e) emission 410–440 nm, (f) 440–600 nm, (g) overlaid e and f, (h) bright-field transmission image. Image reproduced with permission.125

A recent report (2014) by Song also outlined a dicyanoacrylate "switch on" probe (21, Fig. 15) in which a desilylation cascade approach was used to create a red fluorescent iminocoumarin. 127 The probe itself was non-fluorescent and for the product a Stokes shift of more than 140 nm was recorded. Using fluorescence microscopy the probe was shown to be readily internalised and was capable of indicating the presence of fluoride in living human keratinocyte (HaCaT) cells (not shown).

The related probe FP (Fig. 15) from the group of Peng (2014), ¹²⁸ also relies on an additional reaction occurring post Si cleaving. The probe was synthesised from the corresponding quinolinecarbaldehyde and the final product of the reaction sequence is a highly fluorescent ($\phi_F = 0.84$, $\lambda_{ex} = 441$ nm, $\lambda_{em} =$ 485 nm) aminobenzopyranimine. The probe was shown to be relatively non-toxic, localised in the mitochondria of both breast cancer (MCF-7) and fibroblast-like (COS-7) cells and fluorescence was dramatically "switched on" when the cells were treated with dilute solutions of NaF (Fig. 16).

2.1.3 Miscellaneous. A Se-B bond can be selectively cleaved by fluoride and the unusual red emitting BODIPY probe 22 (Fig. 17) reported by Tang (2011) was designed on this principle. 129 The presence of Se quenched fluorescence but upon reaction with fluoride the "usual" F-B bond was formed (23) and red fluorescence (λ_{ex} = 640 nm, λ_{em} = 690 nm) was "switched on" (ca. three-fold enhancement). The chemodosimeter was selective for fluoride and the increased fluorescent response was readily observed in human hepatoma cells (HepG2) pretreated with F-.

2.2 Chloride

Chloride is the most abundant anion in living organisms and its transport across cellular membranes is essential for a number of physiological processes including the maintenance **Review Article**

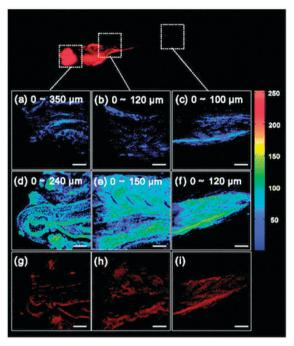


Fig. 15 Top: structure and reaction of aminonaphthalene probe P1 with F⁻ to form extended coumarin **20**. Bottom: accumulated TPM images for three zebrafish parts: (a-c) probe P1 alone (d-i) probe P1 followed by F (a-f) intensity data; (g-i) fluorescence images constructed by image stacking for 0–350 μm depth, with a 2 μm imaging depth step. Scale = $50 \mu m$. View area: $300 \mu m^2$. Image reproduced with permission. $126 \mu m$

of cell volume, acidification of internal compartments and even electrical excitability. Impaired transport of this anion due to a of genetic mutation in a cAMP-regulated Cl⁻ channel defines the condition known as cystic fibrosis (CF). 130 Indeed, the pursuit of biologically active chloride transporters to remedy this condition is an important current goal for supramolecular chemists. 131-138

Other than some recent developments (Section 2.2.3) the strategy employed in the design of chloride imaging agents relies on halide mediated collisional quenching (Section 2.2.1) and as such the majority of Cl⁻ probes are "switch off". Nevertheless by attaching such probes to "constant" fluorophores several ratiometric probes have been successfully designed and used (Section 2.2.2).

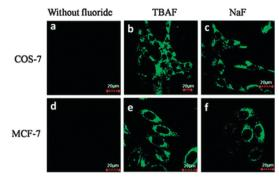


Fig. 16 Images of COS-7 and MCF-7 cells incubated with FP before (a and d) and after (b, c, e, and f) treatment with TBAF or NaF. Image reproduced with permission.¹²⁸

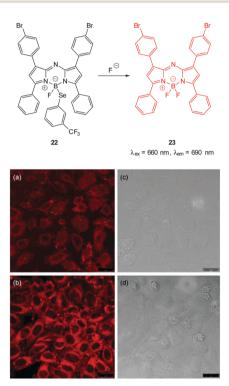


Fig. 17 Top: structure and reaction of Se BODIPY 22 with F⁻. Bottom: images of living HepG2 cells Incubated with (a) probe 22 for 1 h; (b) F- for 1 h then probe 22 for 1 h. Images (c) and (d) are bright field images of (a) and (b), respectively. Image reproduced with permission. 129

2.2.1 Chloride mediated collisional quenching. Due to its recognised physiological importance the development of functionalised quinolones (such as SPQ and MEQ, Fig. 18)102,139-141 as chloride imaging agents was accomplished long before other anions were targeted and several are commercially available. 142 Nevertheless, these quinolone based probes are "switch off"; they are not selective for chloride amongst other halides and they also suffer from photobleaching. 143,144 Furthermore, unless invasive techniques are used to deliver the probe into cells, probes such as MEQ must be reduced (using NaBH₄) to the charge neutral, cell permeable dihydro form (diHMEQ) first which following uptake is oxidised back to the Cl⁻ responsive form.145 Despite their limitations, functionalised quinolone

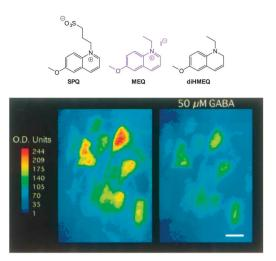


Fig. 18 Top: structure of SPQ, MEQ and the cell permeable diHMEQ probes for Cl⁻. Bottom: images of MEQ-loaded neurons (left) before and (right) 20 min after GABA application. Scale = 15 µm. Image reproduced with permission.146

Fig. 19 Acridine and quinolinium "switch off" probes MACA and lucigenin.

probes have proven very useful. Clear images were obtained by Inglefield who used MEQ ($\lambda_{\rm em}$ = 320 nm) to confirm Cl⁻ transport (mediated by manipulating the GABA_A ion channel, Fig. 18) into neuronal cells obtained from a rat brain slice, ¹⁴⁶ and Durack employed SPQ to measure intracellular chloride in porcine lymphocytes using flow cytometry. 147 Recently this style of probe has also been shown to be compatible with two-photon excitation.148

The identification of N-methylacridinium-9-carboxamide MACA (λ_{em} = 500 nm, Fig. 19) and also the bisacridinium lucigenin (λ_{em} = 506 nm, Fig. 19) as longer wavelength variants was a welcome development. 149 However, while these compounds have been used successfully in vesicle/liposome based studies¹⁵⁰ they were shown to be unstable in cell based studies.149

2.2.2 "Switch on" and ratiometric probes. Ratiometric measurement of intracellular chloride has been achieved by conjugating the chloride sensitive methoxyguinoline to the "constant" dimethylaminoquinoline fluorophore to give bis-DMXPQ $(\lambda_{\rm em} = 450 \text{ for MQ } \nu s. \lambda_{\rm em} = 565 \text{ nm for DMQ, Fig. 20}).^{151} \text{ This}$ dimer distributed uniformly in the cytoplasm and was reported to be stable and non-toxic. Related compounds could be reduced (in a similar process to that for MEQ) for noninvasive cell loading. 151 While not classed as a small molecule the bisacridinium tetramethylrhodamine conjugate BAC-TMR-dextran (Fig. 20) was constructed from the carbohydrate aminodextran. 152



Fig. 20 Ratiometric probes bis-DMXPQ and BAC-TMR-dextran used for chloride imaging

Green emission from the biasacridinium (λ_{em} = 505 nm) was quenched on addition of Cl while red rhodamine emission remained constant. The ratiometric probe was successfully used for intracellular imaging to link chloride concentration to endosomal acidification.

More recently, the ratiometric probe MQAF (Fig. 21) was reported by Tang (2012). 153 The structure consisted of the "switch off" methoxyquinolium combined with aminofluorescein and monitoring at two channels [chloride sensitive emission λ_{ex} = 318 nm, $\lambda_{\rm em}$ = 436 nm and insensitive $\lambda_{\rm ex}$ = 494 nm, $\lambda_{\rm em}$ = 519 nm] gave accurate measurements of Cl⁻ concentration. This probe was successfully used in ventricular myocytes to illustrate that induced ischemia results in increased Clconcentration. In 2014 the same group published the ratiometric methoxyquinolium dansyl combination (MQDS, Fig. 19) and the ratio $\lambda_{\rm em}$ = 440 nm against $\lambda_{\rm em}$ = 560 nm was used to monitor chloride concentration. 154 Imaging of liver cancer cells (HepG2) was performed and intracellular chloride concentration was successfully monitored as the extracellular levels in the surrounding media were deliberately increased (Fig. 21).

2.2.3 Recent developments. A "switch on" probe selective for in vitro or in vivo chloride has yet to be reported however the groups of Fusi and also Smith are getting close. Fusi reported that both the Cd(II) complex with nitrobenzooxadiazoletetraazacyclododecane 24 (λ_{ex} = 410 nm, λ_{em} = 520 nm) and also the bis Zn(II) complex of 25 (λ_{ex} = 325 nm λ_{em} = 543 nm) act as "switch on" sensors for halides (Cl⁻ and F⁻) (Fig. 22). 155,156 It was postulated that for both complexes the metal to nitrogen (nitrobenzooxadiazole) distance and M to N (cyclam) distances change upon binding of chloride and it is the balance between fluorescence enhancement (ICT to nitrobenzooxadiazole) from freeing the N-nitrobenzooxadiazole nitrogen and quenching (PET) of nitrobenzooxadiazole fluorescence by the cyclam that leads to the fluorescence modulation. The ligands have been internalised in human neuroblastoma (HeLa) cells to give fluorescence signals, however, images of the halogen sensitive metal complexes functioning in cells have not yet been published.

Another new, and very interesting, class of chloride probes are the squaraine-rotaxanes developed by Smith (Fig. 23). 157,158

Review Article

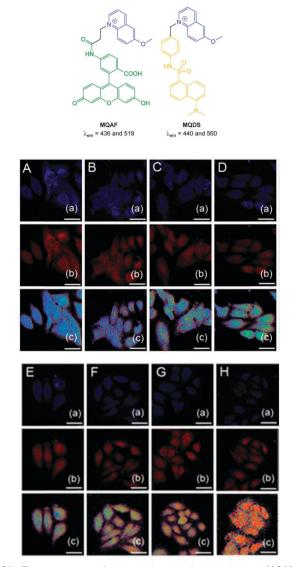


Fig. 21 Top: structures of ratiometric quinolium conjugates MQAF and MQDS. Bottom: images of HepG2 cells loaded with MQDS exposed to: A-H, 0-140 mM chloride. Top in each row is blue channel, middle is red channel and the bottom is a ratio image (F_{red}/F_{blue}). Scale = 25 μ m. Image reproduced with permission. 154

Fig. 22 NBD-cyclam ligand 24 and related ditopic 25

The squaraines have been somewhat overlooked as a biologically compatible fluorophore due to their susceptibility to hydrolysis. In contrast, hydroxysquaraines have been found to be much more stable and for rotaxane 26 (Fig. 23) interaction with chloride shifts the surrounding macrocycle slightly along the squaraine "axle" which in turn leads to fluorescence

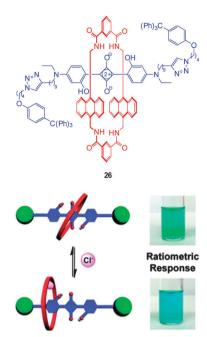


Fig. 23 Fluorescent Cl⁻ sensor 26 based on a squaraine-rotaxane shuttle. Image reproduced with permission. 166

modulation. While not yet demonstrated in an intracellular setting squaraine-rotaxane probes are red emissive, ratiometric (in acetone $\lambda_{\rm em}$ = 698 nm decreases and $\lambda_{\rm em}$ = 665 nm increases) and, unlike the first generation of probes they are selective for chloride (I is not bound; Br binding is 10 fold weaker than that of Cl⁻) and thus have tremendous potential for further development in an intracellular setting.

2.3 Iodide

In the environment iodide occurs naturally in minerals (alutarite and iodargyrite) and it is interesting that AgI is used by humans as a as a nucleation agent in "cloud seeding" programs due a similarity in crystal structure to that of water ice. 159 Iodide is also a common additive to table salt as deficiencies can lead to the condition known as goitre. Indeed the consumption of trace amounts of iodide is essential for human health-the anion is transported to, and accumulated in, the thyroid gland for incorporation into the iodine containing hormones. 160,161

Selective probes for iodide bioimaging are rare. It is interesting to note that the early probes for chloride such as SPQ and MEQ (see Fig. 18) were actually more sensitive to iodide than chloride, 102,140,141 nevertheless the far greater concentration of chloride resulted in minimal interference from iodide.

2.3.1 Recent developments. A recent publication from Mahapatra (2012) outlines a successful displacement approach for the detection of iodide in Candida albicans (IMTECH3018) cells. 162 The complexation of Hg(II) by the thiosemicarbazole ligand 27 (Fig. 24) quenches the inherent fluorescence of the carbazole fluorophore (heavy metal effect). Iodide is capable of displacing Hg(II), liberating the highly fluorescent carbazole (λ_{em} = 425 nm) and a four-fold fluorescence "switch on" (λ_{em} = 425 nm)

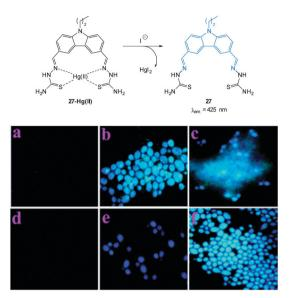


Fig. 24 Top: structure and reaction of iodide probe 27-Ha(II): bottom: fluorescence images of Candida albicans (a) cells only, (b) cells with 27, (c) cells with 27 after addition of Hg(II) (5 μ M), (d) cells with 27 and Hg(II) (25 μ M), (e) cells with the preformed **27-Hg(II)** complex and KI, (f) same as (e) after 10 min. Image used with permission. 162

was observed. Importantly, selectivity for iodide over other halides was excellent.

2.4 Cyanide

Cyanide has a long history of use in industry and is also well known as an environmental poison but for cystic fibrosis (CF) sufferers CN has a particularly sinister role. Infection with Pseudomonas aeruginosa (PA) is common amongst patients with CF and PA is a cyanogenic bacteria (synthesises ⁻CN)¹⁶³ and in vivo cyanide functions as a potent inhibitor of cellular respiration. 164 Indeed PA-mediated cyanogenesis has an acknowledged role in the pathogenesis of CF lung disease. 165 Less common, but more problematic is infection with Burkholderia cepacia complex (Bcc) which is typically multidrug resistant and is also cyanogenic. 165,166 Hence diagnostics for CN in vivo would be welcome for rapid identification of these problematic lung infections. Other sources of in vivo cyanide come from cyanogenic glycosides produced by some plants as part of their innate defence system (for example in almond seeds) and these glycosides can be enzymatically hydrolysed to produce free CN in living tissues. 167

A number of strategies exist for the detection of cyanide but the most common approaches for imaging "CN rely on its (i) nucleophilicity or (ii) affinity for copper ions. 40,168 The nucleophilicity of cyanide has been exploited in the design of chemodosimeters (see Section 2.4.1). Typically, nucleophilic attack of CN at a chemodosimeter incorporating a C=O (aldehyde), C=NR, C=C-CN or related functionality results in a product in which conjugation at some point of the probe is broken and in turn the fluorescence response is modulated. The other successfully used approach involves the *displacement* of copper (Section 2.4.2). These probes are functionalised with copper chelating groups

Coumarin based ESIPT sensor 28 for the detection of cyanide.

such that when Cu(II) is introduced the resultant assembly exists in quenched form (heavy/transition metal ion induced quenching). Cyanide has a very high affinity for copper and is capable of selectively displacing the fluorophore. A very stable Cu(CN)₂ species is formed and the fluorophore is liberated— "switched on".

2.4.1 Cvanide as a nucleophile. A relatively early example (2007) was the coumarin aldehyde 28 (Fig. 25) by Kim and Hong. 169 This probe incorporated a structure known to function by means of the excited state intramolecular proton transfer (ESIPT) principle. 170 Attack at the aldehyde occurs in the vicinity of an acidic OH (phenol) which ultimately leads to formation of a cyanohydrin and a phenoxide anion. As the phenoxide is part of an ICT fluorophore, its formation leads to a dramatic enhancement of fluorescence (λ_{em} = 450 nm). Proton transfer to form 30 was confirmed by the significant upfield shift in the ¹H NMR spectrum as the phenolic proton ($\delta_{\rm H}$ = 10.1 ppm) was "transferred" to the cyanohydrin (δ_H = 6.1 ppm). While microscopy was not performed a fluorescent plate reader was used to confirm selective "switch-on" ($\lambda_{ex} = 350 \text{ nm}, \lambda_{em} = 450 \text{ nm}$) cyanide sensing in murine embryonal carcinoma (P19) cells.

Yoon, designed the ESIPT hydroxyfluorescein aldehyde probes (both mono and di were synthesised; dialdehyde 31 shown in Fig. 26) for microfluidic sensing of cyanide as well as both in vitro and in vivo probes for cyanide. 171,172 Formation of the phenoxide in this instance leads to spirocyclic ring opening and strong fluorescence "switch on" ($\lambda_{em} = 520$ nm). Using dialdehyde 31 the imaging of cyanide in BALB/c nude mouse model was accomplished (Fig. 26) in vivo. 172 This probe was

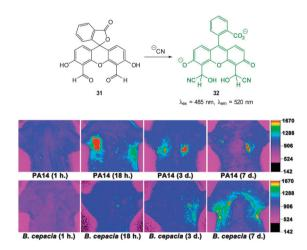


Fig. 26 Top: fluorescein dialdehyde chemodosimeter **31** for ⁻CN. Bottom: in vivo images of CN in the lungs after various incubation times after infection with PA and Bcc. Colour images were reconstructed from inverted fluorescence images. Image reproduced with permission.¹⁷²

Fig. 27 Top: structure and reaction of fluorene based FSal with CN. Bottom: images of SH-SY5Y neuronal cells which were incubated with (left) FSal alone and (right) FSal then TBACN. Image reproduced with permission.¹⁷³

able to detect, in the lungs of the mice, increased levels of cyanide due to infection caused by PA and Bcc. The probe itself did not cause adverse effects when injected as a DMSO solution directly into the lungs of the mice.

The salicylaldehyde functionalised fluorene ESIPT probe FSal (Fig. 27) was reported by Malik in 2014. The sensor could detect cyanide in solution at very low concentration (<0.1 ppb) by reaction to form the corresponding cyanohydrin leading to a strong fluorescence 'switch-on' (λ_{ex} = 329 nm, λ_{em} = 520 nm). The probe was capable of imaging cyanide (as tetrabutylammonium cyanide, TBACN) in human neuroblasts (SH-SY5Y) and the probe was both highly selective and non-toxic.

The "switch off" BODIPY dialdehyde 34 (Fig. 28) was reported by Ravikanth in 2013. 174 Using NMR spectroscopy the probe was clearly shown to react with two equivalents of "CN and fluorescence (λ_{em} = 554 nm) was quenched with the addition of 2.2 equivalents of the anion. In human breast adenocarcinoma cells (MDA-MB-231) the probe was non-toxic and the intense green fluorescence of the probe was quenched upon treatment of the cells with CN.

The ratiometric aminocoumarin probe Coum-1 (Fig. 29) reported by Li (2012)¹⁷⁵ possesses a reactive dicyanoacrylate appendage (readily installed using the reaction of malononitrile with the corresponding coumarin aldehyde). A distinct response (both colourimetric and fluorescent) was observed following the conjugate addition reaction of cyanide to the alkene. The diminished length of the ICT system leads to a shift in both absorption and emission maxima and using excitation at $\lambda = 447$ nm ratiometric measurement of cyanide could be performed [initial coumarin ($\phi_F = 0.45$, $\lambda_{em} = 585$ nm), product **Coum-CN** ($\phi_{\rm F}$ = 0.33, $\lambda_{\rm em}$ = 495 nm)]. An impressive 470 fold increase in F_{495}/F_{585} was realised with the addition of only 1.0 equivalent of CN. The probe was successfully used for the detection of cyanide in HeLa cells by comparing emission from the red and green channels.

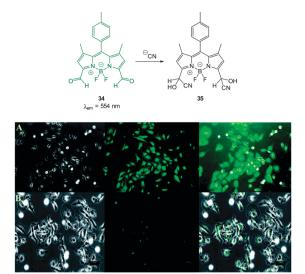


Fig. 28 Top: structure and reaction of BODIPY dialdehyde **34** with ⁻CN. Bottom: images of MDA-MB-231 cells (A) treated with 34 only and (B) after incubation with 34 and CN. Left is bright field, centre is fluorescence and right is overlay image. Scale = $50 \mu m$. Image reproduced with permission. ¹⁷⁴

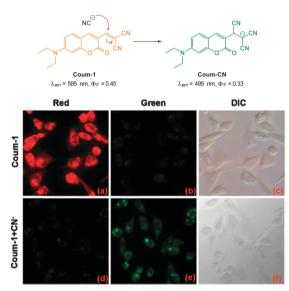


Fig. 29 Top: structure and chemodosimetric reaction of Coum-1 with ⁻CN. Bottom: images of HeLa cells incubated with Coum-1 with and without CN; (a, d) red channel (b, e) green channel and (c, f) brightfield differential interference contrast (DIC). Image reproduced with permission. 175

Also relying on the conjugate addition of CN the BODIPY chemodosimeter 36 (Fig. 30) was developed by Jang (2012). 176 The reaction of cyanide with the dicyanoethylene appendage interrupts the ICT and as a consequence both visible and fluorescent properties were modulated. Interference from fluoride was noted in CH₂Cl₂ but in water the strong solvation of fluoride rendered it less competitive. A clear "switch on" response (λ_{ex} = 480 nm, λ_{em} = 520 nm) was observed in the cytoplasm of HeLa cells that had been incubated with the probe for 20 min then treated with NaCN.

A "switch-on" phenothiazine-hemicyanine probe Phc (Fig. 31) was reported by Yang and Li (2014). 177 The cyanide anion readily

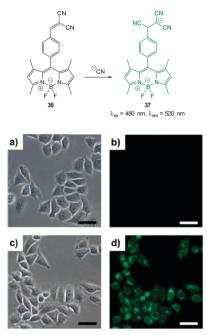


Fig. 30 Top: reaction of dicyanoethylene BODIPY 36 with ⁻CN. Bottom: brightfield (a, c) and fluorescence (b, d) images of HeLa cells with only 36 (a, b) then 20 min after treatment with NaCN (c, d). Scale = 50 μm. Image reproduced with permission. 176

attacked the C=N bond of the indolium and a 20 fold enhancement in fluorescence (λ_{em} = 488 nm) was observed when solutions of the probe were exposed to only 3.0 equivalents of CN. The probe was selective amongst other anions tested and was used in both human breast cancer (GES) and HeLa cells to demonstrate a quick (15 min) "switch on" effect in the presence of in vitro cyanide. Furthermore in adult zebra fish exposed to Phc and cyanide (30 µM) a strong fluorescent response was observed, particularly in the gills and abdomen.

The related red-emitting phenazine(di)cyanine-based chemodosimeters PMI and PDMI (Fig. 32) were reported by Hua (2014)¹⁷⁸ and again these probes rely on nucleophilic attack of cyanide on a indolium cation. As PDMI has two indolium appendages an excess of CN was required before the fluorescence "switch on" (λ_{ex} = 425 nm, λ_{em} = 580 nm) occurred.

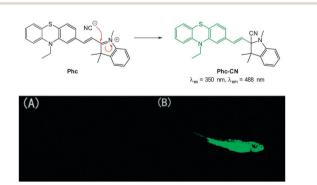


Fig. 31 Top: reaction of CN with indolium Phc. Bottom: images of adult zebrafish under 390 nm light: (A) fish incubated with Phc; (B) fish incubated with **Phc** and ⁻CN. Image reproduced with permission.¹⁷⁷

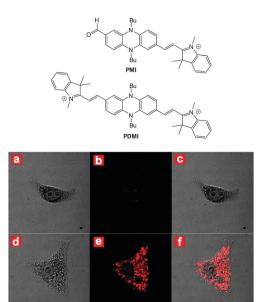


Fig. 32 Top: structures of PMI and PDMI. Bottom: images of HeLa cells incubated with PMI: bright-field (a), dark-field (b) and merged (c). Images of HeLa cells incubated with PMI then CN: bright-field (d), dark-field (e) and merged (f). Image reproduced with permission. 178

In contrast, for PMI an instantaneous response was observed $(\lambda_{\rm ex} = 530 \text{ nm}, \lambda_{\rm em} = 620 \text{ nm})$. Of interest, given that aldehydes are also used as a reactive group for CN, H NMR spectroscopy was used to monitor the intact CHO even as an excess of cvanide was added. The probe located in the cytoplasm In HeLa cells (confirmed using co staining) and a clear "switch on" response to cyanide was noted within 30 minutes of exposure.

2.4.2 Cyanide mediated displacement. Several papers from the group of Yoon describe probes for cyanide bioimaging based on Cu(II) displacement (shown schematically in Fig. 33-the probe is introduced to the cells in the Cu(II) complexed quenched state (heavy metal effect) and upon cyanide mediated displacement of the Cu(II) from the complex fluorescence is restored). The fluorescein tetracarboxylate "switch-on" probe 38-Cu(II) was published in 2009¹⁷⁹ and was one of the first to prove that the copper displacement method could be used both in vitro and in vivo. When 38-Cu(II) was trialled in solution studies, the addition of 100 equivalents of CN increased the quantum yield from 0.057 to 0.53 ($\lambda_{ex} = 505$ nm, $\lambda_{em} = 522$ nm). When Caenorhabditis elegans nematodes (a model host for studying microbial pathogenesis and innate immunity)180 that were initially incubated with 38 and Cu(II) were subsequently incubated with CN a strong fluorescence "switch on" was observed. Of interest when these fluorescent nematodes were again incubated with Cu(II), fluorescence was quenched.

In additional work from the group of Yoon, the NIR emissive cyanine fluorophore (λ_{ex} = 680 nm, λ_{em} = 748 nm) functionalised with picolylamino groups 39 (Fig. 34) was synthesised in a short overall sequence from commercially available cyanine IR-780. 181 In the presence of Cu(II) no significant fluorescence was observed ($\phi_{\rm F} < 0.01$) and initial solution based studies confirmed selective, "switch on" sensing ($\phi_F = 0.65$, $\lambda_{em} = 748$ nm)

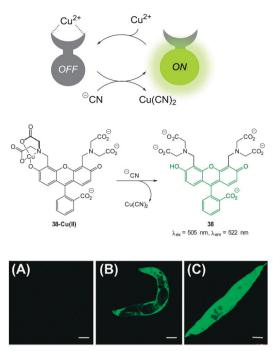


Fig. 33 Top: schematic representation of the Cu(II) displacement approach to sensing cyanide. Middle: structure and displacement reaction of 38-Cu(II). Bottom: fluorescence images of (A) young adult nematodes previously incubated with 38 then incubated with Cu(II), (B) nematodes previously incubated with 38 and Cu(II) then incubated with one equiv. of $^{-}$ CN or (C) with ten equiv. of $^{-}$ CN. Scale = 50 mm. Image reproduced with permission. 179

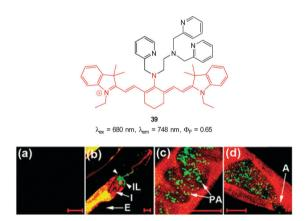


Fig. 34 Top: cyanine based ligand 39. Bottom: imaging of cyanide in C. elegans infected with P. aeruginosa (GFP). Prior to incubation with 39-Cu(II) C. elegans nematodes were fed for 2 d on non-infectious E. coli OP50 (a) or GFP-labelled PA14 (b-d). (b) the anterior end, (c) the medial part, (d) the posterior. (I = intestine; IL = intestinal lumen; I = intestine; E = eggs; PA = PA14-GFP; A = anus). Scale = $20 \mu m$. Image reproduced with permission. ¹⁸¹

of cyanide. Again using the C. elegans nematode as a model organism, aqueous NaCN was readily detected in vivo. Of significant interest when the nematodes were infected with P. aeruginosa (PA14) labeled with green fluorescent protein, the CN that the bacteria are known to produce was also detected in vivo. Such a result neatly conveys the significance of such small fluorescent probes for medically relevant assays.

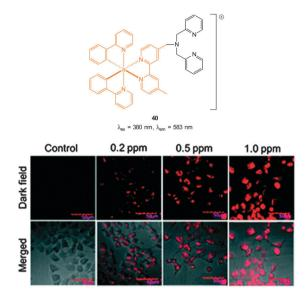


Fig. 35 Structure of DPA functionalised Ir complex 40. Bottom: images of live HeLa cells in the presence of 40-Cu(II) acquired after treatment with increasing concentrations of NaCN. Image reproduced with permission. $^{\rm 182}$

The Cu(II) displacement approach has also been used by Ghosh and Das to develop a "switch on" probe for cyanide, however, in this instance the emitting species (λ_{ex} = 380 nm, $\lambda_{\rm em}$ = 583 nm) was a phosphorescent DPA-functionalised iridium complex 40 (Fig. 35). 182 Detection of cyanide was achieved inside live HeLa cells within 2 minutes using cells pre-incubated with **40-Cu(II)** then exposed to a 0.2 ppm aqueous solution of ⁻CN.

A Cu(II) displacement probe operating by both a colour change and also fluorescent enhancement was reported by Kim. 183 Coumarin imine 41 (Fig. 36) was synthesised in four steps from m-anisidine with the last step involving condensation with 2-aminophenol. A crystal structure of the stable nonfluorescent **41-Cu(II)** ($\phi_{\rm F}$ = 0.02) confirmed that the metal was complexed by both oxygen atoms and the imine nitrogen atom as shown in Fig. 36. Similar to the previous examples the probe operates by means of Cu(II) displacement, however, unlike the Cu(II) complex, the free coumarin imine 41 is prone to hydrolysis (cyanide actually enhances the rate of hydrolysis) and ultimately it is the coumarin aldehyde 42 (λ_{ex} = 479 nm, λ_{em} = 514 nm, $\phi_{\rm F}$ = 0.65) that functions as the reporting species. Again, excellent selectivity for cyanide amongst a selection of anions was reported (CN detected at 10-8 M). No adverse effects were noted when human hepatoma cell line HepG2 cells were treated with the complex and a strong intracellular fluorescence response was detected when cells were treated with solutions of KCN.

An interesting copper displacement probe for cyanide was devised by Zheng (2014). 184 The non-fluorescent Cu(II) schiff base complex of benzimidazole hydroxynaphthalene 43 (Fig. 37) was itself formed by displacing Zn(II) from the corresponding, highly fluorescent Zn complex (both the Cu and the Zn complexes were characterised by means of X-ray diffraction). Displacement of copper from the 43-Cu(II) complex was effected by cyanide to give the fluorescent free 43 ($\lambda_{\rm ex}$ = 366 nm, $\lambda_{\rm em}$ = 425 nm).

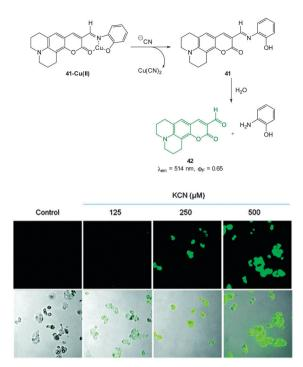


Fig. 36 Top: structure, CN mediated displacement, and hydrolysis of 41-Cu(II). Bottom: images of human HepG2 cells pre-treated with 41-Cu(II) (1.0 μ M) acquired 1 min after addition of KCN (125, 250, and 500 μ M). Image reproduced with permission.¹⁸³

Fig. 37 Structure of the naphthalene-benzimidazole complex 43-Cu(II) developed by Zheng¹⁸⁴ and the **44-Hg(II)** complex from Zhang and Liu.¹⁸⁵

Displacement of Cu(II) was also effected by S²⁻ and it should be noted that this anion (known to have an affinity for Cu) is often omitted from the standard suite of anions used to evaluate the selectivity of many Cu based probes. In HeLa cells incubated with the Zn(II) complex addition of Cu(II) quenched the fluorescence, however, the corresponding addition of CN to restore fluorescence was not performed.

The Hg(II) complex of benzimidazole 44 (Fig. 37) was described by Zhang and Liu (2013)185 for the intracellular sensing of CN. The complex is non-fluorescent (heavy metal effect) and in the presence of cyanide a strong fluorescence "switch on" (λ_{ex} = 345 nm, λ_{em} = 467 nm) was observed due to displacement of Hg(II). Unfortunately both sulphide and also iodide displaced the cation to give an equivalent response. While these competitors might ultimately limit in vivo applications (toxicity was also not evaluated), successful in vitro sensing of cyanide was demonstrated when HeLa cells that had been incubated with 44-Hg(II) were treated with cyanide.

2.4.3 Miscellaneous. Very few *in vitro* or *in vivo* probes that function by means of H-bonding exist—a testament to the lack

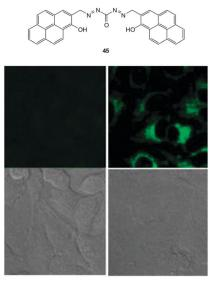


Fig. 38 Top: structure of CN probe 45. Bottom: images of 45 in HeLa cells with (left) 30 μM 45 and (right) 30 μM 45 and 30 μM NaCN. Upper images: fluorescence. Lower images: bright-field. Image reproduced with permission. 186

of truly selective anion sensors that function by H-bonding in highly competitive media. The bispyrenecarbohydrazide 45 (Fig. 38) reported by Yoon (2014)¹⁸⁶ bound cyanide such that excimer emission (λ_{ex} = 500 nm, λ_{em} = 550 nm) was "switched on". A proposed "clamshell" H:G complex of 45 with cyanide was proposed leading to close proximity of both pyrene moieties. In aprotic solvents fluoride also elicited a "turn on" response, however, when small amounts of protic solvents were present CN was targeted more selectively. Again HeLa cells were used for imaging and, in addition to rapid uptake, a distinct fluorescence "switch on" was observed when "CN was added.

3. Anions of biological relevance

Many crucial intracellular processes involve anionic species⁴⁷ and the dysregulation of these species is known to accompany a number disease states. Indeed, the dysregulation of intracellular pyrophosphate (PPi) levels is associated with many conditions including cancer (see Section 3.1). Imaging agents for specific anionic targets in vitro and in vivo can be used to confirm the exact biological role of these anions and importantly they can also function as diagnostics for specific medical conditions. Anions covered in this section are: pyrophosphate, bicarbonate and hydrosulfide.

3.1 Pyrophosphate

Pyrophosphate (PPi) is produced or used in many cellular metabolic processes, such as ATP hydrolysis and DNA/RNA polymerisation reactions. Intracellular PPi concentrations can provide information on important cellular processes and have recently been suggested as a means of cancer diagnosis. 187 The concentration of PPi in other physiological fluids, such as

Review Article

synovial fluid and urine, can also be used to identify diseases

such as chondrocalcinosis or calcium pyrophosphate dihydrate (CPPD) crystal deposition disease. 188

This knowledge has led to the recent development of numerous colourimetric and fluorescent sensors for PPi (see also the review by Yoon in this special issue). 14,36,189 However, significant challenges remain in the development of such probes, due to the difficulties associated with binding PPi in water and distinguishing it from related polyphosphates such as ATP. As many of the fluorescent sensors developed for PPi to date are "switch-off" or only exhibit weak fluorescence they are of only limited use in bioimaging applications. Nevertheless, there are several examples where such compounds have been successfully used to image the presence of cellular PPi and there are a handful of recent examples where "switch on" sensors have been developed and effectively used in imaging applications.

3.1.1 PPi binding to metal complexes. One of the earliest examples of the use of a PPi sensor in cellular imaging was reported by Kim. 190 The 1,8-naphthalimide-DPA-Zn(II) complex 46-2Zn(II) (Fig. 39) was prepared in good overall yield over five steps and in CH3CN:HEPES buffer, ligand 46 exhibited weak emission at 476 nm (λ_{ex} = 360 nm), characteristic of the 4-amino-1,8-naphthalimide fluorophore. Formation of the 46-2Zn(II) complex resulted in a 59-fold fluorescence enhancement together with a 29 nm bathochromic shift to 505 nm, attributed to suppression of PET from the DPA amine. The addition of PPi to 46-2Zn(II) resulted in a hypsochromic shift (23 nm) and ca. 50% quenching of fluorescence (10 equivalents of PPi). Calculations indicated that PPi bound to only one Zn(II)DPA centre and PET quenching was mediated by PPi. Imaging was performed using mouse myoblasts (C2C12) and cells were first incubated with 5 μM Zn(OAc)₂, then with 1 μM 46. Subsequent addition of PPi lead to a dose-dependent decrease in cellular fluorescence (Fig. 39).

Hong and co-workers reported the three step synthesis of the NIR emissive benzothiazolium hemicyanine ligand 47 (Fig. 40), which readily forms a bis Zn(II) complex as a PPi binding site. 191 In aqueous buffer (pH 7.4) Probe 47-2Zn(II) showed weak emission at 548 nm ($\lambda_{\rm ex}$ = 500 nm, $\Phi_{\rm F}$ = 0.08) and addition of PPi (1.0 equivalent) "switched on" emission ($\Phi_{\rm F}$ = 0.10) with a bathochromic shift to 558 nm. While ATP also gave a measurable response, 47-2Zn(II) was used to image PPi uptake in a C2C12 myoblast cell line with a clear increase in intracellular fluorescence observed 30 minutes following addition of 2.5 equivalents of PPi. Importantly, the cells remained viable as determined using Hoechst nuclear stain and the probe had good cell permeability.

3.1.2 PPi mediated displacement. The [DCCA]₂Cu complex, comprising both a dicyanomethylene-4H-chromene fluorophore and a copper(II) complex of iminodiacetic acid group for PPi binding, has been reported as a NIR emissive "switch on" sensor for PPi. 192 In aqueous buffer DCCA (Fig. 41) is highly fluorescent ($\lambda_{\rm ex}$ = 500 nm; $\lambda_{\rm em}$ = 675 nm; $\Phi_{\rm F}$ = 0.79), but upon addition of Cu(II) the fluorescence intensity decreased and complete quenching was observed with five equivalents of Cu(II). On addition of

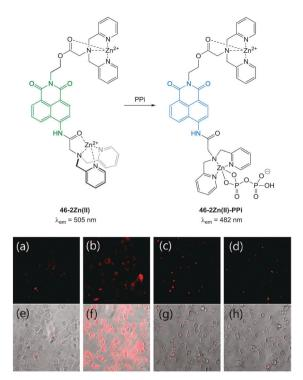


Fig. 39 (a) Fluorescence image of C2C12 cells treated with 46-2Zn(II) (1.0 μ M). (b) Fluorescence images of C2C12 cells treated with **46** (1.0 μ M) and Zn(II) (5.0 μ M). (c) Fluorescence images of C2C12 cells treated with 46 (1.0 μ M), Zn(\shortparallel) (5.0 μ M) and PPi (0.5 mM). (d) Fluorescence images of C2C12 cells treated with 46 (1.0 μ M), Zn(\shortparallel) (5.0 μ M) and PPi (1.0 mM). (e-h) Bright field images of (a-c) respectively. Image reproduced with permission. 190

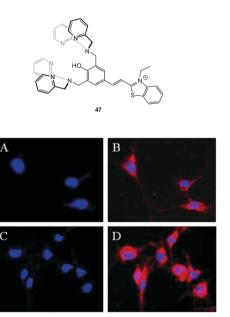


Fig. 40 Fluorescence live-cell pseudo-color images of C2C12 myoblast cells. (A and C) Cells stained by Hoechst nuclear dye. (B) Cells incubated with Hoechst nuclear dye and then with 47-2Zn(II). (D) Cells incubated with Hoechst nuclear dye followed by 47-2Zn(II), then Na₄P₂O₇. Emission collected at (A, C) blue channel and (B, D) Cy3 channel upon excitation at (A, C) 350 \pm 25 nm and (B, D) 543 \pm 11 nm. Image reproduced with permission. 191

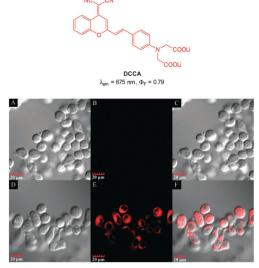


Fig. 41 Top: structure of copper ligand DCCA. Bottom: confocal fluorescence images in KB cells: (A-C) cells incubated with DCCA2-Cu(II) alone. (D-F) Cells incubated with $DCCA_2-Cu(II)$, then $K_4P_2O_7$. Emission collected at 630-730 nm, excitation at 405 nm. Bright field (A and D), fluorescence (B and E) and overlap field (C and F). Image reproduced with permission. 192

PPi to a 1:5 mixture of DCCA and Cu(ClO₄)₂ fluorescence "switch on" was observed, and peaked after 15 equivalents PPi ($\Phi_{\rm F}$ = 0.48). The enhancement was attributed to the displacement of one of the ligands from the Cu(II) complex. This probe was evaluated in KB cells and almost no intracellular fluorescence was observed for the [DCCA]2Cu complex alone. After incubation with PPi, a significant increase in cellular fluorescence was observed within 30 minutes with signals localized in the perinuclear area of the cytosol, indicating a subcellular localisation of PPi and good cell membrane permeability of the [DCCA]₂Cu complex.

The imino-thiophenyl calix[4] arene derivative 48 (Fig. 42) has been used to image both Zn(II) and PPi in HeLa cells. 193 Ligand 48 was prepared in three steps from p-tert-butylcalix[4] arene and upon addition of Zn(II) in a fluorescence turn-on response (λ_{ex} = 390 nm, $\lambda_{\rm em} \sim 450$ nm) was observed. Subsequent addition of PPi resulted in complete quenching of the emission, attributed to the displacement of Zn(II) from the 48-Zn(II) complex as a result of the higher binding affinity of PPi for Zn(II). In HeLa cells incubated with 10 µM 48, very low fluorescence intensity was observed. After subsequent incubation with ZnSO₄/pyrithione for 20 minutes, the cells exhibited highly intense blue fluorescence (4 times higher than with 48 alone). Further treatment with PPi resulted in a decrease in fluorescence intensity (1.5 times higher than 48 alone).

The bis Zn(II) complex of the pyridine-naphthalene based SPHN (Fig. 43) has been reported as a PPi selective fluorescent chemosensor. 194 Compound SPHN was readily prepared by condensation of the bis-glycine adduct of 2,6-diaminopyridine and 2-hydroxy-1-naphthaldehyde. In 7:3 CH₃CN:aqueous HEPES buffer the addition of ZnCl2 to SPHN resulted in a "switch-on" of fluorescence ($\lambda_{\rm ex}$ = 400 nm; $\lambda_{\rm em}$ = 450 nm, $\Phi_{\rm F}$ = 0.940) which was suggested to be a result of the formation of a 1:2 L: Zn(II) complex. The addition of PPi to SPHN-2Zn(II) led to

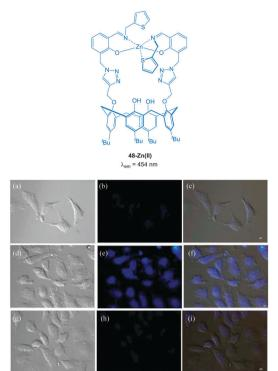


Fig. 42 Fluorescence images in HeLa cells ($\lambda_{\rm ex} \sim 358$ nm and $\lambda_{\rm em} \sim$ 461 nm); (a) DIC image of cells treated with 48 (10 μ M); (b) fluorescence image of (a); (c) merged image of (a) and (b). (d) DIC image of cells treated with 48 then Zn(II)/pyrithione (1:1) solution; (e) fluorescence image of (d); (f) merged image of (d) and (e). (g) DIC image of cells treated with [48 + Zn(II)]followed by PPi; (h) fluorescence image of (g); (i) merged image of (g) and (h). Scale = 10 µm. Image reproduced with permission. 193

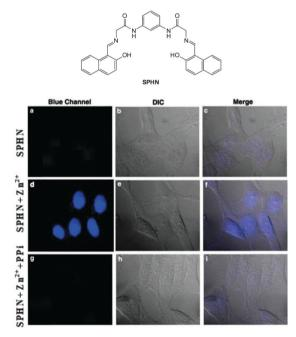


Fig. 43 HeLa cells showed intense blue fluorescence in the presence of both **SPHN** and Zn²⁺ (d) and did not show any fluorescence in the absence of Zn²⁺ (a) and in the presence of PPi (g). Corresponding differential interference contrast (DIC) images (e, b and h) and merge images (f, c and i) of the cells are shown. Image reproduced with permission. 194

Fig. 44 Confocal fluorescence microscopy images of (a) HeLa cells incubated with probe 49-ZnCl₂ (50 µM), (c) single HeLa cell, and (e) single HeLa cell without staining (control). Differential interference contrast images of (b) single HeLa cell incubated with probe 49-ZnCl₂ (50 μM) and (d) single HeLa cell without staining (control). Image reproduced with permission. 195

quenching of this fluorescence as a result of displacement of Zn(II) from **SPHN** and importantly, a selective response for PPi was observed in the presence of ATP. In HeLa cells preincubated with exogenous Zn(II) the addition of SPHN elicited a fluorescence response, however, when PPi was added at the same time as SPHN, significantly lower levels of fluorescence were observed.

More recently, Rissanen and co-workers have reported a terpyridine-Zn(II) complex 49-ZnCl₂ (Fig. 44) capable of the detection of nanomolar PPi concentrations in water, together with the first example of a small molecule probe to image native PPi concentrations in cells (i.e. without the addition of exogenous PPi). 195 The complex was prepared by mixing 4'-(4-N,N'-dimethylaminophenyl)-2,2':6',2"-terpyridine in a 1:1 ratio with ZnCl2 and an X-ray crystallographic structure, confirmed the formation of a 1:1 complex. While 49-ZnCl₂ is fluorescent in the solid state, in water the fluorescence is quenched. The addition of PPi to a solution of 49-ZnCl2 in 0.01 M HEPES buffer resulted in an approximately 500 fold increase in fluorescence ($\lambda_{\rm ex}$ = 440 nm; $\lambda_{\rm em}$ = 591 nm), attributed to the formation of a 1:3 complex between PPi and 49. Cellular imaging was performed in HeLa cells. Cells were treated with 10 µM 49-ZnCl2 for 30 min and bright orangeyellow emission was observed that allowed mapping of PPi concentration in different parts of the cells with the maximum emission observed in the nuclei as well as the cytoplasmic membranes.

3.2 Bicarbonate

The bicarbonate anion is the primary species responsible for maintaining cellular acid-base homeostasis. The enzyme carbonic anhydrase (CA) produces HCO₃⁻ inside cells from dissolved CO2 and dysregulation of CA is associated with a number of tumour types. 196 The bicarbonate anion also plays a role in physiological processes such as cyclic AMP regulation, osteoporosis and kidney disease. 197 Unfortunately only indirect methods have been available for measuring bicarbonate in cells including total H14CO3- concentration or estimates based on pH; each of these are prone to significant error and do not provide spatiotemporal information. As such a more direct means for the bioimaging of this anion using fluorescent probes would be a welcome advance.

3.2.1 Recent developments. Very few small molecule probes exist for the cellular imaging of bicarbonate and these can be divided into two classes: dipyridylalkylbenzenes and luminescent lanthanide complexes.

The dialkynylbenzene probe 50 for the imaging of bicarbonate in vitro was reported by Murphy, Wong and Lee in 2011 (Fig. 45). 198 A NIR multiphoton approach was used for excitation and probe emission also tailed into the NIR region. Solution studies identified strong binding of bicarbonate $(\log K = 7.13)$ and a four-fold enhancement in fluorescence intensity (λ_{em} = 450 nm) was observed as well as a redshift of 30 nm. Binding was tentatively assigned to the δ^+ of the amide N leading to enhanced electron transfer (1:2 H:G binding stoichiometry supported this theory). In solution, binding of citrate was also observed (log K = 7.83), nevertheless, in vitro imaging of HCO₃ was performed in both HeLa and A549 cells ($\lambda_{\rm ex}$ = 900 nm and $\lambda_{\rm em}$ = 400–650 nm) and after 3 h the probes had localised in the cytoplasm and the emission profiled matched the 30 nm red shift observed in solution indicating binding of the target anion.

With the aim of sensing bicarbonate and other oxyanions (such as malate and citrate) "in cellulo" a large body of research

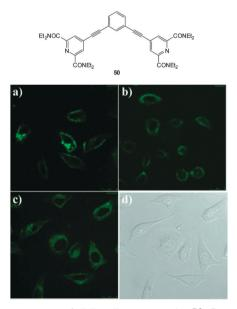


Fig. 45 Top: structure of dialkynylbenzene probe 50. Bottom: in vitro cytoplasmic staining microscopy with **50** (λ_{ex} = 900 nm, λ_{em} = 450-750 nm) in A549 cells after (a) 1 h, (b) 6 h, and (c) 12 h. (d) Bright-field image of panel (c). Image reproduced with permission. 198

effort has been undertaken by the group of Parker using luminescent lanthanide probes. 83,199 The cellular uptake, localisation, stability and toxicity of these probes have all been studied in detail. 45,81,200-202 These sensors have sharp emission bands ($\Delta J = 1, 2, 3$ and 4) and as they rely on energy transfer from a chromophore/sensitiser (normally incorporated as part of the ligand) to the metal the emission can be modulated by the target anion disturbing either the metal excited state or the ligand singlet or triplet states (for excellent overviews of the photophysical properties of lanthanides and how they can be manipulated for sensing and imaging see the excellent recent reviews by Meade, 82 Parker, 83 and Pierre 203). Lanthanide complexes are capable of selectively binding anions if both the ligand and metal are judiciously selected. Typically, but not always, the mode of action involves displacement of a bound water (q) by the target anion leading to a modulated emission profile in which the $\Delta J = 2$ band (e.g. Eu at ca. 620 nm) is considerably altered whereas other bands such as $\Delta I = 1$ (e.g. Eu at ca. 590 nm) are not. Changes in these two distinct outputs allows the probe to function in a very useful ratiometric fashion.82,83,203 Combinations of individual Tb and Eu complexes (one complex is responsive, the other is not) can also function in a ratiometric manner.204

The detection of bicarbonate by the lanthanide complexes 51-Eu(III) and 52-Eu(III) containing the 1-azaxanthone-4-carboxyl sensitiser was reported by Parker in 2011 and in a follow up study in 2012 (Fig. 46). 205,206 The probes were non-toxic and indicated the presence of bicarbonate (HCO₃⁻ formed by exposing the cells to a CO₂ atmosphere) in the mitochondria of a number of cell lines including A549, MCF-7 and HeLa cells. While solution based binding studies indicated little selectivity of the probes over the common carboxylate interferents citrate and lactate, in cells the concentration of bicarbonate is typically 10 fold greater than lactate and 100 times greater than citrate. Of additional interest the same ligands with terbium were unresponsive and could serve as in internal control for ratiometric imaging. Direct detection in A549 cells and selectivity for bicarbonate was confirmed as when the known carbonic anhydrase inhibitor acetazolamide was introduced to the cells little fluorescence was observed. Binding of the bicarbonate anion modulates either triplet sensitiser to metal energy transfer or the lanthanide excited state directly and ultimately leads to significant enhancement of the $\Delta J = 2$ band at ~ 620 nm ($\lambda_{\rm ex} = 340$ nm).

3.3 Hydrosulphide

Hydrogen sulphide (H₂S), along with NO and CO, is considered to be the third gaseous signalling agent, or gasotransmitter.²⁰⁷ Endogenous hydrogen sulphide is produced from homocysteine (Hcy) by the cytosolic enzymes; cystathionine-β-synthase (CBS) and cystathionine-γ-lyase (CGL).²⁰⁸ In addition hydrogen sulphide is also produced from cysteine (Cys) by 3-mercaptopyrate sulfurtransferase (3MST) mediated metabolism; 3MST is present in both the cytosol and mitochondria.208 Considering the first and second pKa values for H2S are 7.05 and 15 respectively (at 25 °C and pH 7.4 the ratio of H₂S/HS⁻/S²⁻ can be calculated as 30:70:0.00002 respectively). 207 As such, for the purpose of this

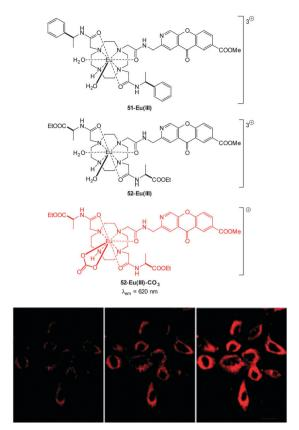


Fig. 46 Top: structure of HCO₃⁻ sensitive probes **51-Eu(III)**, **52-Eu(III)** and the bound 51-Eu(III)-CO3. Bottom: images of HeLa cells incubated with 52-Eu(III), localised in the mitochondrial region under 3, 4 and 5% CO₂ atmosphere. Image reproduced with permission.²¹¹

review we can assume that appreciable quantities of HS are present. Nevertheless the challenge of targeting HS⁻ is complicated as pH varies between subcellular compartments and as such the H₂S/HS⁻ ratio will also vary accordingly.

Hydrogen sulphide has been linked to a number of physiological processes such as inflammation, angiogenesis, respiration, ischaemic reperfusion injury as well as oxidative stress.^{208,209} As such the development of HS⁻ releasing drugs is an active area of research.210

Due to the rapid catabolism of HS by sulphide quinone oxidoreductase (SQR), persulfide dioxygenase (SDO), thiosulfate reductase (TR) and sulphite oxidase (SO), 208,211,212 any probe must react quickly and emit brightly (high quantum yield $(\phi_{\rm F})$ and molar absorptivity (ε)). This formidable challenge is made more difficult by the fact that the typical concentration of HS⁻ in blood are in the order of 10^{-6} M to 10^{-9} M and 30–300 μM in tissues have been reported. 207,212 There is still debate over the physiologically active form of hydrogen sulphide, 212 therefore a selective means to detect low concentrations of the anionic form could unlock some of the secrets of its remarkable biology.

The development of fluorescent indicators to sense HS in living systems is a rapidly developing field. 52,213-216 Given the large number of examples this review will highlight bioimaging agents that either (i) present significant advances in sensitivity, (ii) target particular cellular locations, (iii) emit in the NIR range

and (iv) have been demonstrated to be applicable to in vivo studies.

For probes that target hydrosulphide, three strategies are commonly employed to modulate fluorescence. The first two are chemodosimeter approaches that rely on HS as a nucleophile or HS⁻ mediated reduction. The third strategy is sulphide mediated metal displacement. Nucleophilic reactions (typically S_NAr or nucleophilic addition) are used to restore ICT or remove a group involved in a PET process, displace a trigger or interrupt a conjugated system. Anionic HS⁻ is a superior nucleophile compared to thiols (p $K_a > 8.5$) at physiological pH. When two proximal electrophiles are present interference from endogenous sulphur species such as cysteine (Cys), homocysteine (Hcy) and glutathione (GSH) is further circumvented. Reduction of an azide is an often utilised approach as the azide can be introduced directly to a fluorophore bearing an arylamine as a component of an ICT system, or as a sulfonylazide. Reduction of nitro groups, hydroxyl amines, and N-oxides are related examples of this strategy, however the reduction of the nitrogroup invariably suffers from poor reaction kinetics. The displacement of a metal, typically $Cu(\Pi)$ or $Zn(\Pi)$, from a chelating ligand has also been widely used for bioimaging HS⁻. There are obvious parallels between this approach and the probe design for CN selective probes (see Section 2.4).

3.3.1 Hydrosulfide as a nucleophile. Lin et al. made use of both the donor photoelectron transfer (d-PET) properties and HS reactivity of the 2,5-dinitrophenylether in their hybrid cyanine-BODIPY probe, NIR-H₂S (Fig. 47).²¹⁷ NIR-H₂S is essentially non-fluorescent due to the d-PET process, however, upon treatment with HS- the fluorescent phenol 53 $(\lambda_{\rm ex} = 650 \text{ nm}, \lambda_{\rm em} = 708 \text{ nm})$ is revealed. NIR-H₂S has a detection limit of 50 nM although this value was determined at pH 7.0. Using probe NIR-H₂S visualisation of varying concentrations of exogenous HS in MCF-7 cells was achieved. Notably higher fluorescent intensity at the mitochondria was observed which was confirmed by colocalisation studies using Hoechst 33342.

NIR-H₂S
$$\begin{array}{c}
O_2N \\
O_3N
\\
O_4PET
\\
O_5B \\
F
\end{array}$$

$$\lambda_{ex} = 650 \text{ nm}, \lambda_{em} = 708 \text{ nm}$$

$$A_{ex} = 650 \text{ nm}, \lambda_{em} = 708 \text{ nm}$$

Fig. 47 Structure and reaction of cyanine-BODIPY hybrid probe NIR-H₂S with HS⁻; INSET shows fragmentation mechanism.

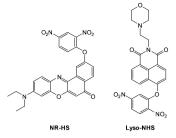


Fig. 48 Structures of NR-HS and Lyso-NHS

Zheng and Cui (2014) functionalised nile red with this trigger to give a NIR-emissive (λ_{ex} = 488 nm, λ_{em} = 655 nm) HS⁻ responsive probe NR-HS (Fig. 48).²¹⁸ Upon reaction with HS⁻ the quantum yield of **NR-HS** ($\Phi_{\rm F}$ = 0.05 in simulated physiological conditions) increased to 0.32 as nile red was regenerated. Maximum fluorescence was obtained after 20 minutes with a limit of detection of 270 nM. Fluorescence microscopy experiments were carried out using MCF-7 cells and NR-HS responded to exogenous HS-.

The 2,5-dinitrophenylether trigger was incorporated onto a 4-hydroxynaphthalimide fluorophore by Liu et al. to give Lyso-NHS (Fig. 48). The probe also contained a basic morpholine substituent (**Lyso-NHS** $pK_a = 3.12$) which was responsible for compartmentalisation of the sensor into the lysosome (Fig. 49). 100 The reaction of HS with Lyso-NHS led to a significant increase in fluorescent intensity ($\lambda_{ex} = 450 \text{ nm}$, $\lambda_{em} = 555 \text{ nm}$) with a maximal response after 20 minutes. The probe had a nanomolar (480 nM) detection limit and was used to visualise exogenous HS in MCF-7 cell lysosomes (confirmed by co-staining with neutral red (NR) a known lysosomal stain) and was not toxic (MTT assay) at the concentrations used.

Also using the 2,5-dinitrophenylether trigger, the group of Govindaraju synthesised the HS⁻ probe **DNOPCy** (Fig. 50).²¹⁹ Dislodging the 2,5-dinitrophenyl group of **DNOPCy** (λ_{em} = 555 nm) gave Cy-quinone which has a red-shifted emission maximum



Fig. 49 Colocalisation images of Lyso-NHS in MCF-7 cells. (a) Lyso-NHS with HS⁻ (green channel. (b) Neutral red (red channel). (c) Merged images of (a) and (b). Image reproduced with permission. 100



Fig. 50 NIR emissive HS⁻ probe **DNOPCy**.

Fig. 51 Structure and reaction mechanism of benzothiazole probe 54 with HS-.

at λ = 695 nm. This change in fluorescence emission was ideal for ratiometric detection and visualisation of exogenous NaSH in human embryonic kidney cells (HEK293T) was successfully accomplished.

Through the judicious placement of a proximal aldehyde, Feng (2014) developed the dinitrophenyl ether probe 54 (Fig. 51) that reacted fully within two minutes of exposure to HS to give maximum fluorescence.²²⁰ The reaction generates the modified HMBT ESIPT fluorophore 55 ($\lambda_{\rm ex}$ = 450 nm, $\lambda_{\rm em}$ = 555 nm, $\Phi_{\rm F}$ = 0.18) and HS⁻ at concentrations as low as 48 nM were detected in simulated physiological conditions. This probe was successfully used for the visualisation of exogenous HS⁻ in HeLa cells.

In 2012 Qian and co-workers reported a rapidly reacting HBMT based HS⁻ activated fluorescent probe (Scheme 1).²²¹ Probe E1 can undergo thiol exchange with both HS⁻ and thiols, however only the persulfide generated from HS can cyclise to release the fluorescent **HBMT** (λ_{ex} = 295 nm, λ_{em} = 487 nm). Probe E1 was weakly fluorescent due to PET from the pendant dithiol and reacted rapidly (2 min) with HS with an detection limit of ca. 120 nM. Once again this probe readily detected exogenous HS in HeLa cell.

In 2013 the Tang group reported the HS responsive ratiometric probe HS-Cy (Fig. 52) which incorporates a proximal electrophile.222 Nucleophilic addition of HS at the aldehyde of HS-Cy leads to a rapid (within 3 min) loss of fluorescence

Scheme 1 Structure and reaction mechanism of E1 with HS-.

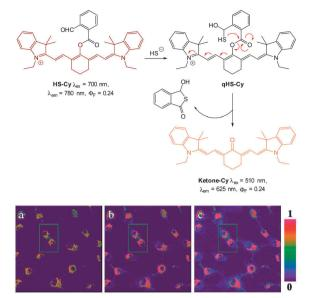


Fig. 52 Top: structure and reaction of HS-Cy with HS⁻. Bottom: confocal fluorescence ratiometric images of endogenous HS⁻ in living A549 cells. A549 cells loaded with 5 mM HS-Cy for 30 min (a). Cells were prestimulated with SNP, then incubated with HS-Cy for 10 min (b) and 20 min (c). Scale = 50 mm. Image reproduced with permission.²²²

emission ($\lambda_{\rm em}$ = 780 nm, $\Phi_{\rm F}$ = 0.24). This decrease in fluorescence was speculated to be caused by a PET process from the free hydroxyl or sulfhydryl groups of the intermediate qHS-Cy. The intramolecular cyclisation between the free sulfhydryl and the ester the releases the ketone cyanine (ketone-Cy) resulting in a 155 nm blue-shifted emission ($\lambda_{\rm em}$ = 625 nm). The cyclisation step is a much slower process, with the emission at 625 nm increasing slowly over 35 min. In the mitochondria of HepG2 cells (pH 8.0) the nucleophilic addition and substitution occurred within 30 s and 5 min respectively. The fluorescence intensity ratio F_{625}/F_{780} rises from 0.01 to 24.8 following the addition HS-. Probe HS-Cy was used to image exogenous HSin HepG2 cells and could detect endogenous HS⁻ in A549 cells stimulated with sodium nitroprusside (SNP). A decrease in the F_{625}/F_{780} ratio was observed when an inhibitor (DL-propargylglycine, PPG) of the HS producing enzymes (CBS and CES) was added to the cells, confirming HS as the analyte responsible for the response.

Guo and co-workers reported a fast reacting flavylium derived ratiometric HS⁻ probe 59 (Fig. 53).²²³ Nucleophilic attack of HS⁻ on this NIR emissive probe ($\lambda_{ex} = 450 \text{ nm}$, $\lambda_{ex} = 690 \text{ nm}$) disrupts conjugation and the fluorescent product is essentially a substituted aminocoumarin (λ_{ex} = 485 nm). In pure PBS buffer, the reaction was complete in 20 s, making probe 59 one of the fastest probes yet reported. Upon treatment with HS a 694-fold increase in the ratio F_{485}/F_{690} (0.07-83.90) was noted allowing a detection limit of 140 nM. While this probe did react with mercaptoethanol, selectivity for HS over cysteine and GSH was apparent. It was suggested that electrostatic repulsion between the benzopyrylium ion and the protonated amines of Cys and GSH prevents addition. Probe 59 was found to be non-toxic (MTT assay) and was subsequently used for the ratiometric imaging of exogenous HS in HeLa cells.

Fig. 53 Structure and reaction of 59 with HS

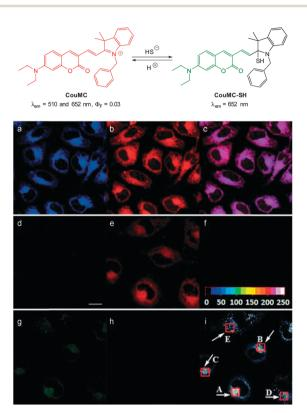


Fig. 54 Top: structure and reversible reaction of CouMC with HS-Bottom: (a-c) fluorescence images of MCF-7 cells co-stained by CouMC and Mito marker Deep Red 633. (a) Pseudocoloured image obtained with band path of 660-750 nm ($\lambda_{\rm ex}$ = 488 nm); (b) image from band path of 665–750 nm upon excitation of Deep Red (λ_{ex} = 633 nm); (c) overlay of (a) and (b). (d-i) Fluorescence imaging of MCF-7 cells (λ_{ex} = 488 nm). (d-f) Images of cells stained by CouMC; (q-i) images of cells preincubated with CouMC followed by NaSH. (d, g) Green-channel images collected with band path of 500-560 nm; (e, h) red-channel images collected with band path of 640-700 nm; (f, i) ratiometric image scale bar in (d): 20 mm. Image reproduced with permission.²²⁴

The mitochondria selective HS⁻ probe CouMC (Fig. 54) was reported by the groups of He and Guo in 2013.224 The coumarin-hemicyanine probe CouMC has two fluorescent emissions (λ_{em} = 510 and 652 nm) with the red emission, which corresponds to the full conjugated system, being the more intense. Nucleophilic attack of HS at the indolium C=N interrupts the conjugated system of CouMC and the resultant truncated π-system of CouMC-SH exhibits coumarin-like fluorescence (λ_{em} = 510 nm). Maximum fluorescence emission was achieved in 30 s in simulated physiological conditions. The red fluorescence could be reinstated when the media containing CouMC-SH was acidified to pH 2.5; CouMC itself, was stable over the pH range of 2.5 to 8.0. In vitro ratiometric

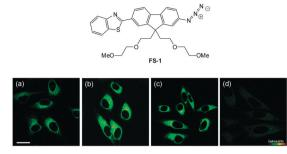


Fig. 55 Top: structure of hydrosulphide probe FS-1. Bottom: (a) twophoton microscopy images of HeLa cells labelled with FS-1. (b-d) Cells pre-treated with cysteine (b), GSH (c), or PMA (d) before labelling with FS-1. The TPEF was collected at 400-680 nm upon excitation at 750 nm. Scale = 30 mm. Image reproduced with permission.²²⁵

imagining studies with CouMC in MCF-7 cells revealed high localisation in the mitochondria (colocalisation with Deep Red 633). The intracellular reaction of the probe with HS⁻ occurred rapidly (<80 s) and as such this probe may find utility in the spatiotemporal tracking of this anion.

3.3.2 Hydrosulfide mediated reduction. In 2012 Cho reported FS-1 (Fig. 55), the earliest example of a two-photon probe for HS⁻.²²⁵ The sensor employed the azide "trigger", which was pioneered by the Chang group for bioimaging.²²⁶ When treated with HS⁻, a 21-fold increase in fluorescent enhancement ($\lambda_{\rm em}$ = 548 nm, $\Phi_{\rm F}$ = 0.46) was observed. The probe also displayed an increase in two-photon cross section under the same conditions (HEPES buffer, $\Phi\delta$ = 15–302 GM). Endogenous HS⁻ was visualised in live HeLa cells using FS-1, pre-treatment with cysteine and GSH both led to enhanced twophoton excited fluorescence (TPEF) (λ_{ex} = 750 nm, λ_{em} = 520 nm). Phorbol 12-myristate 13-acetate (PMA) induced oxidative stress led to a decrease in observed emission intensity.

In 2012 Han and co-workers reported the NIR-emitting ratiometric cyanine-azide probe Cy-N₃ (Fig. 56).²²⁷ Upon treatment with NaSH the azide probe (λ_{ex} = 625 nm, λ_{em} = 710 nm $\Phi_{\rm F}$ = 0.11) is reduced to give Cy-NH₂ ($\lambda_{\rm em}$ = 750 nm, $\Phi_{\rm F}$ = 0.12) with a concomitant increase in molar absorptivity (ε_{660} = 130 000 M⁻¹ cm⁻¹). The maximum fluorescence response was achieved in 20 min which was superior to related examples at that time. The ratio of emission intensities (F_{750}/F_{710}) increased from 0.6-2.0 with the addition of 10 equivalents of NaSH, and a detection limit of 80 nM was established. The probe was successfully used to detect endogenous HS in live RAW264.7 macrophages (stimulated using PMA). The fluorescence emission intensity also increased in cells treated with NaSH and Cy-N3 was also used to study the time dependent decomposition of the HS⁻ releasing agent 5-(4-hydroxyphenyl)-3H-1,2-dithiole-3thione (ADT-OH) in fetal bovine serum.

In 2013 the groups of Xu and Peng independently reported the red emitting dicyanomethylenebenzopyran probe DCMC-N₃ (Fig. 57). 228,229 Probe DCMC-N₃ is essentially non-fluorescent, however, upon reaction with HS- fluorescence was "switched on" ($\lambda_{\rm em}$ = 670 nm in 1:1 PBS buffer: DMSO or $\lambda_{\rm em}$ = 655 nm in 1:1 phosphate buffer: MeCN). The Xu group showed that

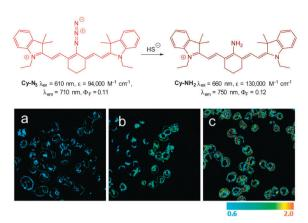


Fig. 56 Top: structure and reaction of Cy-N₃ with HS⁻. Bottom: ratiometric fluorescence images (F_{750}/F_{710}) of living RAW264.7 macrophage cells with Cy-N3. Images displayed in pseudo colour represent the ratio of emission intensities. (a) Cells were pretreated with PMA before loading Cy-N₃. (b) Cells incubated with Cy-N₃. (c) RAW264.7 cells incubated with NaSH and Cy-N₃ was added. Image reproduced with permission.²²⁷

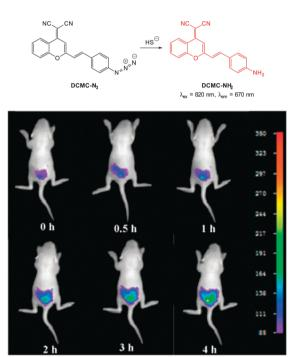


Fig. 57 Top: structure and reaction of probe DCMC-N₃ with sulphide. Bottom: representative fluorescence images of mice (pseudo-colour) given a skin popping injection of probe DCMC-N₃ and then injected with NaSH. Images were taken after incubation of NaSH for different times (0, 0.5, 1, 2, 3 and 4 h). Image reproduced with permission.²²⁹

DBMC-N₃ could be used to indicate the presence of exogenously administered HS in human umbilical vein endothelial cells (HUVEC). Similarly, preliminary experiments by the Peng group used DBMC-N₃ to image exogenous HS⁻ in HeLa cells. The Peng group also utilised the favourable properties of **DCMC-N₃** (NIR, large Stokes shift and good $\Phi \delta_{\text{max}} = 50$ GM at 820 nm in DMSO) to visualise the presence of HS⁻ in MCF-7 cells using two photon microscopy. Furthermore, a skin-pop injection of probe DCMC-N3 and NaSH (25 equiv.) into ICR

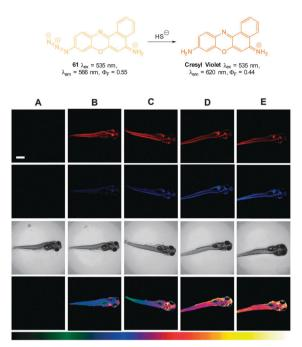


Fig. 58 Top: structure and reaction of **61** with HS⁻. Bottom: fluorescent images of HS⁻ in living 5-day-old zebrafish. (A) Zebrafish only (control). The zebrafish were treated with 61 and then with various concentrations of NaSH: (B) 0 mM, (C) 10 mM, (D) 100 mM, and (E) 500 mM. First row (570-600 nm), second row (640-670 nm) and third row (corresponding DIC images). The images of the fourth row are the ratio channel. The bottom color strip represents pseudocolor correlation with HS⁻ concentration. Scale = 500 mm. Image reproduced with permission.²³⁰

mice revealed that the probe could be used in vivo as an enhanced fluorescent response ($\lambda_{\rm ex}$ = 530 nm, $\lambda_{\rm em}$ = 655 \pm 20 nm) was observed. The development of the fluorescent response over 4 h is shown in Fig. 57.

Through a simple two-step azidation procedure Ma (2012) converted cresyl violet to the ratiometric azide probe 61 (Fig. 58). ²³⁰ Both **61** ($\lambda_{\rm em}$ = 566 nm, $\Phi_{\rm F}$ = 0.54) and cresyl violet $(\lambda_{\rm em} = 620 \text{ nm}, \Phi_{\rm F} = 0.44)$ were strongly fluorescent $(\lambda_{\rm em} =$ 620 nm). The emission ratio (F_{620}/F_{566}) ranged from 0.34–10.5 upon addition of HS- and a detection limit of 100 nM was determined. Probe 61 was used to visualise exogenous HSadded to MCF-7 cells, and the emission could be quenched with addition of ZnCl₂ to the cells, confirming that switching is a result of azide reduction. The utility of 61 to visualise HS in vivo was demonstrated in live zebrafish. As the concentration of HS was increased (10-500 μM) fluorescence emission ratio (F_{620}/F_{566}) of the probe (10 μ M) ranged from 0.73–1.64 with no visible fluorescence decrease on standing for elongated times, indicating that probe 61 was stable in vivo.

Chang in 2013 reported probe SF7-AM; which incorporated AM-esters to facilitate passive diffusion into cells. Intracellular ester hydrolysis gave the free carboxylates and the probe was subsequently retained within the cells (Fig. 59).²³¹ The inclusion of two azide triggers to the rhodamine-based fluorophore gave enhanced sensitivity and SF7-AM was used as a tool to study vascular endothelial growth factor (VEGF) stimulated HUVEC HS production as a model for angiogenesis.

Fig. 59 Structure, intracellular esterase and sulphide reactions of $\bf SF7-AM$.

As an advancement on their **Lyso-NHS** probe (Fig. 48) Cui and Xu developed the lysosome targeting probe **Lyso-AFP** (Fig. 60). When HS⁻ mediated reduction of the essentially non-fluorescent azide ($\Phi_{\rm F}=0.012$) occurred an increase in fluorescence response ($\Phi_{\rm F}=0.263$, $\lambda_{\rm ex}=426$ nm, $\lambda_{\rm em}=535$ nm) was observed over 20 min. As with **Lyso-NHS** the pendant morpholine of **Lyso-AFP** lead to lysosomal localisation.

Another lysosome specific probe; rhodamine-based **SulpHensor** (Fig. 61) was described by Yang (2014). No fluorescent response at physiological pH was observed for this probe upon treatment with HS $^-$. The acidic lysosome environment is required to open the spirocycle which results in a weakly fluorescent species ($\lambda_{\rm ex}=540$ nm, $\lambda_{\rm em}=550$ nm, $\Phi_{\rm F}=0.05$). Subsequent azide reduction by HS $^-$ greatly enhances the ICT fluorescent emission at 550 nm ($\Phi_{\rm F}=0.05$) and a limit of detection of 500 nM for HS $^-$ was determined. The HS $^-$ /H $^+$ induced fluorescent response of

Lyso-NFP
$$\lambda_{\rm ex}=370$$
 nm, $\lambda_{\rm em}=535$ nm, $\lambda_{\rm F}=0.012$

Fig. 60 Structure and reaction of Lyso-AFP.

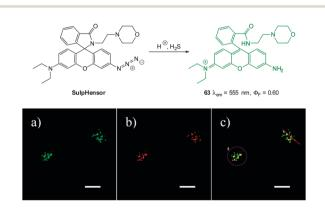


Fig. 61 Top: structure and reaction of **SulpHensor**. Bottom: HeLa cells stained with (a) LysoTracker Green (Ch1, green) and (b) **SulpHensor** (Ch2, red) with NaSH solution (c) overlay of (a) and (b). Scale = 10 μ m. Image reproduced with permission.²³³

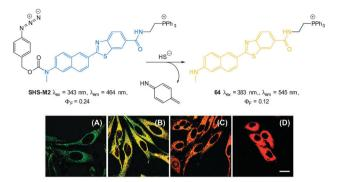


Fig. 62 Top: two-photon fluorescent probe **SHS-M2** developed by Kim. Bottom: (A–D) Pseudocoloured ratiometric TPM images F_{545}/F_{464} of (A, D) HeLa cells with (A) **SHS-M2** or (D) **SHS-M2** and (B, C) HeLa cells pretreated with (B) GSH or (C) cysteine prior to **SHS-M2**. Image reproduced with permission. 234

SulpHensor was demonstrated *in vitro* using HeLa cells. Lysosomal accumulation was confirmed by co-staining with Lyso-Tracker green and comparing the intensity profiles (Fig. 61) from the red (**SulpHensor**) and green channels (LysoTracker) over a selected region.

Bae et al. employed the 4-azidobenzylcarbamate trigger in their two photon fluorescent probe SHS-M2 (Fig. 62). Hydrosulphide mediated reduction initially yields the aminobenzylcarbamate which subsequently fragments to give the observed products. In addition, the attachment of a pendant triphenylphosphonium moiety lead to mitochondrial accumulation in astrocytes.234 Upon reduction with HS- the emission wavelength of **SHS-M2** ($\lambda_{\rm em}$ = 464, $\Phi_{\rm F}$ = 0.24) was red-shifted by 81 nm ($\lambda_{\rm em}$ = 545 nm, $\Phi_{\rm F}$ = 0.12) and despite a decrease in quantum yield the two photon cross section was improved $(\Phi \delta_{\text{max}} = 17-55 \text{ GM})$. The probe was successfully used to detect mitochondrial HS⁻ in HeLa cells; metabolic precursors (GSH or Cys) of HS- were added prior to the SHS-M2 and an increase in the F_{545}/F_{464} ratio was recorded. The probe was also used to demonstrate the relationship between the DJ-1 gene and CBS mediated HS⁻ production in astrocytes as a model of Parkinson's disease.

The 4-aminonaphthalimide-based HS⁻ probes **NAP-1** and **AcSH-2** also bearing the 4-azidobenzylcarbamate trigger were independently reported by Zhao and Song in 2014. ^{235,236} Reaction of **NAP-1** (**AcSH-1**) with HS⁻ gives the fluorescent aminonaphthalimide and a corresponding red-shift in emission (from $\lambda_{\rm em}$ = 474 nm to $\lambda_{\rm em}$ = 540 nm). ²³⁵ A low limit of detection for HS⁻ was determined (50 nM at pH 7.0 and 110 nM at pH 7.4) and the probe was used by Song for monitoring endogenous HS⁻ production in sodium nitroprusside stimulated MCF-7 cells (Fig. 63) as well as quantifying HS⁻ levels in murine hippocampus. Zhao used **AcSH-2** to visualise exogenous HS⁻ in MCF-7 cells using TPM ($\lambda_{\rm ex}$ = 800 nm, F_{530}/F_{468} = 0.38–2.90). It was also evident that the *N*-(2-hydroxylethyl)-imide of **AcSH-2** promoted mitochondrial localisation. ²³⁶

Chen and co-workers built the m-nitrophenyloxycyanine **Cy-NO**₂ (Fig. 64) as a d-PET based probe for HS $^-$.²³⁷ The 3-nitrophenylether attached to the cyanine framework could accept an

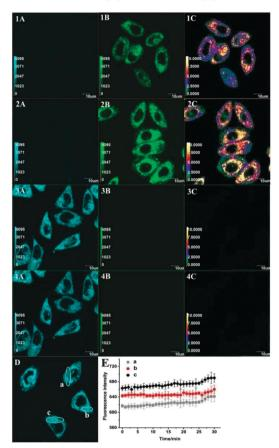


Fig. 63 Confocal fluorescence images of endogenous HS⁻ in living MCF-7 cells with NAP-1. Cells were pre-stimulated with SNP, then with NAP-1 (1A, 1B, 1C). Cells were pre-stimulated with SNP, and then with NAP-1 (2A, 2B, 2C). Cells were pre-treated with DL-propargylglycine (PPG), and then with NAP-1 (3A, 3B, 3C). Cells in (3A, 3B, 3C) were thereafter treated with SNP (4A, 4B, 4C). Cells were incubated with NAP-1 alone (D). The average fluorescence intensity from the regions of interest a, b and c in (D) was recorded with 60 s intervals (E) (n = 3). Ratiometric images (F_{530}/F_{468}) generated by the Olympus software (1C, 2C, 3C, 4C). Scale bars = $10 \mu m$. Image reproduced with permission.²³⁵

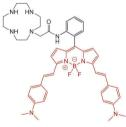
OPET
$$NNO_2$$
 NNO_2
 NH_2
 NH_2

Fig. 64 Structure and reaction of hydrosulphide probe Cy-NO₂.

electron from the excited state of the cyanine fluorophore. Reduction of the nitro group with HS⁻ disrupts the d-PET process resulting in significantly enhanced emission

(from $\Phi_{\rm F} = 0.05$ to $\Phi_{\rm F} = 0.11$, $\lambda_{\rm ex} = 755$ nm, $\lambda_{\rm em} = 789$ nm). The probe localised in the cytosol of RAW264.7 macrophages and was used to detect exogenous HS-. A significant drawback associated with unassisted nitro group reduction is that it is a kinetically slow process, and in this instance fluorescence intensity peaked only after 60 min, even at 37 °C.

3.3.3 Hydrosulfide mediated metal displacement. In 2014 Huang and Deng reported a NIR emitting probe based on Cu(II) displacement from the Cu(II)-cyclen complex 68-Cu(II) (Fig. 65).²³⁸ The probe was originally designed to function by means of HS⁻ mediated NO₂ reduction, but no reaction occurred at ambient temperatures. The probe was redesigned and the nitro group was reduced to an amine and functionalised with the cyclen-macrocycle. Complexation of 68 with Cu(II) gave the non-fluorescent probe which, when treated with HS⁻ in buffered solution studies gave a significant fluorescence "switch on" response ($\lambda_{\rm ex}$ = 716 nm, $\lambda_{\rm em}$ = 765 nm). Visualisation of exogenous HS in RAW264.7 macrophages was successfully demonstrated as was the detection of endogenous HSwhich was produced by the overexpression of wild-type (WT) cystathionine-γ lyase (CSE) in human embryonic kidney (HEK293). In vivo studies were then performed by injecting imprinting control region (ICR) mice with 68-Cu(II) by skin-pop injection. One 68-Cu(II) treated mouse was then injected with Na2S (as source of HS-) and the fluorescence images were recorded (λ_{ex} = 670 nm, λ_{em} = 790 nm). The fluorescence signal increased seven-fold 1 h after treatment with HS (compared to the control) and continued to rise gradually over 5 h.



68 $\lambda_{ex} = 716 \text{ nm}, \lambda_{em} = 765 \text{ nm}$

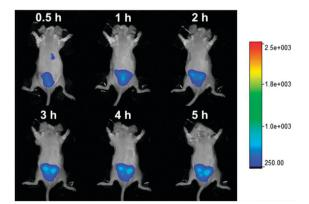


Fig. 65 Top: NIR emissive cyclen dosimeter 68 by Deng and Huang. Bottom: representative fluorescence images of mice (pseudocolour) that were injected with 68-Cu(II) (40 mm), followed by Na₂S. The images were recorded after the injection of Na₂S within 5 h. Image reproduced with permission.²³⁸

In order to keep this section to a reasonable length and highlight the most relevant recent examples it was not possible to include all recent examples of probes functioning by way of (i) nucleophilicity^{100,218,219,223,224,239-247} (ii) reduction (arylazides, ^{226-228,231-235,248-258} sulfonylazides, ²⁵⁹⁻²⁶¹ nitro groups, ^{262,263} hydroxyl amines, ²⁶⁴ and N-oxides ²⁶⁵) as well as (iii) displacement ^{53,266-269} and readers are referred to these citations for additional information.

4. Reactive anions

In addition to the well-known oxidative stress caused by reactive oxygen and nitrogen species, it is becoming increasingly apparent that these moieties are involved in a wide range of physiologically essential processes (such as cellular migration and circadian rhythm).²⁷⁰ Reactive oxygen/nitrogen species can be neutral, anionic, radicals or even radical anions (Table 2) and as many of these species exist only fleetingly they are exceptionally challenging targets for small molecular probes.^{50,271}

At physiological pH (*ca.* 7.4) several of these species exist to a considerable extent as an anion (peroxynitrite, hypochlorite and hypobromite) and can therefore be considered biologically relevant anionic targets. Given their diverse roles interest in detecting these species *in vitro* and *in vivo* has been strong and several reviews on the topic are available.^{34,60,271,272}

4.1 Peroxynitrite

Peroxynitrite is formed from the rapid reaction of two other RO/N species: superoxide $O_2^{\bullet-}$ and nitric oxide NO^{\bullet} (Fig. 66) and its detection in living systems is hampered by a number of factors including (i) its reactivity (it is a potent nucleophile and is a more powerful oxidant than superoxide) with a number of *in vivo* targets such as proteins, nucleic acids and lipids (especially those containing thiols) and (ii) degradation to other highly reactive species (including both the hydroxyl radical and the nitrogen dioxide radical).^{57,273} The pK_a of ONOOH is 6.8 and as a result $\sim 80\%$ of the species is found in the anionic form at pH 7.4. Typically the anion adopts a cisoid structure that is responsible for its 'relative' stability compared to the parent acid.²⁷⁴

Elevated levels of this species are associated with cardiovascular and neurodegenerative disorders, metabolic diseases, inflammation, pain, and cancer.^{275,276} Hence the development of probes for its detection *in vivo* is an important task *en route* to fully understanding its diverse physiological roles.⁵⁷

$$NO' + OO'^{\ominus} \longrightarrow ONOO^{\ominus}$$

$$O_{O-N'}^{\ominus}$$

Fig. 66 Formation and cisoid structure of peroxynitrite.

Peroxynitrite has long been known as a cellular oxidant and hence sensors to monitor this anion emerged last century. Probes for peroxynitrite rely on the same reactivity that the anion exhibits *in vivo*; ONOO⁻ is both nucleophilic (reacts with CO₂ *in vivo* to form carbonate²⁷⁷) and highly oxidative (by one and two electron processes) and is a known nitrating agent. All three of these reaction types has been employed in the design of imaging agents for the species however probes that employ the oxidation power of ONOO⁻ are by far the most prominent (Section 4.1.1). Amongst these, probes based on the oxidation of B, Se, and Te form an interesting subset (Section 4.2.2). Common interferents with the detection of ONOO⁻ are typically other ROS in particular hypochlorite (ClO⁻) and nitroxide radical (*NO).

Early anion sensors for peroxynitrite inside cells include the "switch on" probes dichlorodihydrofluorescein **DCHF** and dihydrorhodamine **DHR-123** (Fig. 67).^{278–280} While many imaging studies, and even flow cytometry assays,²⁸¹ were performed using these, (and similar) probes they are somewhat non-selective and in some instances light sensitive.²⁷²

4.1.1 Peroxynitrite mediated oxidation/fragmentation. A recent report by Shivanna (2013) detailed the use of rhodamine B phenyl hydrazide RBPH (Fig. 68). The probe was readily oxidised by ONOO⁻ to give the highly fluorescent (λ_{em} = 580 nm) ring open **rhodamine-B**; the product confirmed by H NMR spectroscopy ESMS. Interferents such as H₂O₂ did not elicit the same reaction (ClO⁻ was not tested) and as such some selectivity was noted. Live MCF-7 cells incubated with the probe gave a clear "switch on" response within 30 min when exogenous ONOO⁻ was added.

A strategy developed by Yang involves ONOO⁻ nucleophilic attack on a reactive trifluoromethyl ketone group followed by

Fig. 67 Early chemodosimeter based agents for peroxynitrite; dihydro-dichlorofluorescein (DCHF) and dihydrorhodamine (DHR-123).

Table 2	Reactive	oxygen/	/nitrogen	species

Neutral	Anionic	Radical anion	Radical
Hydrogen peroxide HOOH Singlet oxygen $^1\mathrm{O}_2$	Peroxynitrite ONOO ⁻ Hypochlorite ClO ⁻ Hypobromite BrO ^{- a}	Superoxide O₂•¯	Nitric oxide NO° Hydroxyl HO° Nitrogen dioxide NO ₂ ° Peroxy radicals ROO°

^a A percentage of this species can also be found in neutral form (HOBr $pK_a = 8.7$).

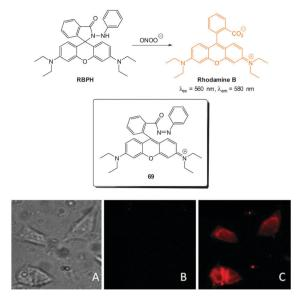


Fig. 68 Top: structure and reaction of RBHP with ONOO-; inset shows the diazo intermediate 69 that forms prior to fragmentation. Bottom: (A) bright-field image of MCF-7 cells incubated with **RBPH**. (B) Corresponding fluorescence image (C) fluorescence image of MCF-7 cells incubated with RBPH then peroxynitrite. Image reproduced with permission.²⁸²

formation of a spirohemiacetal via a dioxirane intermediate. 283 Three separate probes have been developed: employing dichlorofluorescein **HKGreen1**, ²⁸⁴ BODIPY **HKGreen2**, ²⁸⁵ and rhodol **HKGreen3**⁹² fluorophores (Fig. 69). For these chemodosimeters fluorescence is quenched in the ketone form but following spirohemiacetal formation (and for HK1 and HK3 fragmentation) fluorescence is "switched on". For HKGreen2 a 21-fold enhancement of fluorescence ($\lambda_{\rm em}$ = 539 nm) was observed upon reaction with just one equivalent of ONOO. The probes react to a small extent with HO• but not the common ClO interferent. Evaluation in cells was performed for all probes (Results for HKGreen3 in RAW264.7 macrophages shown in Fig. 69). This cell line is known to produce ROS/RNS, including ONOO-, in response to immunological and inflammatory stress and after stimulation of endogenous ONOO production using bacterial endotoxin lipopolysaccharide (LPS), interferon-γ (IFN-γ) and phorbol 12-myristate 13-acetate (PMA) strong fluorescence was noted. No fluorescence enhancement was noted when ONOOproduction was inhibited by (2,2,6,6-tetramethylpiperidin-1-yl)oxy (TEMPO) a superoxide scavenger or aminoguanidine (AG) an inhibitor of NO synthase286 confirming that endogenous production of ONOO was being detected.

In a more recent article from the Yang group a functionalised rhodol chemodosimeter HKGreen-4 (Fig. 70) was described in which the oxidation of electron rich aromatics was exploited.²⁸⁷ The "switch on" probe (290-fold increase in λ_{em} = 535 nm) was capable of discriminating between peroxynitrite and other reactive oxygen species including hydroxyl radical and hypochlorite. **HKGreen4** also performed in the presence of CO₂, a molecule known to react quickly with ONOO. The probe was water soluble and was successfully used with either conventional or two photon microscopy to image endogenous ONOO production in E. coli

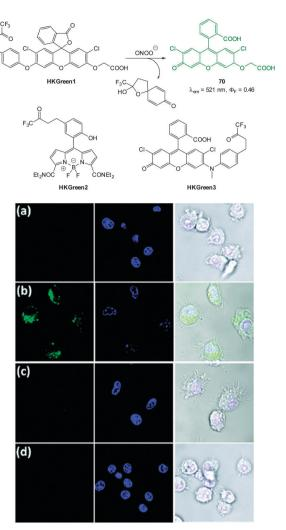


Fig. 69 Top: structure of HKGreen1, 2 and 3 and reactivity of BODIPY based chemodosimeters **HKGreen1** with peroxynitrite to form **70**. Bottom: images of live RAW264.7 cells were treated with stimulants to elicit endogenous ONOO- production then stained with HKGreen-3 (green channel) and Hoechst 33342 (blue channel). (a) Cells without stimulation. (b) Cells stimulated with LPS, IFN- γ , and PMA. (c) Cells pre-treated with TEMPO, and then stimulated with LPS, IFN- γ , and PMA. (d) Cells pretreated with AG, then stimulated with LPS, IFN-γ, and PMA. Image reproduced with permission.92

challenged RAW264.7 cells. In conjunction with a number of enzymatic inhibitors the probe was used to further confirm the generation of endogenous ONOO production in response to the presence of E. coli. Generation of ONOO is thought to be an immune effector for bacterial clearance, and the results of this study suggest that the ONOO formation in E. coli challenged macrophages is enzymatically regulated.

The "switch on" coumarin pyridinium probe C-Py-1 was reported by Yu in 2014 (Fig. 71). 288 The probe was selective for peroxynitrite amongst other reactive oxygen/nitrogen species with a 25-fold enhancement of emission at $\lambda_{\rm em}$ = 493 nm. The emitting species was identified (1H NMR spectroscopy and ESI-MS) to be the coumarin aldehyde 72 formed from oxidative cleavage of the alkene in the presence of ONOO-. Excellent cell

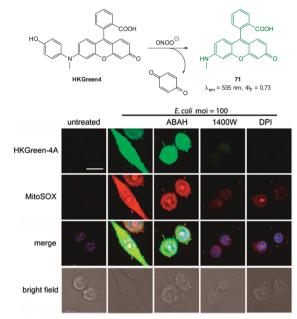


Fig. 70 Top: structure and reaction of **HKGreen4** with ONOO⁻. Bottom: images of RAW264.7 macrophages. Cells were co-treated with heat-killed E. coli and various enzyme inhibitors then stained with HKGreen4A, MitoSOX, and Hoechst 33342 before imaging. Aminobenzoic acid hydrazide (ABAH) is an inhibitor of myeloperoxidase that produces ClO-; 1400 W and DPI are inhibitors for iNOS and NOX, respectively. The merged images are overlays of all fluorescence channels. Scale = 10 μm. Image reproduced with permission.²⁸⁷

membrane permeation and low cytotoxicity were noted and the probe was successfully applied to the imaging of endogenous ONOO in RAW264.7 cells. In vitro fluorescence was "switched on" within 30 min of the addition of lipopolysaccharide (LPS) to the cells to stimulate endogenous production of ONOO-.

The related hemicyanine probe CHCN (Fig. 72) has recently been published by Yoon (2015).²⁸⁹ Oxidative cleavage of the alkene gives coumarin aldehyde 73 and 1,3,3-trimethyloxindole; both products confirmed using ESMS and ¹H NMR spectroscopy. This probe indicated ONOO⁻ in a linear ratiometric fashion (F_{515}/F_{635} increase), had a low LOD (49.7 nM) and displayed excellent

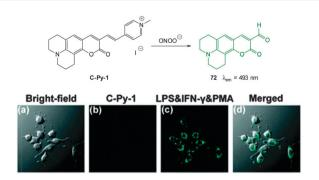


Fig. 71 Top: structure and reaction of ONOO probe C-Py-1. Bottom: images of RAW264.7 cells. (a) Bright-field image; (b) cells stained with **C-Py-1**; (c) cells were stained with LPS and IFN- γ then PMA and finally with C-Py-1; (d) merged image of (a) and (c). Scale = 10 μm. Image reproduced with permission.²⁸⁸

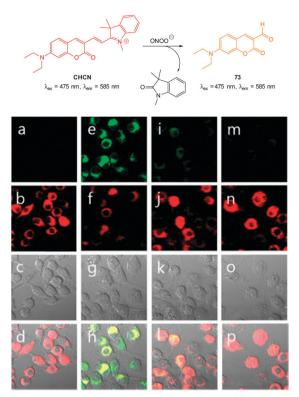


Fig. 72 Top: structure and reaction of coumarinindolium probe CHCN. Bottom: images of RAW264.7 cells for endogenous ONOO- during phagocytic immune response. The cells were stained with CHCN. (a) Control; (e) LPS, IFN- γ and PMA; (i) LPS, IFN- γ and PMA then AG; (m) LPS, IFN- γ and PMA then TEMPO. Green channel (a, e, i, m); red channel (b, f, j, n); images (c, g, k, o) are differential interference contrast; images (d, h, l, p) are merged red and green channels. Image reproduced with permission.²⁸

selectivity—only a very slight response to a large excess of hypochlorite was noted. The probe was shown to operate successfully in RAW264.7 macrophages when the cells were stimulated to produce ONOO using a number of agents (LPS, IFN- γ and PMA). No response was observed when inhibitors of endogenous ONOO- production were introduced (TEMPO and aminoguanidine).

A multichannel probe PN₆₀₀ (Fig. 73) that can clearly distinguish ONOO from ClO has been developed by Yang (2012).²⁹⁰ While both hypochlorite and peroxynitrite can oxidise the coumarin PN₆₀₀ to the corresponding aminophenol 74, only ONOO is powerful enough to oxidise 74 to the red emitting iminoquinone 75. Due to differing excitation yet similar emission wavelengths either of OCl or the ONOO could be inferred by monitoring emission at 620 nm and selectively exciting at 355, 465 or 575 to identify which fluorophore had formed and hence which oxidant was present. In human glioma cell line U87 the probe was shown to quickly penetrate the cell membrane and was non-toxic (MTT assay). Using 3-morpholinosydnonimine (SIN-1), a compound known to decompose to NO which in turn forms ONOO^{-,291} a clear fluorescent response was observed.

Probes containing boron have recently emerged for the cellular sensing of peroxynitrite. 292 The nucleophilicity of ONOO leads to initial formation of a C-O-B bond in place of the original C-B

Fig. 73 Top: probe PN₆₀₀ showing reaction with both ONOO⁻ and ClO⁻ to form 74, however only ONOO⁻ can oxidise 74 to the red iminoquinone 75. Bottom: live-cell imaging using PN₆₀₀. Phase contrast and fluorescence images of human glioma cells treated with (A, B) PN₆₀₀, (C, D) PN₆₀₀ + ClO⁻, and (E, F) PN_{600} + SIN-1. Scale = 50 μm . Image reproduced with permission. 290

Scheme 2 Conversion of arylboronates to phenols using ONOO-.

bond (Scheme 2). This insertion is followed by hydrolysis to afford C-O-H. The process is similar to the established hydroboration/ oxidation using alkaline H₂O₂ however the reaction of boronates with ONOO is nearly 1×10^7 times faster than the reaction with H2O2 and hence discrimination between these species is possible.293

The naphthalimide-based "switch off" probe 80 was reported by James in 2014 (Fig. 74).²⁹⁴ The fluorescent D-fructose complex (λ_{em} = 525 nm) of **79** in which PET from the spacer N is prevented was "switched off" by ONOOmediated oxidation to the corresponding phenol 81. The product again has a free amine and PET quenches fluorescence. All other ROS except ClO⁻ did not elicit a significant response. In RAW264.7 macrophages ONOO production was stimulated by a number of immunological factors (again including LPS) and the "switch off" was easily visualised. When TEMPO or aminoguanidine was added to the stressed cells prior to addition of the probe fluorescence was maintained due to a lack of endogenous ONOO-.

In 2012 Han reported the "switch on" dioxaborolane pyrene probe PyBor (Fig. 75) which was synthesised in three steps from pyrene.²⁹⁵ Reaction with ONOO was complete in seconds (PyBor is converted to PyOH) and was accompanied by a significant increase in quantum yield from $\phi_{\rm F}$ = 0.08 to 0.60 (**PyOH**, $\lambda_{\rm ex}$ = 347, $\lambda_{\rm em}$ = 410 nm). While slightly sensitive to

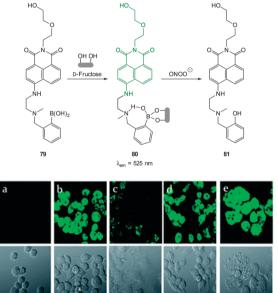


Fig. 74 Structure and three stage reaction of naphthalimide boronate 79 with D-fructose and ONOO-. Bottom: fluorescent imaging for endogenous ONOO in RAW264.7 cells. The probe 80 was formed by mixing 79 and p-fructose in situ. (a) Blank without probe; (b) probe 80 only; (c) probe 80 and LPS, IFN-γ, PMA; (d) c + aminoquanidine; (e) c + TEMPO. Image reproduced with permission.²⁹⁴

H₂O₂, ClO⁻ and BrO⁻ co-staining confirmed **PyBor** localised in the cytoplasm of RAW264.7 cells and intense intracellular fluorescence was observed when cells that had been incubated with **PvBor** were treated with LPS, IFN-γ and PMA. When the cells were pre-treated with aminoguanidine, only weak fluorescence was detected.

4.1.2 ONOO mediated chalcogen oxidation. Fully reversible, NIR emissive, phenylselenylaniline probes BzSe-Cy, Cy-PSe and a related Te containing cyanine probe Cy-NTe have been developed by Tang and Han (Fig. 76). The first, benzylselenylcyanine BzSe-Cy, 296 is a "switch off" probe that can be recycled with ascorbic acid. In BzSe-Cy the selenium is an electron donating

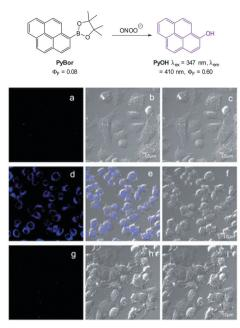


Fig. 75 Top: structure and reaction of PyBor with ONOO-. Bottom: images of RAW264.7 macrophages treated with PyBor in the absence or presence of stimulants for 30 min. (a-c) Controls; (d-f) LPS and IFN- γ then PMA; (g-i) AG, LPS, IFN- γ and PMA. (a, d, g) fluorescence Images; (b, e, h) overlay images; (c, f, i) bright-field images. Image reproduced with permission.²⁹⁵

component of the cyanine system, however, in its oxidised Se=O form (readily accomplished by ONOO-) electron donation is "switched off" and fluorescence is quenched. The second probe, Cy-PSe²⁹⁷ is a "switch on" probe that uses PET from the dibenzylselenoether to quench BODIPY fluorescence. When oxidised to Se=O, electron transfer is inhibited and fluorescence is "switched on". The third, Cy-NTe²⁹⁸ another "switch on" probe also operates using this principle. The Te component required six steps to construct prior to coupling with commercially available cyanine chloride. Both Cy-PSe and Cy-NTe are easily oxidised by ONOO and also easily reduced by glutathione (GSH) which makes them mimics of the Se containing glutathione peroxidase enzymes (GPx). In the non-oxidised state the metals quench fluorescence by PET, however PET is not possible in the oxidised forms and strong fluorescence enhancement is observed (23-fold for Cy-PSe and 13-fold for Cy-NTe). The successful "switch on" oxidation, "switch off" reduction cycles for both Cy-PSe and Cy-NTe were demonstrated in RAW264.7 cells by successive treatment with LPS then an ROS scavenger glutathione S-transferase (GST) to "switch off" fluorescence. Mitochondrial localisation of Cy-NTe was reported as was a lack of toxicity (MTT assay) and the switching behaviour of the probe was sensitive enough to be visualised in vivo using BALB/c mice.

The selenium containing "switch off" BODIPY probe BOD-Se (Fig. 77) was reported by Han in 2012.²⁹⁹ The authors proposed that, in light of the long time required to elicit a response, oxidation of the Se itself by ONOO did not modulate fluorescence but that the product containing Se=O was hydrolysed

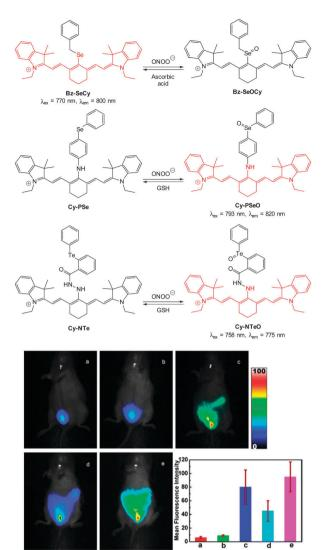


Fig. 76 Top: structure of BzSe-Cy, Cy-PSe and Cy-NTe probes and their oxidation products. Bottom: imaging of redox cycles between peroxynitrite and GSH in peritoneal cavity of BALB/c mice. (a) Cy-NTe and L-cysteine were injected in the i.p. cavity. (b) Mice injected i.p. with **Cy-NTe**. (c) Mice injected with LPS, IFN- γ then PMA followed by **Cy-NTe** (d) mice treated as described in (c), then injected i.p. with AG, GST and L-cysteine (e) mice treated as described in (d), then injected with SIN-1. Bar graph indicates total number of photons from the entire peritoneal cavity of the mice (a-e). Image reproduced with permission. 298

(Fig. 78) to liberate a new selenium free florescent BODIPY 82. The **BOD-Se** probe itself was highly fluorescent ($\lambda_{em} = 572$ nm, $\phi_{\rm F}$ = 0.96) and a colour change from red to blue was noted upon exposure to ONOO with an isosbestic point at 567 nm. Fluorescence intensity decreased more than 200-fold along with a shift of the emission maximum ($\lambda_{\rm em}$ = 680 nm, $\phi_{\rm F}$ = 0.05). Again murine macrophage RAW264.7 cells were stressed using LPS/ IFN-γ and PMA to induce endogenous production of ONOO⁻ prior to imaging.

4.1.3 Peroxynitrite mediated nitration/nitrosylation. The Ds-DAB probe (Fig. 78) was described by Wang in 2013 and its synthesis was remarkably easy—one step from commercially available materials.300 Fluorescence was initially quenched

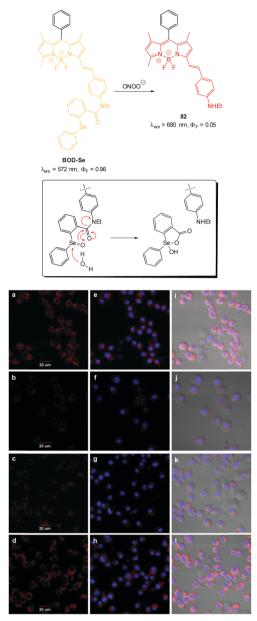


Fig. 77 Top: structure and reaction of BOD-Se with ONOO-; inset: proposed tandem hydrolysis/cyclisation of oxidised BOD-Se leading to fragmentation. Bottom: images RAW264.7 cells incubated with BOD-Se then treated with (a, e, i) controls. (b, f, j) SIN-1 (c, g, k) LPS, IFN- γ then PMA. (d, h, l) AG, LPS and IFN- γ then PMA (e-h) overlay showing **BOD-Se** fluorescence and Hoechst dye; (i-l) bright-field overlay of BOD-Se and Hoechst dye. Image reproduced with permission.²⁹⁹

(presumably by PET) and the selective, "switch on" (6.5-fold enhancement) chemodosimeter reacts readily with ONOO to form fluorescent dansyl acid ($\phi_{\rm F}$ = 0.15, $\lambda_{\rm em}$ = 505 nm, $\lambda_{\rm ex}$ = 350 nm) and benzotriazole as indicated by ESMS, ¹H NMR spectroscopy and LC-MS. The proposed mechanism involves formation of a nitrosamine which subsequently fragments. Rapid uptake of the probe was reported as was no toxicity and again the probe was used to visualise production of endogenous ONOO⁻ inside RAW264.7 macrophages when treated with LPS and PMA to induce cell stress.

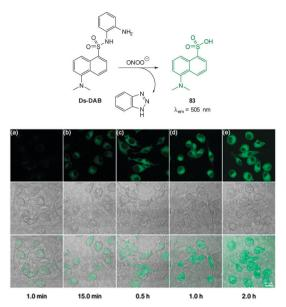


Fig. 78 Top: structure and reaction of **Ds-DAB** with peroxynitrite. Bottom: in vitro detection of ONOO in RAW264.7 macrophages. Cells were treated with LPS then PMA and subsequently incubated with Ds-DAB for the time stated prior to imaging. Top = fluorescence, middle = bright-field, bottom = overlay; scale = 20 μ m. Image reproduced with permission.³⁰⁰

A probe for nitrative stress (NiSPY-3, Fig. 79) was rationally designed by Nagano (2006)301 and is an interesting example in which nitration leads to fluorescence "switch on" ($\lambda_{ex} = 505$ nm, $\lambda_{\rm em}$ = 520 nm) based on an a-PET process. The probe was selective for peroxynitrite and was successfully used to visualise exogenous ONOO in live HeLa cells.

4.1.4 Miscellaneous. An interesting lanthanide-based probe for ONOO bioimaging was reported by Guan in 2010 (see Section 3.2 for the general principles by which Ln emission is modulated).93 The DTTA ligand (a combination of dimethoxyphenyl and terpyridinetetraacid, Fig. 80) was designed to be both a Ln chelator and also sensitive to a d-PET process. In practice the terbium complex [(DTTA)Tb]⁻ (λ_{ex} = 335 nm, λ_{em} = 612 nm) was sensitive to ONOO whereas the corresponding europium complex (λ_{ex} = 335 nm, λ_{em} = 541 nm) was not. The authors postulated that quenching by charge transfer, not PET, was responsible for the quenching, however, the electron rich dimethoxyphenyl substituent of DTTA is similar to that of NiSPY-3 (shown in Fig. 79). Thus, with a "cocktail" of both lanthanides [DTTA-Eu(III)] and [DTTA-Tb(III)] ratiometric measuring was possible with only very slight interference noted from nitrate. The tetraacetoxymethyl ester form AM-DTTA readily entered HeLa cells esters along with solutions of both lanthanides. Ester hydrolysis inside cells was followed by assembly of the lanthanide complexes and their formation could be visualised using microscopy. Again using SIN-1 as a source of NO° (reacts immediately with superoxide to form ONOO⁻) a clear decrease in Tb emission in proportion to increasing SIN-1 concentration was observed.

An interesting example of a probe for the sensing of ONOO by means of luciferin bioluminescence was reported in 2013 by **Review Article**

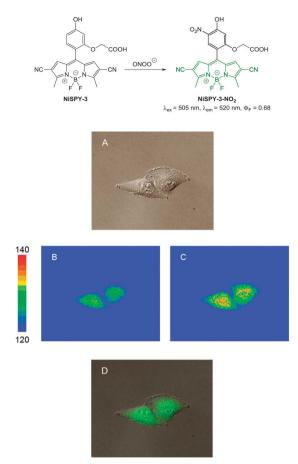


Fig. 79 Top: structure of NiSPY-3 and its reaction with ONOO. Bottom: differential interference contrast (A), pseudo-colour fluorescence (B, C) and merged images (D) of HeLa cells loaded with NiSPY-3. Pseudo-colour images were obtained before (B) and after (C) addition of peroxynitrite. Image reproduced with permission. 301

Bonini using the peroxy-caged luciferin PCL-1 (Fig. 81).302 Unfortunately, cell images were not shown in this instance. The boronic acid based chemodosimeter PCL-1 (originally designed and used by Chang for the in vivo bioimaging of H₂O₂ in mice)³⁰³ reacts far more rapidly with ONOO⁻ than it does with H2O2 to form luciferin which in turn forms oxyluciferin with concomitant emission of light (λ_{em} = 560 nm).

4.2 Hypochlorite

Hypochlorite plays an important physiological role defending against invading pathogens and endogenous hypochlorite is produced from the reaction of H2O2 with Cl and is catalysed by the heme enzyme myeloperoxidase (MPO). Over stimulation of the MPO immune response, and increased hypochlorite levels can lead to host tissue damage and inflammation that is associated with a number of serious disorders such as cancer, neurodegeneration, arthritis and cardiovascular disease.

$$H_2O_2 + Cl^{\ominus} \rightarrow H_2O + ClO^{\ominus}$$
 (1)

Bioimaging agents must be selective for ClO⁻ over H₂O₂ if the MPO-H₂O₂-Cl⁻ enzymatic system is used to generate endogenous

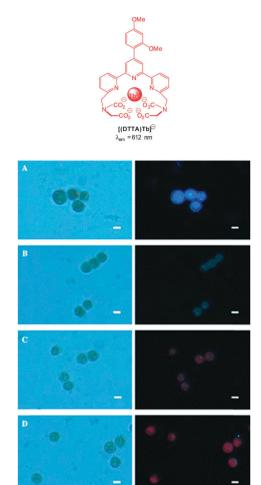


Fig. 80 Top: structure of the DTTA-Tb(III) complex. Bottom: bright-field (left) and normal luminescence (right) images of the [Eu(III)/Tb(III)(DTTA)]loaded HeLa cells in the presence of ONOO- generated from SIN-1 (A: negative control; B: 100 μ M; C: 200 μ M; D: 500 μ M of SIN-1). Scale = 10 μm. Image reproduced with permission.⁹³

Fig. 81 Structure and reaction of luciferin based probe PCL-1 with ONOO-.

ClO otherwise the fluorescent signal may be due to exogenous $\mathrm{H}_2\mathrm{O}_2$. Another consideration is pH; the parent acid HOCl has a p K_a of 7.463 at 35 °C, ³⁰⁴ therefore at physiological pH approximately 50% of the acid is dissociated; so it possible that either the hypochlorite anion or the protonated form could be the detected species. Most researchers evaluate their probe over a pH range to identify whether hypochlorite or hypochlorous acid is being detected.

The majority of chemodosimeter for hypochlorite rely on oxidation; indeed ClO- is well known, even at a household level, as a strong oxidising agent. The most common triggers include the oxidation of p-hydroxy and p-aminophenyl ethers to give quinones or iminoquinones (Section 4.2.1) although the p-aminophenyl ethers typically elicit a larger response to ClO and are more selective over ONOO (versus p-hydroxy). Oximes provide a pathway for non-radiative decay and are also readily react with hypochlorite (Section 4.2.2). As for probes that target ONOO⁻, the oxidation of S, Se, and Te has been employed in spirocyclic ring opening triggers for fluorescein and rhodamine dyes. This class of probe (notably the Se and Te based examples) are conveniently reversible as they can be reduced back to the parent structure by thiols (e.g. Cys, GSH) or hydrosulfide.

4.2.1 Hypochlorite mediated oxidation/fragmentation. An early example of a "switch on" probe for ClO was reported by Nagano in 2003. 305 Nagano's fluorescein system used hypochlorite to oxidise either a pendant p-hydroxyphenyl ether (HPF) or p-aminophenyl ether (APF) attached to the fluorescein fluorophore. Removal of the phenyl ethers (as the corresponding quinone or aminoquinone) restored ICT and gave rise to high fluorescence emission ($\lambda_{\rm em}$ = 514 nm, $\Phi_{\rm F}$ = 0.81). Unfortunately, and confirming the challenging nature of selective ClO- detection, HPF was more reactive towards HO and to a lesser extent ONOO. The second probe APF also gave a fluorescence response to HO* and ONOO- which was greater than HPF but unlike HPF, APF gave a large response when treated with hypochlorite. While HPF and APF were not completely selective, the difference in reactivity was demonstrated in neutrophils which contain azurophilic granules that are abundant in the ClO generating MPO enzyme. Both APF and HPF loaded neutrophils were stimulated with PMA to stimulate endogenous ClO production and fluorescence images were collected after 10 minutes. Only the cells containing APF exhibited a significant increase in fluorescent emission.

An extension on the Nagano fluorescein system was reported in 2007 by Libby, 306 whereby the p-aminophenyl ether moiety was attached to a water soluble sulfonaphthofluorescein (SNAPF, Fig. 82). Oxidation with hypochlorite resulted in the expulsion of the aminoquinone moiety to reveal a fluorescein derivative with an extended π -system $(\lambda_{\rm em}$ = 676 nm). **SNAPF** was then used to detect hypochlorite produced by human neutrophils stimulated with PMA (Fig. 83). When a MPO inhibitor was co-administered in stimulated cells no fluorescence was observed, indicating that MPO produced hypochlorite was being detected. SNAPF was also used to detect hypochlorite in stimulated mouse macrophages transgenic for human MPO (h-MPOTg) and stimulated human MPO-containing macrophages. Using SNAPF the successful bioimaging of hypochlorite generated in vivo was also performed in h-MOPTg mice with thioglycollate induced peritonitis. The SNAPF probe was administered 24 hours after thioglycollate stimulation, and after a further hour a 1.4-fold increase in fluorescence was observed.

$$\begin{array}{c} CIO^{\bigcirc} \\ CO_{2} \\ CO_{$$

Fig. 82 Structures of "switch on" probes for ClO- that function by oxidative cleavage.

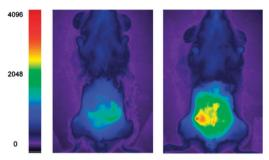


Fig. 83 In vivo demonstration of SNAPF: (left) h-MPOtg mouse with thioglycollate induced peritonitis pre-SNAPF injection; (right) the same animal post-injection of SNAPF. No visible fluorescence was observed when **SNAPF** was injected into mice that had been injected with saline solution as opposed to thioglycollate, nor was there any increase in fluorescence of a wavelength-matched control dye, SNAPF, when injected into mice with peritonitis compared to saline-injected animals (n = 4 per group). Image reproduced with permission. 306

In conjunction with a rhodamine fluorophore the *p*-aminophenyl ether trigger (MitoAR, Fig. 82) was also exploited by Nagano (2007).³⁰⁷ It was envisaged that the inherent positive charge of the ring open rhodamine would lead to accumulation of the probe within the mitochondria of living cells. In this instance the phenyl ether was located in the 2-position of the phenyl substituent in an effort to facilitate PET to the xanthene. Hypochlorite mediated oxidation of the p-aminophenyl ether correlated with a large increase in fluorescence response (λ_{em} = 574 nm) but only moderate selectivity over HO• was noted. Nevertheless, MitoAR was used to monitor the MPO-catalysed production of mitochondrial ROS in HL-60 cells using H₂O₂ stimulation (Fig. 84).

Yuan et al. successfully employed the 4-amino-3-nitrophenyl moiety as a hypochlorite responsive PET trigger to modulate the luminescence of terpyridine polyacid lanthanide complexes, ANMTTA-Tb(III) and ANMTTA-Eu(III) (Fig. 85).308 Oxidation of the 4-amino-3-nitrophenyl substituent gave the benzofurazan-1-oxide (BFO), which reacted with a further equivalent of ClO to restore the luminescent terbium and europium complexes HTTA-Tb(III) and HTTA-Eu(III). Probe ANMTTA-Eu(III) was used for the time-gated spatiotemporal luminescence visualisation

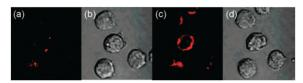


Fig. 84 Detection of endogenous ClO⁻ generation in mitochondria using MitoAr: (a, b) fluorescence and bright-field images of HL-60 cells loaded with MitoAR (c, d) 10 min after addition of H2O2. Image reproduced with permission. 307

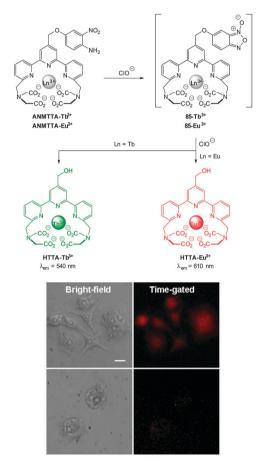


Fig. 85 Top: structures of ANMTTA-Tb(III), ANMTTA-Eu(III) and their reaction with ClO-. Bottom: time-gated luminescence images of the ANMTTA-Eu(III) loaded RAW264.7 macrophage cells after stimulation with LPS/IFN-γ/PMA (top) or stimulated with LPS/IFN-γ/PMA/4-aminobenzoic acid hydrazide (ABAH). Scale bar: 10 µm. Image reproduced with permission.308

of exogenous hypochlorite in HeLa and in LPS/IFN-γ/PMAstimulated RAW264.7 macrophages. Addition of the MPO inhibitor, ABAH, to cells resulted in no fluorescence emission.

An elegantly designed system HKOCl-1 (Fig. 86), related to the aforementioned probes, was reported by Yang in 2008.³⁰⁹ This example used a BODIPY fluorophore which was suitably quenched ($\Phi_{\rm F}$ < 0.01) by a p-methoxyphenol substituent by means of PET. Oxidative demethylation of HKOCl-1 to the quinone (HKOCl) was effected by hypochlorite; the greater oxidation potential of the quinone makes PET unfavourable and fluorescence is "switched on" (λ_{em} = 541 nm). This process

Fig. 86 Structure and reaction of **HKOCl-1** with ClO⁻.

was selective for hypochlorite, with ONOO eliciting a response only at a 10-fold higher concentration. The probe was used for the visualisation of live MPO producing RAW264.7 murine macrophages stimulated using lipopolysaccharide (LPS), interferon-γ (IFN-γ) and PMA. Stimulated cells showed an increase in the fluorescent output compared to the control. Additionally, when cells were stimulated in the presence of 2,2,6,6-tetramethylpiperidinooxy (TEMPO), much weaker fluorescent was observed. TEMPO is a known superoxide (O2 •) scavenger which is an intermediate in hypochlorite synthesis from the MPO system.

In 2012 Yao reported the dihydrofluorescein based probe FCN2 (Fig. 87) which, unlike preceding examples, is triggered by oxidation dealkylation rather than spirocycle ring opening.310 Ether cleavage from FCN2 restores the ICT of the dihydrofluorescein system (86) and results in a 1643-fold increase in fluorescent intensity ($\lambda_{\rm em}$ = 485 nm, $\Phi_{\rm F}$ = 0.71). FCN2 was completely soluble in aqueous solution and, although some autooxidation was noted (over 24 h), reacted rapidly enough (30 min) to be applicable for in vitro (NIH3T3 cells) and in vivo applications (larval and adult zebrafish). The fluorescent response generated from the treatment of 3 month old zebrafish with exogenous hypochlorite and FCN2, indicated the accumulation of hypochlorite in gall bladder, intestine, eye, liver and eggs.

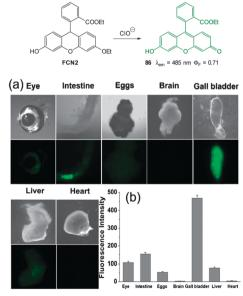


Fig. 87 Adult zebrafish were (a) exposed to ClO- in E3 embryo media then incubated with FCN2. (b) The average emission intensities of isolated organs. Image reproduced with permission. 310

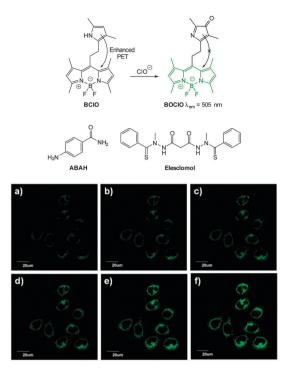


Fig. 88 Top: structure and reaction of BCIO with hypochlorite. Middle: structures of ABAH and elesclomol. Bottom: live MCF-7 cells were cultured with BCIO then confocal fluorescence images were recorded after the addition of elesclomol at different time points: (a) 0, (b) 30, (c) 60, (d) 90, (e) 120, and (f) 180 min. Image reproduced with permission.³¹¹

Peng and co-workers reported the oxidation-activated "enhanced PET" BODIPY-based probe BClO (Fig. 88) which was synthesised in an exquisite two step procedure from 2,4-dimethylpyrrole.311 The PET quenching was mediated by a pendant pyrrole unit which was envisaged to provide "enhanced PET" compared to single electron donors (such as heavy metal containing probes). The resultant probe, BClO was essentially non-fluorescent at $\lambda_{\rm em}$ = 505 nm ($\Phi_{\rm F}$ = 0.006), however, oxidation with hypochlorite afforded the pyrrol-3one BOClO in which PET was restricted and a 56-fold "switch on" fluorescence response was observed ($\Phi_{\rm F}$ = 0.347). In solution studies BClO was highly sensitive to hypochlorite with a limit of detection of 0.56 nM. Facilitated by the remarkable sensitivity of BClO the authors determined the basal hypochlorite levels in MCF-7 and HeLa cancer cell lines. When incubated with BClO (1 μ M) for 20 min at 37 °C, both MCF-7 and HeLa displayed an increased fluorescence response (in relation to healthy COS-7 and RAW264.7 cells) corresponding to intracellular ClO⁻ concentrations of 9.45 nM and 8.23 nM respectively. In both of the cancer cell lines visualised, pre-treatment with the antioxidant GSH or 4-aminobenzoic acid hydrazide (ABAH, an MPO inhibitor) resulted in a significant drop in fluorescence response. The authors suggest that it may be possible to use BCIO in a diagnostic capacity; differentiating healthy and cancer cells based on endogenous hypochlorite concentration. The utility of BCIO was further demonstrated by the detection of hypochlorite produced in MCF-7 cells stimulated with elesclomol (an ROS generating anticancer agent).

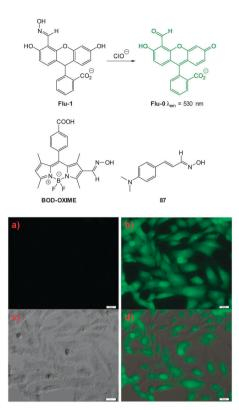


Fig. 89 Top: structure, and reaction of, Flu-1 with ClO-. Middle: structures of BODOXIME and 87. Bottom: (a) image of HeLa cells incubated with Flu-1 (20 μM) for 30 min. (b and c) Fluorescence and bright-field images of cells pre-treated with Flu-1 then incubated with ClO⁻ for 30 min. (d) Overlay image of (b) and (c). Image reproduced with permission. 313

4.2.2 Hypochlorite mediated oxime/imine oxidation. An early example of a probe that used the oxime oxidation approach (Flu-1, Fig. 89) was published by the Li group in 2011. The emissive species ($\lambda_{\rm em}$ = 530 nm, $\Phi_{\rm F}$ = 0.65) was an aldehyde containing fluorescein derivative (Flu-0) and when the aldehyde was protected as the oxime (Flu-1), fluorescence was effectively quenched ($\Phi_{\rm F}$ = 0.01). Probe Flu-1 displayed good selectivity against a suite of anionic species, however screening against ROS such as ONOO $^-$, HO $^\bullet$, O $_2^{\bullet-}$ etc. was not performed. Importantly, Flu-1 failed to illicit a fluorescent response with H₂O₂ and bioimaging of exogenous hypochlorite was successfully demonstrated using HeLa cells incubated with Flu-1.

Wu, Zeng and Wu (2013) employed the same oxime/aldehyde strategy using a BODIPY fluorophore.313 The water soluble **BOD-OXIME** (Fig. 89) was poorly fluorescent ($\Phi_{\rm F} = 0.04$) but reacted in a dose dependant "switch on" manner (LOD = 17.7 nm) with hypochlorite to give BOD-CHO which exhibited extraordinary fluorescence in aqueous solutions ($\Phi_{\rm F}$ = 0.96, $\lambda_{\rm em}$ = 525 nm). The visualisation of both exogenous (ClO⁻) and endogenous hypochlorite (PMA stimulation) in RAW264.7 macrophages was successfully demonstrated. Selectivity for ClOin vitro was excellent as no emission was observed when ABAH or taurine (a ClO⁻ scavenger) were added to the PMA stimulated cells.

A recent report from the Kumar group in 2014 identified 4-dimethylaminocinnimaldehyde oxime 87 ($\Phi_F = 0.008$, Fig. 89) **Review Article** Chem Soc Rev

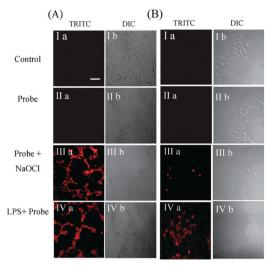


Fig. 90 Fluorescence and DIC images of C6 glial (A) and BV2 microglial (B) cell lines. (Ia) Control of C6 glial and BV2 microglial cell lines respectively. (Ib) DIC images of Ia. (IIa) Images of C6 glial and BV2 microglial cells with 87. (IIb) DIC images of IIa. (IIIa) Red fluorescence images of C6 glial and BV2 microglial cells with 87 and NaOCl. (IIIb) DIC images of IIIa. (IVa) Red fluorescence images of C6 glial and BV2 microglial cells with 87 and LPS. (IVb) DIC images of IVa. Scale = 50 nm. Image reproduced with permission.314

as a selective "switch on" probe for hypochlorite. 314 Oxidation with hypochlorite gave the nitrile oxide and this group participates in an extended ICT system leading to strong emission at 556 nm ($\Phi_{\rm F}$ = 0.51). The formation of the nitrile oxide was confirmed by spectroscopic means (¹H and ¹³C NMR) and by in situ trapping using 2-butene to give the 4,5-dihydroisoxazole. The ability of probe 87 to visualise endogenous and exogenous hypochlorite was demonstrated using the brain resident murine macrophages (BV2 microglial) and C6 glial cell lines (Fig. 90). Addition of exogenous NaOCl and also LPS stimulated endogenous hypochlorite production led to increased fluorescence.

The first ratiometric fluorometric probe for hypochlorite was developed by Yuan using an analogous approach to those above. 315 The probe consists of a diaminomaleonitrile derived imine 88 of aminocoumarin aldehyde 89 (Fig. 91) The weakly fluorescent imine ($\lambda_{\rm em}$ = 585 nm, $\Phi_{\rm F}$ = 0.02) reacted with hypochlorite to give the parent aldehyde and a bathochromic shift to an emission maximum centred at $\lambda_{\rm em}$ = 505 nm ($\Phi_{\rm F}$ = 0.59) was observed. At physiological pH a marked increase in emission ratio (F_{505}/F_{585}) from 0.12 to 28.2 was observed after the probe was treated with hypochlorite. Probe 88 was successfully used to visualise exogenous hypochlorite in MCF-7 cells.

4.2.3 Hypochlorite mediated ring opening. A number of rhodamine based systems which react specifically with hypochlorite have been reported in recent years. Work in this area was pioneered by Nagano in 2007 with the rhodamine thioether spirocycle HySOx.316 The thioether was critical for the stability of the closed form of the HySOx probe, particularly at higher pH. Hypochlorite oxidation of the thioether triggers ring opening and fluorescence "switch on" (λ_{em} = 575 nm, $\Phi_{\rm F}$ = 0.34). Utilising this sensitivity to hypochlorite

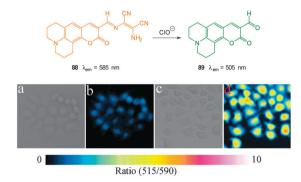


Fig. 91 Top: structure and reaction of aminocoumarinimine 88 with ClO⁻ (a) bright-field image of live MCF-7 cells incubated with only probe 88 (b) fluorescence ratio image (F_{505}/F_{585}) of (a); (c) bright-field image of live MCF-7 cells incubated with probe 88 then with ClO-; (d) fluorescence ratio image (F_{505}/F_{585}) of (c). Image reproduced with permission.³¹⁵

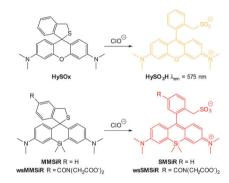


Fig. 92 Structure and spirocycle ring opening reactions of HySOx and MMSiR with hypochlorite.

the authors were able to image phagocytosis in porcine neutrophils.

In an extension of this work, Nagano (2011) reported the silylrhodamine analogue MMSiR (Fig. 92).317 The isosteric replacement of oxygen with silicon resulted in a significant red-shift in the emission wavelength to the near-infrared (NIR) region ($\lambda_{\rm em}$ = 670 nm, $\phi_{\rm F}$ = 0.31). Similar to HySOx, the MMSiR probe was also used in the imaging of phagocytosis. In addition the hydrophilic probe wsMMSiR was synthesised and applied to the in vivo imagining of hypochlorite in a mouse peritonitis model (Fig. 93). In this study C57BL/6 mice were treated with an intraperitoneal injection of zymosan to stimulate neutrophil invasion of the peritoneal cavity. Injection of wsMMSiR and PMA resulted in enhanced fluorescence emission in the abdomen.

Using a more traditional rhodamine fluorophore, Yoon (2007) developed both a thio- and selenoester trigger for selective ClO sensing.318 Upon reaction with hypochlorite, the non-fluorescent R19-S, R19-Se and R101-S undergo ring opening and fluorescence is "switched on" at λ_{em} = 550 nm, 545 nm and 585 nm respectively (Fig. 94). Probe R19-S was used to visualise hypochlorite production in phagocytes and microbial hypochlorite generation in intestinal epithelia of Drosophila melanogaster.

Chem Soc Rev **Review Article**

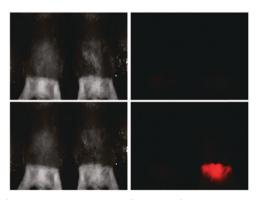


Fig. 93 Comparison of white light (left panels) and fluorescence (right panels) images of unstimulated mouse (left) and the peritonitis model mouse stimulated with zymosan and PMA (right). wsMMSiR and PMA were successively administered by intraperitoneal injection. Images were obtained just before (top) and 60 min after (bottom) PMA injection. Image reproduced with permission.317

Fig. 94 Structure of the rhodamine probes developed by Yoon containing S and Se triggers.

In the last few years a number of diacylhydrazine-rhodamine probes have been reported. These probes rely on selective oxidation by hypochlorite to give a diacyl diimide, then subsequent hydrolysis reveals the fluorescent rhodamine. An early example of this approach was reported by Ma and co-workers although high pH was required (pH 12).319 Modifications to the benzoyl substituent can be used to tailor probes which are more suited for imaging purposes. For example, by using a pendant alkoxyquinoline moiety (RHQ, Fig. 95) Goswami and co-workers were able to image endogenous hypochlorite in human peripheral blood mononuclear cells (PBMCs). 320 A similar fluorescein based system (90 R=O and 91 R=S, Fig. 95) from the Li group was used to monitor hypochlorite in Rhodobacter ferrooxidans prokaryotes as a potential model for hypochlorite induced stress.³²¹

In the last few years a number of diacylhydrazine-rhodamine probes have been reported. These probes rely on selective oxidation by hypochlorite to give a diacyl diimide, then subsequent hydrolysis reveals the fluorescent rhodamine. An early example of this approach was reported by Ma and co-workers although high pH was required (pH 12).319 Modifications to the benzoyl substituent can be used to tailor probes which are more suited for imaging purposes. For example, by using a pendant alkoxyquinoline moiety (RHQ, Fig. 95) Goswami and co-workers were able to image endogenous hypochlorite in human peripheral blood mononuclear cells (PBMCs).³²⁰ A similar fluorescein based system (90 R=O and 91 R=S, Fig. 95) from the Li group was used to monitor hypochlorite in Rhodobacter ferrooxidans prokaryotes as a potential model for hypochlorite induced stress.321

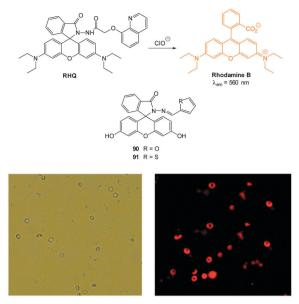


Fig. 95 Top: structure of RHQ probe and related probes 90 and 91. Bottom: (left) bright field image of PBMCs (40×), (right) fluorescence image of PBMCs (40x) treated with RHQ. Image reproduced with permission.320

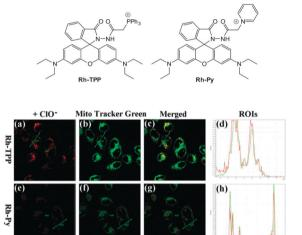


Fig. 96 Top: structure of mitochondria targeting probes Rh-TPP and Rh-Pv Bottom: HeLa cells were stained with Rh-TPP or Rh-Pv, incubated with ClO-, then Mito Tracker Green was added. (a) and (e): Fluorescence images of Rh-TPP and Rh-Py with ClO⁻; (b) and (f): the fluorescence images of Mito Tracker Green; (c) and (g): merged images; (d) and (h): intensity profile of ROIs across HeLa cells. Red lines represent the intensity of synthetic probes and green lines represent the intensity of Mito Tracker Green. Scale = 25 μm. Image reproduced with permission.⁹⁹

In 2014 Hou et al. employed this trigger in the mitochondria targeting probes Rh-TPP and Rh-Py (Fig. 96).99 The incorporation of a phosphonium (Rh-TPP) or pyridinium ion (Rh-Py) onto the probe facilitated the imaging of exogenous hypochlorite in the mitochondria of HeLa cells.

The ability of Rh-TPP and Rh-Py to visualise hypochlorite in vivo was also demonstrated (Fig. 97). Nude mice were injected with either probe followed by an injection with a ClO-

Review Article Chem Soc Rev

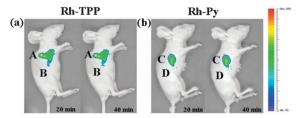


Fig. 97 Representative fluorescence images (pseudocolor) of nude mice given a skin-pop injection of (a) Rh-TPP and (b) Rh-Py (region A and C, respectively) and a subsequent skin-pop injection of ClO-. Representative fluorescence images (pseudocolor) of nude mice given a skin-pop injection of (a) Rh-TPP and (b) Rh-Py region B and D, respectively). Images were taken after incubation for 20 and 40 min, respectively. Image reproduced with permission.99

solution. In each case a persistent fluorescent response was elicited from hypochlorite.

A hydroxamic acid variant of this approach was outlined by Shin and Tae in 2013.322 In this case it was proposed that the hydroxamic acid was oxidised to the corresponding ring opened acyl nitroso group and it was anticipated that this product was rapidly hydrolysed to **rhodamine 19** (λ_{em} = 547 nm). Probe **92** (Fig. 98) could detect hypochlorite concentration at ca. 25 nM. Of interest, when the exocyclic amines had an additional ethyl substituent, or were replaced by hydroxyl groups (fluorescein) the probes did not respond to hypochlorite, even when a 20-fold excess was administered.

Probe 92 could be used to detect exogenous hypochlorite in A549 lung cancer cells with a clear dose responsive fluorescence "switch on" with increasing ClO concentration (Fig. 99). Furthermore 92 was successfully used for the in vivo detection of exogenous hypochlorite added to live zebrafish.

4.2.4 Hypochlorite mediated chalcogen oxidation. In 2013 Wu and Liu described the PET based BODIPY probe HCSe (Fig. 100) for hypochlorous acid. 323 In this instance the BODIPY fluorophore was functionalised with a 2-(phenylselenyl)phenyl substituent and the presence of the selenide quenches fluorescence by PET ($\Phi_{\rm F}$ = 0.005). When oxidised by hypochlorite, the corresponding selenoxide (HCSeO) is formed and PET is unfavoured and BODIPY fluorescence is restored (λ_{em} = 526 nm, $\Phi_{\rm F}$ = 0.690). Using RAW264.7 cells the utility of this probe in vitro was explored; cells were pre-treated with HCSe

92 Rhodamine 19
$$\lambda_{em}$$
 = 547 nm

Fig. 98 Structure and reaction of 92 with hypochlorite. Inset shows proposed acylnitroso intermediate 93

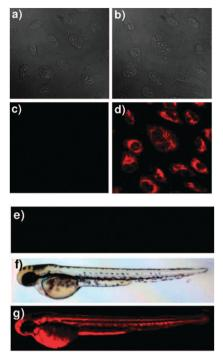


Fig. 99 Bright field image of A549 cells treated with (a) 92 in the absence of ClO-. (b) With both ClO- and 92. Fluorescence image of A549 cells treated with (c) 92 in the absence of ClO-. (d) Both ClO- and 83. Fluorescence images of zebrafish treated with (e) 92 in the absence of CIO-. (f) Bright field image of zebrafish treated with 92 and CIO- (g) fluorescence images of zebrafish treated both 92 and ClO-. Image reproduced with permission.322

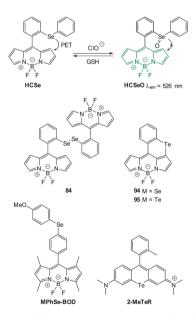


Fig. 100 Structures of Se and Te containing probes for ClO⁻.

and upon addition of ClO enhanced fluorescence emission was detected. Subsequent treatment of these cells with glutathione (GSH) resulted in the loss of fluorescence intensity, indicating that the selenoxide (HCSeO) could be reduced back to its non-emissive precursor. Similarly, the endogenous Chem Soc Rev

production of hypochlorite could be visualised in RAW264.7 cells that were stimulated using PMA.

Structurally similar annulated BODIPY chalcogenides (discovered somewhat serendipitously during the synthesis of dichalcogenides such as 93) were reported by Churchill in 2013. 324 These unexpected annulated heterocycles were formed by base induced S_EAr reaction of the dipyrrole dichalcogenide (93) and their structure confirmed by means of an X-ray structure of the selenide derivative (94). It is of note that the diselenide 93 has been utilised as a reversible superoxide probe.325 Despite not being applied to a living system, the annulated tellurium BODIPY (95) was shown to be at least 62-fold selective for ClO⁻ over other ROS (O₂•⁻, H₂O₂, ^tBuOOH, ClO[−], HO[•], and ^tBuO[•]) under physiological conditions (0.1 M PBS/EtOH (99:1 v/v), pH 7.5). Following oxidation with hypochlorite, PET from the tellurium was blocked and fluorescence was "switched on" ($\lambda_{\rm em}$ = 597 nm, $\Phi_{\rm F}$ increased from 0.06 to 0.23). Similar to HCSe, telluride oxidation could be reversed by treatment with GSH.

MPhSe-BOD is weakly fluorescent ($\Phi_F = 0.13$, $\lambda_{em} = 510$ nm) due to a Se modulated PET process.326 Hypochlorite oxidation interrupts the PET process and restores strong fluorescence (MPhSeO-BOD, $\Phi_{\rm F}$ = 0.96). The reverse process (reduction) is selectively performed by HS-. The probe was used to visualise endogenously produced hypochlorite in PMA stimulated RAW264.7 macrophages. The role of hypochlorite was confirmed by comparison to taurine and xanthine-xanthine oxidase controls. Imaging of the redox cycling between hypochlorite and HS⁻ was also demonstrated in RAW264.7 cells.

The tellurium containing rhodamine system (2-MeTeR, $\Phi_{\rm F} < 0.001$) presented by Nagano in 2012 has the advantage that its oxidised form (2-MeTeOR) is red emissive (λ_{em} = 686 nm, $\Phi_{\rm F}$ = 0.18). However, this probe suffers from interference from other ROS such as HO• and ONOO-. Nevertheless the probe was used to visualise endogenously produced ROS in human promyelocytic leukemia (HL-60) cells following stimulation with H2O2. As the added H2O2 was consumed by MPO and/or the reaction was reversed by intracellular reductants, the increased fluorescent intensity was short lived. Fluorescence was restored following a second addition of H₂O₂ (Fig. 101). Fluorescence intensity was also reduced when the cells were treated with aminobenzoic acid hydrazide (ABAH).

In 2013 the Han group reported the 4-aminonaphthalimidebased hypochlorite sensor NI-Se, shown in Fig. 102.³²⁸ While related to the aforementioned examples, the selenide was nonfluorescent ($\Phi_{\rm F}$ = 0.04) and oxidation gave the fluorescent selenoxide NI-SeO ($\lambda_{\rm em}$ = 523 nm, $\Phi_{\rm F}$ = 0.45). Unlike the previously described selenide-selenoxide systems fluorescence was not modulated by a PET mechanism. Instead, the 2-(phenylselenyl)benzyl moiety induced an excited state configurational twist which was not present in the oxidised NI-SeO. The reduction of the selenoxide could be reversed by the addition of HS⁻ to the system; this process was repeated up to six times with a decrease in fluorescence intensity of 50%. Cellular imagining of NI-Se was performed using mouse macrophage RAW264.7 cells stimulated with LPS and PMA and enhanced

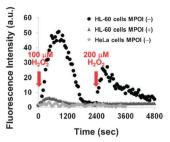


Fig. 101 Time courses of the change in fluorescence intensity observed with **2-MeTeR** for H_2O_2 -stimulated or unstimulated HL-60 cells or H_2O_2 stimulated HeLa cells. H_2O_2 (100 μ M and 200 μ M final concentration) was added at 100 s and 2400 s, respectively. The myeloperoxidase inhibitor (MPOI) is aminobenzoic acid hydrazide (ABAH; 2 mM). The fluorescence intensity was measured at 690 nm with excitation at 660 nm. Image reproduced with permission.327

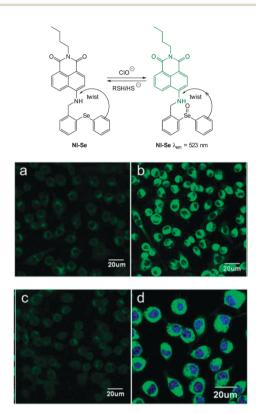


Fig. 102 Top: structure and reaction of NI-Se with hypochlorite. Bottom: fluorescence images of ClO in living RAW264.7 cells. (a-c) Cells were pretreated with LPS. (a) Incubated with NI-Se. (b) Incubated with NI-Se and then with PMA. (c) Incubated with SHA and co-incubated with PMA, then incubated with NI-Se. (d) RAW264.7 cells loaded with Hoechst 33342 and NI-Se. Image reproduced with permission. 328

fluorescence was observed. Weak fluorescence was also observed when cells were pre-treated with salicylhydroxamic acid (SHA), a known inhibitor of MPO. A similar result was obtained with the use of a ROS scavenger glutathione S-transferase (GST, EC: 2.5.1.18). Co-staining with Hoechst 33342 revealed that probe was located mainly in the cytosol.

NI-Se was also used in living mice for the in vivo imaging of hypochlorite produced in a LPS model of acute inflammation (Fig. 103). Similar to the in vitro study, when LPS was injected,

Review Article Chem Soc Rev

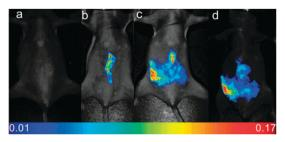


Fig. 103 Fluorescent images of CIO⁻ production and HS⁻ reduction in the peritoneal cavity of the mice with NI-Se. (a) Control, neither LPS nor NI-Se was injected; (b) saline was injected in the intraperitoneal (i.p.) cavity of mice, followed by i.p. injection of NI-Se; (c) LPS was injected into the peritoneal cavity of the mice, followed by i.p. injection of NI-Se. (d) An additional HS- was injected in parallel to (c). Image reproduced with permission. 328

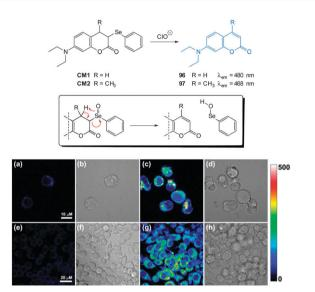


Fig. 104 Top: structure of CM1 and CM2 and the mechanism of their reaction with ClO-. Bottom: (a) fluorescence images of HL-60 cells with **CM1** (b) bright-field images of cells in panel (a). (c) After addition of H_2O_2 (d) bright-field images of cells in panel (c). (e) Fluorescence images of RAW264.7 cells with CM1 (f) bright-field images of cells in panel (e). (g) Cells loaded with CM1 then LPS (h) bright-field images of cells in panel (g). Image reproduced with permission. 329

followed by NI-Se, an enhanced signal was collected compared to the control (NI-Se only). Injection of HS resulted in a decrease in fluorescence emission.

A new strategy for the detection of hypochlorite involving a selenide containing probe was presented by Li et al. in 2013.³²⁹ The partially reduced coumarin derivatives CM1 and CM2, (Fig. 104) each bearing a 3-phenylselenyl moiety were synthesised and both were non-fluorescent ($\Phi_{\rm F} < 0.001$). In this instance the selenoxide produced from hypochlorite oxidation underwent a cope-type elimination to give the corresponding fluorescent reporters 96 ($\lambda_{\rm em}$ = 480 nm, $\Phi_{\rm F}$ = 0.036) and 97 ($\lambda_{\rm em}$ = 468 nm, $\Phi_{\rm F}$ = 0.047). The utility of probe **CM1** was demonstrated in vitro, by the quantitative determination of exogenous hypochlorite in NIH3T3 cells. CM1 was also used to indicate the endogenous formation of hypochlorite in H₂O₂ stimulated HL-60 human progranulocytic leukemia cell lines and RAW264.7 macrophages stimulated with lipopolysaccharide (LPS). In both of these instances there was a significant enhancement of the fluorescent response in relation to the controls.

A PET-based Ru(bpy)₃²⁺ based probe for the monitoring of ClO⁻/HS⁻ redox cycle was developed by the Sun group in 2014 (Fig. 105).³³⁰ A pendent phenothiazine (PTZ) was attached to one of the 2.2'-bipyridine ligands, which suppressed fluorescence emission from the complex. Upon oxidation of the PTZ sulfur with ClO the fluorescence emission was restored $(\lambda_{\rm em} = 605 \text{ nm}, \lambda_{\rm ex} = 450 \text{ nm}, \Phi_{\rm F} = 0.39)$. This process could be reversed with HS⁻ in a recyclable fashion (12 cycles). The authors were able to visualise this ClO⁻/HS⁻ redox cycle in live mice; weak fluorescence was observed after administration of probe 98 and this response was modulated during alternating additions of ClO and HS.

The groups of Wang and Peng reported a cyaninephenothiazine hybrid probe, PTZ-Cy2 which was sensitive to both hypochlorite and HO[•].331 The sulphur atom of the nonfluorescent probe was initially oxidised by OCl- and/or HO• to give the fluorescent sulfoxide OPTZ-Cy2 which gave a pink emission (λ_{em} = 595 nm). Continued addition of OCl⁻ to **OPTZ-Cy2** led to a blue shifted emission ($\lambda_{em} = 470 \text{ nm}$) resulting from the degradation of the conjugated cyanine alkene to the aldehyde OPTA. This blue shifted emission was not seen during HO[•] addition, rather, excessive HO[•] lead to a decrease in the total emission indicating decomposition. PTZ-Cv2 was used to visualise the ROS in PMA stimulated HeLa cells (Fig. 106). Co-staining with MitoTracker Deep Red FM indicates that fluorescence resulting from PTZ-Cy2 and OPTZ-Cy2 was localised in the mitochondria. Non-mitochondrial fluorescence was ascribed to the non-charged OPTA diffusing away from the mitochondria.

4.2.5 Miscellaneous. Lin and co-workers developed a series of rhodamine-merocyanine hybrid probes which absorb and

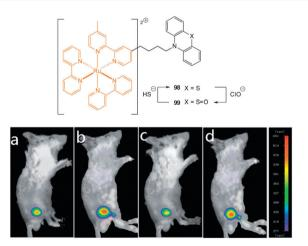


Fig. 105 The luminescence imaging of the redox cycle between ClOand HS⁻ in live mice: (a) 98 was loaded into the leg cortex of the mice; (b) ClO⁻ was loaded in the same position; (c) HS⁻ was loaded in the same position; and (d) another ClO was loaded in the same position. Image reproduced with permission. 330

Chem Soc Rev **Review Article**

Fig. 106 Top: structure and reaction of PTZ-Cy2 with ClO-. Bottom: HeLa cells pre-treated with PMA then PTZ-Cy2 plus MitoTracker Deep Red FM. (a) Emission of PTZ-Cy2 at 470 nm; (b) emission of PTZ-Cy2 at 590 nm; (c) merged image of (a) and (b) with bright-field image; (d) pseudocolour ratiometric images (F_{470}/F_{590}); (e) fluorescence image of MitoTracker Deep Red FM (λ_{em} = 690 nm); (f) overlay of (a) and (e). Image reproduced with permission. 331

emit in the NIR range. 332 The non-fluorescent spirocyclic benzoyl thiosemicarbazide 100 (Fig. 107), in the presence of hypochlorite undergoes oxidative cyclisation to give the 2-amino-1,3,4oxadiazole (101) which simultaneously opens the spirocycle and restores ICT ($\lambda_{\rm ex}$ = 690 nm, $\lambda_{\rm em}$ = 746 nm). Imaging of hypochlorite in LPS and PMA stimulated RAW264.7 macrophages established the viability of probe 100 in vitro and also revealed mitochondrial localisation. Probe 100 was applicable as a hypochlorite responsive probe in imprinting control region (ICR) mice treated with LPS; higher fluorescent emission was recorded when compared with the control or 100 alone.

Ma (2010) described the PET system 9-AEF consisting of an anthracene linked by an alkene to ferrocene (Fig. 108).333 The electron rich ferrocene instigates PET to the anthracene and fluorescence is quenched ($\Phi_{\rm F} < 0.001$). Hypochlorite could oxidise the alkene, and in the product (not characterised) PET is unfavoured and anthracene-like emission was observed ($\lambda_{\rm em}$ = 441 nm, $\Phi_{\rm F}$ = 0.12). It should be noted that no single product was identified, nevertheless, the response to hypochlorite was dose dependant and the probe was successfully used to image hypochlorite in HeLa cells. No fluorescence was observed in cells containing 9-AEF unless they were pre- or post-treated with hypochlorite.

4.3 Hypobromite

In an analogous manner to hypochlorite, hypobromous acid/ hypobromite can be produced endogenously by macrophages

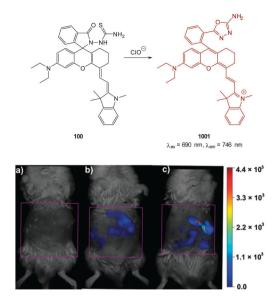


Fig. 107 Representative fluorescent images (pseudocolour) of in vivo CIO production from the peritoneal cavity of the mice with 100 during an LPS-mediated inflammatory response: (a) negative control, neither LPS nor 100 was injected; (b) saline was injected in the intraperitoneal (i.p.) cavity of mice, followed by i.p. injection of 100; (c) LPS was injected into the peritoneal cavity of the mice, followed by i.p. injection of 100. Image reproduced with permission.332



Fig. 108 Structure of hypochlorite sensitive probe 9-AEF as described by Ma.³³³

and eosinophils from the reaction between H₂O₂ and bromide which is catalysed by eosinophil peroxidase (EPO) in response to invading pathogens. Overproduction of HOBr can lead to diseases such as cancer, arthritis, cardiovascular disease and asthma. There is a demonstrated correlation between clinical severity in asthma patients and serum EPO levels. While the fraction of HOBr/BrO $^-$ is likely to be high (the p K_a for HOBr is 8.7-8.8 at 25 °C) a small percentage of the anionic species is likely to exist at physiological pH and in certain compartments such as mitochondria a considerable percentage of BrO is likely. The design of fluorescent probes for *in vitro* of detection of this species has recently received attention.

4.3.1 Recent developments. In 2012, the Han group reported two reversible fluorescent probes for the in vitro imagining of redox stress caused by HOBr. 334 Both probes, mCyTem-OH and CyTem-OH (Fig. 109), respond through the HOBr mediated oxidation of a 2,2,6,6-tetramethylpiperidine-Noxyl moiety to the corresponding oxyammonium cation which leads to a donor-excited PET (d-PET) quenching mechanism ($\Phi_{\rm F}$ decrease from 0.11 to 0.02 for mCy-TemOH). Oxidation of **mCyTemOH** (λ_{em} = 550 nm) results in a red-shifted emission centred at 632 nm. In vitro investigations used mCy-TeOH to monitor changes in endogenous HOBr concentration in

Review Article Chem Soc Rev

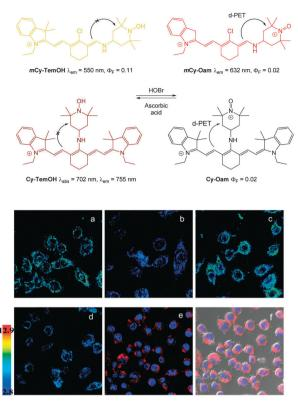


Fig. 109 Top: structure of **mCy-TemOH** and **Cy-TemOH** and their reaction with BrO $^-$. Bottom: ratiometric fluorescence images (F_{632}/F_{550}) of living RAW264.7 cells with **mCy-TemOH** (a)–(d). pseudo color images represent the ratio of emission intensities. (a) Control. (b) **mCy-TemOH**-loaded cells incubated with H₂O₂, EPO and KBr. (c) **mCy-TemOH** loaded, EPO, and H₂O₂ treated cells incubated with glutathione S-transferase, then ascorbic acid. (d) Cells exposed to a second dose of EPO, KBr and H₂O₂. (e) and (f) Confocal microscopy imaging for subcellular locations of **mCy-TemOH** in living RAW264.7 cells. (e) Cells incubated with **mCy-TemOH** (red) and co-staining with Hoechst dye (blue). (f) Overlay of (e) and its bright-field image. Image reproduced with permission. 334

RAW264.7 macrophages; treatment with EPO, $\rm H_2O_2$ and KBr resulted in an increased in the F_{632}/F_{550} ratio from 2.8 to 12.9. Addition of ascorbic acid to the system resulted in reduction of the oxyammonium cation and a decrease in the F_{632}/F_{550} ratio.

The full cyanine probe, **Cy-TemOH**, exhibited NIR absorption (λ_{abs} = 702 nm) and emission (λ_{em} = 755 nm). **Cy-TemOH** also responded to the HOBr/ascorbic acid redox cycle but suffered from severe bleaching after three cycles. Nevertheless, **Cy-TemOH** was successfully used to visualise the redox cycle in RAW264.7 cells. Both **Cy-TemOH** and **mCy-TemOH** localised in the cytoplasm and cells remained viable (MTT assay).

The same group then developed a NIR-reversible BODIPY-based probe which could monitor the redox cycle between HOBr and HS $^{-}$. The probe, **diMPhSe-BOD** (Fig. 110) absorbs strongly ($\epsilon_{672}=22\,770~{\rm M}^{-1}~{\rm cm}^{-1}$) but was weakly fluorescent ($\lambda_{\rm em}=711~{\rm nm},\,\Phi_{\rm F}=0.00083$) due to the electron transfer (PET) from the diarylselenides. Oxidation with HOBr leads to a blue-shifted emission ($\lambda_{\rm em}=635~{\rm nm}$) and 118-fold increase in the F_{635}/F_{711} ratio. The reverse reaction is accomplished by HS $^-$ (selectively over other RSS such as Cys, Hcys and GSH). It is also

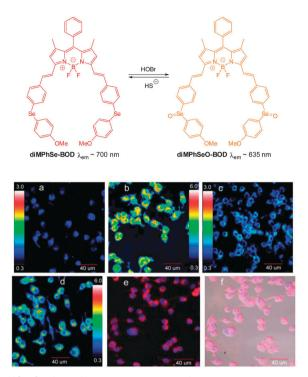


Fig. 110 Confocal fluorescence images of the redox cycles between HOBr and H_2S in RAW264.7 cells. Macrophage cells. (a) Control; (b) **diMPhSe-BOD**-loaded cells with H_2O_2 , EPO, and KBr; (c) cells in (b) after addition of HS^- ; (d) (c) was treated with a second dose of H_2O_2 , EPO and KBr; (e) overlay of images showing fluorescence from **diMPhSe-BOD** and Hoechst dye; (f) overlay of bright-field, **diMPhSe-BOD**, and Hoechst dye images. Image reproduced with permission. 335

notable that the emission ratio generated from the reaction with HOBr was *ca.* 6-fold greater than with ClO⁻. The HOBr/HS⁻ redox cycle could be visualised in RAW264.7 cells and using **diMPhSe-BOD** HOBr and H₂S could be detected at concentrations as low as 50 and 100 nM respectively.

5. Conclusion and future work

One of the key purposes of this review was to highlight that the strategies employed for the design of small fluorescent anion sensors can be applied to *in vitro* and *in vivo* bioimaging.

As such further developments in fluorophore design and strategies for signal modulation³³⁶ are likely to have immediate imaging applications. The emerging use of multiphoton excitation is already having an impact. Developments in the use of fluorescence lifetime³³⁷ will also broaden the range of approaches that can be used. Probes that are compatible with a superresolution approach would also be beneficial for the ultimate aim of pinpointing the origin and/or fate of the species of interest.

Despite some impressive examples, many of the probes described herein do not meet the highly demanding criteria set out for an "ideal probe" in Section 1.2. Complete selectivity for the analyte of interest is not always realised and probes that are not dependent on a chemical transformation are currently the most prone to interference. Indeed it is a truly formidable

Chem Soc Rev **Review Article**

challenge to design a selective, reversible, recognition process that operates by means of non-covalent forces in an exceptionally competitive media! Further refinement of fundamental recognition principles and the ability to readily synthesise (or assemble) sophisticated structures is required to overcome this hurdle. While the selectivity of chemodosimeters is often excellent the reactions are typically irreversible and hence they are incapable of mapping in a truly spatiotemporal manner.

Furthermore, despite the obvious potential that these probes offer, many are destined to be research tools only; the widespread use of fluorescent probes in clinical settings is hampered by expensive operational set-up and sample by sample analysis. Nevertheless, several of the probes included herein have been successfully used in flow systems 147,171,281 and with the current rapid progress in the field of micro-fluidics and micro-optics the goal of cost effective, "smartphone style", point of care diagnostics using selective fluorescent probes is sure to be realised. 338-342

It is also interesting to note that for many small anions (Cl-, I-, HCO₃⁻, and BrO⁻) the complete list of probes is very short and hence any progress would be welcome. Nevertheless, the field of anion sensing is rapidly advancing, and for the researchers involved in this field these challenges should be seen as nothing more than an excellent opportunity to further the fundamental understanding of our natural world.

Glossary of cell lines

	RAW264.7	Murine/mouse	macrophages
--	----------	--------------	-------------

PC3 Prostate cancer

Human umbilical vein endothelial cell HUVEC

NIH3T3 Murine/mouse fibroblast HeLa Epithelial cervical cancer

MCF-7 Breast cancer

HEK-293 Human embryonic kidney cells

L929 Murine/mouse fibroblast

A549 Adenocarcinomic human alveolar basal

epithelial cells

Fibroblast-like COS-7

B16-F10 Murine/mouse skin melanoma

U266 Human myeloma

HepG2 Hepatocellular carcinoma

PMN Human polymorphonuclear neutrophils BV2 microglial Brain resident murine macrophages MDA-MB-231 Human breast adenocarcinoma SH-SY5Y Human neuronal neuroblasts Human promyelocytic leukemia HL-60 Human breast cancer cells **GES**

Acknowledgements

The authors TDA, KJ and FP would like to thank the Australian Research Council (ARC DP140100227) and TDA and FP also thank the Strategic Research Centre for Chemistry and Biotechnology (Deakin University) for financial support.

References

- 1 Supramolecular Chemistry: From Molecules to Nanomaterials, ed. P. A. Gale and J. W. Steed, John Wiley and Sons, Chichester,
- 2 Recognition of Anions, ed. R. Vilar, Springer-Verlag, Berlin,
- 3 Anion Receptor Chemistry, ed. J. L. Sessler, P. A. Gale and W.-S. Cho, The Royal Society of Chemistry, Cambridge,
- 4 Encyclopedia of Supramolecular Chemistry, ed. J. L. Atwood and J. W. Steed, Marcel Dekker, New York, 2004.
- 5 Supramolecular Chemistry of Anions, ed. A. Bianchi, K. Bowman-James and E. García-España, Wiley-VCH, New York, 1997.
- 6 M. M. G. Antonisse and D. N. Reinhoudt, Chem. Commun., 1998, 443-448.
- 7 S. Kubik, C. Reyheller and S. Stuwe, J. Inclusion Phenom. Macrocyclic Chem., 2005, 52, 137-187.
- 8 E. A. Katayev, Y. A. Ustynyuk and J. L. Sessler, Coord. Chem. Rev., 2006, 250, 3004-3037.
- 9 F. P. Schmidtchen, Coord. Chem. Rev., 2006, 250, 2918–2928.
- 10 P. Blondeau, M. Segura, R. Perez-Fernandez and J. de Mendoza, Chem. Soc. Rev., 2007, 36, 198-210.
- 11 J. W. Steed, Chem. Soc. Rev., 2009, 38, 506-519.
- 12 S. Kubik, Chem. Soc. Rev., 2010, 39, 3648-3663.
- 13 F. P. Schmidtchen, Chem. Soc. Rev., 2010, 39, 3916-3935.
- 14 A. E. Hargrove, S. Nieto, T. Zhang, J. L. Sessler and E. V. Anslyn, Chem. Rev., 2011, 111, 6603-6782.
- 15 M. Wenzel, J. R. Hiscock and P. A. Gale, Chem. Soc. Rev., 2012, 41, 480-520,
- 16 P. A. Gale, N. Busschaert, C. J. E. Haynes, L. E. Karagiannidis and I. L. Kirby, Chem. Soc. Rev., 2014, 43, 205-241.
- 17 M. J. Langton and P. D. Beer, Acc. Chem. Res., 2014, 47, 1935-1949.
- 18 H. D. P. Ali, P. E. Kruger and T. Gunnlaugsson, New J. Chem., 2008, 32, 1153-1161.
- 19 T. Gunnlaugsson, A. P. Davis and M. Glynn, Chem. Commun., 2001, 2556-2557.
- 20 H. Miyaji and J. L. Sessler, Angew. Chem., Int. Ed., 2001, 40, 154-157.
- 21 T. Gunnlaugsson, A. P. Davis, J. E. O'Brien and M. Glynn, Org. Lett., 2002, 4, 2449-2452.
- 22 R. Martinez-Manez and F. Sancenon, Chem. Rev., 2003, 103, 4419-4476.
- 23 C. Suksai and T. Tuntulani, Chem. Soc. Rev., 2003, 32, 192–202.
- 24 F. P. Schmidtchen, in Anion Sensing, ed. I. Stibor, 2005,
- 25 C. Suksai and T. Tuntulani, in Anion Sensing, ed. I. Stibor, 2005, pp. 163-198.
- 26 T. Gunnlaugsson, M. Glynn, G. M. Tocci, P. E. Kruger and F. M. Pfeffer, Coord. Chem. Rev., 2006, 250, 3094-3117.
- 27 B. T. Nguyen and E. V. Anslyn, Coord. Chem. Rev., 2006, 250, 3118-3127.
- 28 R. M. Duke, E. B. Veale, F. M. Pfeffer, P. E. Kruger and T. Gunnlaugsson, Chem. Soc. Rev., 2010, 39, 3936-3953.

29 M. E. Moragues, R. Martinez-Manez and F. Sancenon, *Chem. Soc. Rev.*, 2011, **40**, 2593–2643.

Review Article

- 30 J. Du, M. Hu, J. Fan and X. Peng, *Chem. Soc. Rev.*, 2012, **41**, 4511–4535.
- 31 L. E. Santos-Figueroa, M. E. Moragues, E. Climent, A. Agostini, R. Martinez-Manez and F. Sancenon, *Chem. Soc. Rev.*, 2013, 42, 3489–3613.
- 32 H. T. Ngo, X. J. Liu and K. A. Jolliffe, *Chem. Soc. Rev.*, 2012, **41**, 4928–4965.
- 33 P. A. Gale and C. Caltagirone, *Chem. Soc. Rev.*, 2015, DOI: 10.1039/C4CS00179F.
- 34 X. Li, X. Gao, W. Shi and H. Ma, *Chem. Rev.*, 2014, **114**, 590–659.
- 35 K. Kaur, R. Saini, A. Kumar, V. Luxami, N. Kaur, P. Singh and S. Kumar, *Coord. Chem. Rev.*, 2012, **256**, 1992–2028.
- 36 S. K. Kim, D. H. Lee, J.-I. Hong and J. Yoon, *Acc. Chem. Res.*, 2009, **42**, 23–31.
- 37 M. Cametti and K. Rissanen, *Chem. Commun.*, 2009, 2809–2829.
- 38 T. W. Hudnall, C.-W. Chiu and F. P. Gabbai, *Acc. Chem. Res.*, 2009, **42**, 388–397.
- 39 C. R. Wade, A. E. J. Broomsgrove, S. Aldridge and F. P. Gabbaï, *Chem. Rev.*, 2010, **110**, 3958–3984.
- 40 F. Wang, L. Wang, X. Chen and J. Yoon, *Chem. Soc. Rev.*, 2014, 43, 4312–4324.
- 41 Q. Xu, C. Jin, X. Zhu and G. Xing, *Chin. J. Org. Chem.*, 2014, 34, 647–661.
- 42 D. Zhang, J. R. Cochrane, A. Martinez and G. Gao, RSC Adv., 2014, 4, 29735–29749.
- 43 M. H. Lee, J. S. Kim and J. L. Sessler, *Chem. Soc. Rev.*, 2015, DOI: 10.1039/C4CS00280F.
- 44 Y. Zhou and J. Yoon, Chem. Soc. Rev., 2012, 41, 52-67.
- 45 E. J. New, D. Parker, D. G. Smith and J. W. Walton, *Curr. Opin. Chem. Biol.*, 2010, **14**, 238–246.
- 46 X. J. Liu, H. T. Ngo, Z. J. Ge, S. J. Butler and K. A. Jolliffe, Chem. Sci., 2013, 4, 1680–1686.
- 47 J. L. Sessler, P. A. Gale and W.-S. Cho, in *Anion Receptor Chemistry*, ed. J. L. Sessler, P. A. Gale and W. -S. Cho, The Royal Society of Chemistry, 2006, pp. 1–26.
- 48 J. Chan, S. C. Dodani and C. J. Chang, *Nat. Chem.*, 2012, 4, 973–984.
- 49 Y. Yang, Q. Zhao, W. Feng and F. Li, *Chem. Rev.*, 2012, **113**, 192–270.
- 50 L. M. Hyman and K. J. Franz, Coord. Chem. Rev., 2012, 256, 2333–2356.
- 51 Y. Urano, Curr. Opin. Chem. Biol., 2012, 16, 602-608.
- 52 N. Kumar, V. Bhalla and M. Kumar, *Coord. Chem. Rev.*, 2013, 257, 2335-2347.
- 53 J. Wang, L. Long, D. Xie and Y. Zhan, *J. Lumin.*, 2013, **139**, 40–46.
- 54 L. Yuan, W. Lin, K. Zheng, L. He and W. Huang, *Chem. Soc. Rev.*, 2013, 42, 622–661.
- 55 Z. Guo, S. Park, J. Yoon and I. Shin, *Chem. Soc. Rev.*, 2014, 43, 16–29.
- 56 E. Pershagen and K. E. Borbas, *Coord. Chem. Rev.*, 2014, 273–274, 30–46.

- 57 S. F. Peteu, R. Boukherroub and S. Szunerits, *Biosens. Bioelectron.*, 2014, **58**, 359–373.
- 58 K. Wang, H. Peng and B. Wang, *J. Cell. Biochem.*, 2014, **115**, 1007–1022.
- 59 X. Wu and W. Zhu, *Chem. Soc. Rev.*, 2015, DOI: 10.1039/ C4CS00152D.
- 60 S. Wang, N. Li, W. Pan and B. Tang, TrAC, Trends Anal. Chem., 2012, 39, 3-37.
- 61 K. P. Carter, A. M. Young and A. E. Palmer, *Chem. Rev.*, 2014, **114**, 4564–4601.
- 62 R. Y. Tsien, Annu. Rev. Neurosci., 1989, 12, 227-253.
- 63 R. Y. Tsien, in *Methods in Cell Biology*, ed. D. Lansing Taylor and Y.-L. Wang, Academic Press, 1989, pp. 127–156.
- 64 S. A. Hilderbrand, Live Cell Imaging, 2009, pp. 17-45.
- 65 S. A. Hilderbrand and R. Weissleder, *Curr. Opin. Chem. Biol.*, 2010, **14**, 71–79.
- 66 R. Weissleder and V. Ntziachristos, *Nat. Med.*, 2003, 9, 123–128.
- 67 J. O. Escobedo, O. Rusin, S. Lim and R. M. Strongin, *Curr. Opin. Chem. Biol.*, 2010, **14**, 64–70.
- 68 W. R. Zipfel, R. M. Williams and W. W. Webb, *Nat. Biotechnol.*, 2003, **21**, 1369–1377.
- 69 F. Helmchen and W. Denk, Nat. Methods, 2005, 2, 932-940.
- 70 P. Klán and J. Wirz, Photochemistry of Organic Compounds, John Wiley & Sons, Ltd, 2009, pp. 25–72.
- 71 K. Baathulaa, Y. Xu and X. Qian, *J. Photochem. Photobiol.*, *A*, 2010, **216**, 24–34.
- 72 P. Abbyad, W. Childs, X. Shi and S. G. Boxer, *Proc. Natl. Acad. Sci. U. S. A.*, 2007, **104**, 20189–20194.
- 73 P. Horváth, P. Šebej, T. Šolomek and P. Klán, *J. Org. Chem.*, 2015, DOI: 10.1021/jo502213t.
- 74 N. Boens, V. Leen and W. Dehaen, *Chem. Soc. Rev.*, 2012, **41**, 1130–1172.
- 75 H. Lu, J. Mack, Y. Yang and Z. Shen, Chem. Soc. Rev., 2014, 43, 4778–4823.
- 76 X. Chen, T. Pradhan, F. Wang, J. S. Kim and J. Yoon, *Chem. Rev.*, 2011, **112**, 1910–1956.
- 77 H. Zheng, X.-Q. Zhan, Q.-N. Bian and X.-J. Zhang, *Chem. Commun.*, 2013, 49, 429–447.
- 78 Y. Q. Sun, J. Liu, X. Lv, Y. Liu, Y. Zhao and W. Guo, *Angew. Chem.*, *Int. Ed.*, 2012, **51**, 7634–7636.
- 79 S. T. Manjare, Y. Kim and D. G. Churchill, Acc. Chem. Res., 2014, 47, 2985–2998.
- 80 X. Wang, H. Chang, J. Xie, B. Zhao, B. Liu, S. Xu, W. Pei, N. Ren, L. Huang and W. Huang, *Coord. Chem. Rev.*, 2014, 273–274, 201–212.
- 81 C. P. Montgomery, B. S. Murray, E. J. New, R. Pal and D. Parker, *Acc. Chem. Res.*, 2009, 42, 925–937.
- 82 M. C. Heffern, L. M. Matosziuk and T. J. Meade, *Chem. Rev.*, 2013, **114**, 4496–4539.
- 83 S. J. Butler and D. Parker, Chem. Soc. Rev., 2013, 42, 1652-1666.
- 84 A. Demchenko, J. Fluoresc., 2010, 20, 1099–1128.
- 85 J. Fan, M. Hu, P. Zhan and X. Peng, *Chem. Soc. Rev.*, 2013, **42**, 29–43.
- 86 D.-G. Cho and J. L. Sessler, *Chem. Soc. Rev.*, 2009, **38**, 1647–1662.

- 87 X. Lou, D. Ou, Q. Li and Z. Li, *Chem. Commun.*, 2012, 48, 8462–8477.
- 88 F. Zheng, F. Zeng, C. Yu, X. Hou and S. Wu, *Chem. Eur. J.*, 2013, **19**, 936–942.
- 89 B. Ke, W. Chen, N. Ni, Y. Cheng, C. Dai, H. Dinh and B. Wang, *Chem. Commun.*, 2013, **49**, 2494–2496.
- 90 R. Y. Tsien, Nature, 1981, 290, 527-528.

Chem Soc Rev

- 91 J. P. Crow, Nitric oxide, 1997, 1, 145-157.
- 92 T. Peng and D. Yang, Org. Lett., 2010, 12, 4932-4935.
- 93 C. Song, Z. Ye, G. Wang, J. Yuan and Y. Guan, *Chem. Eur. J.*, 2010, **16**, 6464–6472.
- 94 F. Di Virgilio, T. H. Steinberg, J. A. Swanson and S. C. Silverstein, *J. Immunol.*, 1988, **140**, 915–920.
- 95 R. Horobin, J. Stockert and F. Rashid-Doubell, *Histochem. Cell Biol.*, 2013, **139**, 623–637.
- 96 F. Rashid and R. W. Horobin, *Histochemistry*, 1990, **94**, 303–308.
- 97 S. Trapp and R. Horobin, Eur. Biophys. J., 2005, 34, 959–966.
- 98 S. Trapp, G. Rosania, R. Horobin and J. Kornhuber, *Eur. Biophys. J.*, 2008, **37**, 1317–1328.
- 99 J. T. Hou, M. Y. Wu, K. Li, J. Yang, K. K. Yu, Y. M. Xie and X. Q. Yu, Chem. Commun., 2014, 50, 8640–8643.
- 100 T. Liu, Z. Xu, D. R. Spring and J. Cui, *Org. Lett.*, 2013, 15, 2310–2313.
- 101 Y. Zhou, J. F. Zhang and J. Yoon, *Chem. Rev.*, 2014, 114, 5511–5571.
- 102 C. D. Geddes, K. Apperson, J. Karolin and D. J. S. Birch, *Anal. Biochem.*, 2001, **293**, 60–66.
- 103 H. S. Horowitz, J. Public Health Dent., 2003, 63, 3-8.
- 104 S. Ayoob and A. K. Gupta, *Crit. Rev. Environ. Sci. Technol.*, 2006, 36, 433–487.
- 105 E. Bassin, D. Wypij, R. Davis and M. Mittleman, *Cancer Causes Control*, 2006, **17**, 421–428.
- 106 A. L. Choi, G. Sun, Y. Zhang and P. Grandjean, *Environ. Health Perspect.*, 2012, **120**, 1362–1368.
- 107 E. Galbraith and T. D. James, Chem. Soc. Rev., 2010, 39, 3831–3842.
- 108 Z. Guo, I. Shin and J. Yoon, *Chem. Commun.*, 2012, 48, 5956-5967.
- 109 T. Gunnlaugsson, P. E. Kruger, T. C. Lee, R. Parkesh, F. M. Pfeffer and G. M. Hussey, *Tetrahedron Lett.*, 2003, 44, 6575–6578.
- 110 T. Gunnlaugsson, P. E. Kruger, P. Jensen, F. M. Pfeffer and G. M. Hussey, *Tetrahedron Lett.*, 2003, 44, 8909–8913.
- 111 L. S. Evans, P. A. Gale, M. E. Light and R. Quesada, *Chem. Commun.*, 2006, 965–967.
- 112 S. Camiolo, P. A. Gale, M. B. Hursthouse and M. E. Light, *Org. Biomol. Chem.*, 2003, **1**, 741–744.
- 113 X. Zheng, W. Zhu, D. Liu, H. Ai, Y. Huang and Z. Lu, *ACS Appl. Mater. Interfaces*, 2014, **6**, 7996–8000.
- 114 R. Liu, Y. Gao, Q. Zhang, X. Yang, X. Lu, Z. Ke, W. Zhou and J. Qu, *New J. Chem.*, 2014, **38**, 2941–2945.
- 115 A. K. Mahapatra, R. Maji, K. Maiti, S. S. Adhikari, C. Das Mukhopadhyay and D. Mandal, *Analyst*, 2014, **139**, 309–317.

- 116 F. M. Pfeffer, K. F. Lim and K. J. Sedgwick, *Org. Biomol. Chem.*, 2007, 5, 1795–1799.
- 117 J. L. Sessler, D.-G. Cho and V. Lynch, *J. Am. Chem. Soc.*, 2006, **128**, 16518–16519.
- 118 G. Sivaraman and D. Chellappa, *J. Mater. Chem. B*, 2013, **1**, 5768–5772.
- 119 P. G. M. Wuts and T. W. Greene, *Greene's Protective Groups in Organic Synthesis*, John Wiley & Sons, Inc., 2006, pp. 16–366.
- 120 S. Y. Kim, J. Park, M. Koh, S. B. Park and J.-I. Hong, *Chem. Commun.*, 2009, 4735–4737.
- 121 B. Zhu, H. Kan, J. Liu, H. Liu, Q. Wei and B. Du, *Biosens. Bioelectron.*, 2014, **52**, 298–303.
- 122 B. Zhu, F. Yuan, R. Li, Y. Li, Q. Wei, Z. Ma, B. Du and X. Zhang, *Chem. Commun.*, 2011, 47, 7098–7100.
- 123 Z. Luo, B. Yang, C. Zhong, F. Tang, M. Yuan, Y. Xue, G. Yao, J. Zhang and Y. Zhang, *Dyes Pigm.*, 2013, 97, 52–57.
- 124 G. Wei, J. Yin, X. Ma, S. Yu, D. Wei and Y. Du, *Anal. Chim. Acta*, 2011, **703**, 219–225.
- 125 L. Gai, H. Chen, B. Zou, H. Lu, G. Lai, Z. Li and Z. Shen, *Chem. Commun.*, 2012, **48**, 10721–10723.
- 126 D. Kim, S. Singha, T. Wang, E. Seo, J. H. Lee, S.-J. Lee, K. H. Kim and K. H. Ahn, *Chem. Commun.*, 2012, 48, 10243–10245.
- 127 P. Hou, S. Chen, H. Wang, J. Wang, K. Voitchovsky and X. Song, *Chem. Commun.*, 2014, **50**, 320–322.
- 128 S. Zhang, J. Fan, S. Zhang, J. Wang, X. Wang, J. Du and X. Peng, *Chem. Commun.*, 2014, **50**, 14021–14024.
- 129 W. Gong, R. Su, L. Li, K. Xu and B. Tang, *Chin. Sci. Bull.*, 2011, **56**, 3260–3265.
- 130 T.-Y. Chen and T.-C. Hwang, *Physiol. Rev.*, 2008, **88**, 351–387.
- 131 P. A. Gale, Acc. Chem. Res., 2011, 44, 216-226.
- 132 N. Busschaert, I. L. Kirby, S. Young, S. J. Coles, P. N. Horton, M. E. Light and P. A. Gale, *Angew. Chem., Int. Ed.*, 2012, **51**, 4426–4430.
- 133 C. J. E. Haynes and P. A. Gale, Chem. Commun., 2011, 47, 8203–8209.
- 134 P. R. Brotherhood and A. P. Davis, *Chem. Soc. Rev.*, 2010, **39**, 3633–3647.
- 135 A. P. Davis, D. N. Sheppard and B. D. Smith, *Chem. Soc. Rev.*, 2007, **36**, 348–357.
- 136 J. T. Davis, O. Okunola and R. Quesada, *Chem. Soc. Rev.*, 2010, **39**, 3843–3862.
- 137 G. W. Gokel and N. Barkey, New J. Chem., 2009, 33, 947-963.
- 138 B. A. McNally, W. M. Leevy and B. D. Smith, *Supramol. Chem.*, 2007, **19**, 29–37.
- 139 A. S. Verkman, Am. J. Physiol., 1990, 259, C375-C388.
- 140 S. Jayaraman, L. Teitler, B. Skalski and A. S. Verkman, *Am. J. Physiol.*, 1999, 277, C1008–C1018.
- 141 C. D. Geddes, K. Apperson, J. Karolin and D. J. S. Birch, Dyes Pigm., 2001, 48, 227–231.
- 142 Molecular Probes Handbook, A Guide to Fluorescent Probes and Labeling Technologies, ed. I. Johnson, Life Technologies Corporation, 2010.
- 143 A. S. Verkman, in *Physiology and Pathology of Chloride* Transporters and Channels in the Nervous System, ed.

F. J. Alvarez-Leefmans and E. Delpire, Academic Press,

San Diego, 2010, pp. 109–123. 144 D. Arosio and G. M. Ratto, *Front. Cell. Neurosci.*, 2014,

Review Article

- 145 J. Biwersi and A. S. Verkman, *Biochemistry*, 1991, 30, 7879-7883.
- 146 J. R. Inglefield and R. D. Schwartz-Bloom, *J. Neurosci. Methods*, 1997, 75, 127–135.
- 147 B. Pilas and G. Durack, Cytometry, 1997, 28, 316-322.

8, 258, DOI: 10.3389/fncel.2014.00258.

- 148 Y. Kovalchuk and O. Garaschuk, *Cold Spring Harb. Protoc.*, 2012, DOI: 10.1101/pdb.prot070037.
- 149 J. Biwersi, B. Tulk and A. S. Verkman, *Anal. Biochem.*, 1994, 219, 139–143.
- 150 B. A. McNally, A. V. Koulov, B. D. Smith, J.-B. Joos and A. P. Davis, *Chem. Commun.*, 2005, 1087–1089.
- 151 S. B. J. V. A. S. Jayaraman, Am. J. Physiol., 1999, 276, C747–C757.
- 152 N. D. Sonawane, J. R. Thiagarajah and A. S. Verkman, J. Biol. Chem., 2002, 277, 5506-5513.
- 153 P. Li, T. Xie, N. Fan, K. Li and B. Tang, *Chem. Commun.*, 2012, **48**, 2077–2079.
- 154 P. Li, S. Zhang, N. Fan, H. Xiao, W. Zhang, W. Zhang, H. Wang and B. Tang, Chem. - Eur. J., 2014, 20, 11760-11767.
- 155 S. Amatori, G. Ambrosi, M. Fanelli, M. Formica, V. Fusi, L. Giorgi, E. Macedi, M. Micheloni, P. Paoli, R. Pontellini, P. Rossi and M. A. Varrese, *Chem. – Eur. J.*, 2012, 18, 4274–4284.
- 156 S. Amatori, G. Ambrosi, E. Borgogelli, M. Fanelli, M. Formica, V. Fusi, L. Giorgi, E. Macedi, M. Micheloni, P. Paoli, P. Rossi and A. Tassoni, *Inorg. Chem.*, 2014, 53, 4560–4569.
- 157 J. J. Gassensmith, S. Matthys, J.-J. Lee, A. Wojcik, P. V. Kamat and B. D. Smith, *Chem. – Eur. J.*, 2010, **16**, 2916–2921.
- 158 C. G. Collins, E. M. Peck, P. J. Kramer and B. D. Smith, *Chem. Sci.*, 2013, 4, 2557–2563.
- 159 P. J. DeMott, Atmos. Res., 1995, 38, 63-99.
- 160 C. D. Geddes, Meas. Sci. Technol., 2001, 12, R53.
- 161 G. Dai, O. Levy and N. Carrasco, *Nature*, 1996, 379, 458–460.
- 162 A. K. Mahapatra, J. Roy, P. Sahoo, S. K. Mukhopadhyay and A. Chattopadhyay, *Org. Biomol. Chem.*, 2012, **10**, 2231–2236.
- 163 P. Castric, Curr. Microbiol., 1994, 29, 19-21.
- 164 J. L. Way, Annu. Rev. Pharmacol. Toxicol., 1984, 24, 451–481.
- 165 J. R. Govan and V. Deretic, *Microbiol. Rev.*, 1996, **60**, 539–574.
- 166 B. Ryall, X. Lee, J. Zlosnik, S. Hoshino and H. Williams, *BMC Microbiol.*, 2008, **8**, 108.
- 167 Cyanide in Water and Soil: Chemistry, Risk, and Management, ed. D. A. Dzombak, R. S. Ghosh and G. M. Wong-Chong, CRC Press, Boca Raton, Florida, 2005.
- 168 Z. Xu, X. Chen, H. N. Kim and J. Yoon, *Chem. Soc. Rev.*, 2010, **39**, 127–137.
- 169 K.-S. Lee, H.-J. Kim, G.-H. Kim, I. Shin and J.-I. Hong, Org. Lett., 2007, 10, 49–51.

- 170 J. Zhao, S. Ji, Y. Chen, H. Guo and P. Yang, *Phys. Chem. Chem. Phys.*, 2012, **14**, 8803–8817.
- 171 S. K. Kwon, S. Kou, H. N. Kim, X. Chen, H. Hwang, S.-W. Nam, S. H. Kim, K. M. K. Swamy, S. Park and J. Yoon, *Tetrahedron Lett.*, 2008, **49**, 4102–4105.
- 172 S. W. Nam, X. Chen, J. Lim, S. H. Kim, S. T. Kim, Y. H. Cho, J. Yoon and S. Park, *PLoS One*, 2011, 6, e21387.
- 173 M. K. Bera, C. Chakraborty, P. K. Singh, C. Sahu, K. Sen, S. Maji, A. K. Das and S. Malik, *J. Mater. Chem. B*, 2014, 2, 4733.
- 174 S. Madhu, S. K. Basu, S. Jadhav and M. Ravikanth, *Analyst*, 2013, 138, 299–306.
- 175 X. Cheng, R. Tang, H. Jia, J. Feng, J. Qin and Z. Li, ACS Appl. Mater. Interfaces, 2012, 4, 4387–4392.
- 176 C.-H. Lee, H.-J. Yoon, J.-S. Shim and W.-D. Jang, *Chem. Eur. J.*, 2012, **18**, 4513–4516.
- 177 M. Sun, S. Wang, Q. Yang, X. Fei, Y. Li and Y. Li, RSC Adv., 2014, 4, 8295–8299.
- 178 L. Yang, X. Li, Y. Qu, W. Qu, X. Zhang, Y. Hang, H. Ågren and J. Hua, *Sens. Actuators*, *B*, 2014, **203**, 833–847.
- 179 S. Y. Chung, S. W. Nam, J. Lim, S. Park and J. Yoon, *Chem. Commun.*, 2009, 2866–2868.
- 180 C. D. Sifri, J. Begun and F. M. Ausubel, *Trends Microbiol.*, 2005, 13, 119–127.
- 181 X. Chen, S. W. Nam, G. H. Kim, N. Song, Y. Jeong, I. Shin, S. K. Kim, J. Kim, S. Park and J. Yoon, *Chem. Commun.*, 2010, 46, 8953–8955.
- 182 U. Reddy G, P. Das, S. Saha, M. Baidya, S. K. Ghosh and A. Das, *Chem. Commun.*, 2013, **49**, 255–257.
- 183 H. S. Jung, J. H. Han, Z. H. Kim, C. Kang and J. S. Kim, *Org. Lett.*, 2011, **13**, 5056–5059.
- 184 W. Cao, X.-J. Zheng, D.-C. Fang and L.-P. Jin, *Dalton Trans.*, 2014, **43**, 7298–7303.
- 185 Y.-Y. Guo, X.-L. Tang, F.-P. Hou, J. Wu, W. Dou, W.-W. Qin, J.-X. Ru, G.-L. Zhang, W.-S. Liu and X.-J. Yao, *Sens. Actuators, B*, 2013, **181**, 202–208.
- 186 M. Lee, J. H. Moon, K. M. K. Swamy, Y. Jeong, G. Kim, J. Choi, J. Y. Lee and J. Yoon, *Sens. Actuators, B*, 2014, 199, 369–376.
- 187 S. Xu, M. He, H. Yu, X. Cai, X. Tan, B. Lu and B. Shu, *Anal. Biochem.*, 2001, **299**, 188–193.
- 188 A. E. Timms, Y. Zhang, R. G. G. Russell and M. A. Brown, *Rheumatology*, 2002, **41**, 725–729.
- 189 S. Lee, K. K. Y. Yuen, K. A. Jolliffe and J. Yoon, *Chem. Soc. Rev.*, 2015, DOI: 10.1039/c1034cs00353e.
- 190 J. F. Zhang, S. Kim, J. H. Han, S.-J. Lee, T. Pradhan, Q. Y. Cao, S. J. Lee, C. Kang and J. S. Kim, *Org. Lett.*, 2011, 13, 5294–5297.
- 191 D.-N. Lee, A. Jo, S. B. Park and J.-I. Hong, *Tetrahedron Lett.*, 2012, **53**, 5528–5530.
- 192 W. Zhu, X. Huang, Z. Guo, X. Wu, H. Yu and H. Tian, *Chem. Commun.*, 2012, **48**, 1784–1786.
- 193 R. K. Pathak, K. Tabbasum, A. Rai, D. Panda and C. P. Rao, *Anal. Chem.*, 2012, **84**, 5117–5123.
- 194 S. Goswami, A. K. Das, B. Pakhira, S. Basu Roy, A. K. Maity, P. Saha and S. Sarkar, *Dalton Trans.*, 2014, 43, 12689–12697.

195 S. Bhowmik, B. N. Ghosh, V. Marjomaki and K. Rissanen, J. Am. Chem. Soc., 2014, 136, 5543-5546.

- 196 M. Leppilampi, P. Koistinen, E.-R. Savolainen, J. Hannuksela, A.-K. Parkkila, O. Niemelä, S. Pastoreková, J. Pastorek, A. Waheed, W. S. Sly, S. Parkkila and H. Rajaniemi, *Clin. Cancer Res.*, 2002, 8, 2240–2245.
- 197 W. S. Sly and P. Y. Hu, Annu. Rev. Biochem., 1995, 64, 375-401.
- 198 W. Wu, H.-K. Kong, H. Li, Y.-M. Ho, Y. Gao, J. Hao, M. B. Murphy, M. H.-W. Lam, K.-L. Wong and C.-S. Lee, *Eur. J. Org. Chem.*, 2011, 5054–5060.
- 199 D. Parker, Aust. J. Chem., 2011, 64, 239-243.

Chem Soc Rev

- 200 B. S. Murray, E. J. New, R. Pal and D. Parker, *Org. Biomol. Chem.*, 2008, 6, 2085–2094.
- 201 E. J. New and D. Parker, *Org. Biomol. Chem.*, 2009, 7, 851–855.
- 202 S. J. Butler, L. Lamarque, R. Pal and D. Parker, *Chem. Sci.*, 2014, 5, 1750–1756.
- 203 A. Thibon and V. Pierre, *Anal. Bioanal. Chem.*, 2009, **394**, 107–120.
- 204 M. S. Tremblay, M. Halim and D. Sames, *J. Am. Chem. Soc.*, 2007, **129**, 7570–7577.
- 205 D. G. Smith, G. L. Law, B. S. Murray, R. Pal, D. Parker and K. L. Wong, *Chem. Commun.*, 2011, 47, 7347–7349.
- 206 D. G. Smith, R. Pal and D. Parker, *Chem. Eur. J.*, 2012, **18**, 11604–11613.
- 207 P. Nagy, Z. Palinkas, A. Nagy, B. Budai, I. Toth and A. Vasas, *Biochim. Biophys. Acta*, 2014, **1840**, 876–891.
- 208 K. R. Olson, J. A. Donald, R. A. Dombkowski and S. F. Perry, *Respir. Physiol. Neurobiol.*, 2012, **184**, 117–129.
- 209 A. Stein and S. M. Bailey, Redox Biol., 2013, 1, 32-39.
- 210 J. L. Wallace, Trends Pharmacol. Sci., 2007, 28, 501–505.
- 211 P. Kamoun, Amino Acids, 2004, 26, 243-254.
- 212 J. I. Toohey, Anal. Biochem., 2011, 413, 1-7.
- 213 R. E. Hansen and J. R. Winther, *Anal. Biochem.*, 2009, **394**, 147–158.
- 214 M. Vendrell, D. Zhai, J. C. Er and Y. T. Chang, *Chem. Rev.*, 2012, **112**, 4391–4420.
- 215 V. S. Lin and C. J. Chang, *Curr. Opin. Chem. Biol.*, 2012, **16**, 595–601.
- 216 B. Peng and M. Xian, Asian J. Org. Chem., 2014, 3, 914-924.
- 217 X. Cao, W. Lin, K. Zheng and L. He, *Chem. Commun.*, 2012, 48, 10529–10531.
- 218 C. Tang, Q. Zheng, S. Zong, Z. Wang and Y. Cui, *Sens. Actuators*, *B*, 2014, **202**, 99–104.
- 219 D. Maity, A. Raj, P. K. Samanta, D. Karthigeyan, T. K. Kundu, S. K. Pati and T. Govindaraju, *RSC Adv.*, 2014, 4, 11147.
- 220 Z. Huang, S. Ding, D. Yu, F. Huang and G. Feng, *Chem. Commun.*, 2014, **50**, 9185–9187.
- 221 Z. Xu, L. Xu, J. Zhou, Y. Xu, W. Zhu and X. Qian, *Chem. Commun.*, 2012, 48, 10871–10873.
- 222 X. Wang, J. Sun, W. Zhang, X. Ma, J. Lv and B. Tang, *Chem. Sci.*, 2013, **4**, 2551.
- 223 J. Liu, Y. Q. Sun, J. Zhang, T. Yang, J. Cao, L. Zhang and W. Guo, *Chem. Eur. J.*, 2013, **19**, 4717–4722.

- 224 Y. Chen, C. Zhu, Z. Yang, J. Chen, Y. He, Y. Jiao, W. He, L. Qiu, J. Cen and Z. Guo, *Angew. Chem., Int. Ed.*, 2013, 52, 1688–1691.
- 225 S. K. Das, C. S. Lim, S. Y. Yang, J. H. Han and B. R. Cho, Chem. Commun., 2012, 48, 8395–8397.
- 226 A. R. Lippert, E. J. New and C. J. Chang, J. Am. Chem. Soc., 2011, 133, 10078–10080.
- 227 F. Yu, P. Li, P. Song, B. Wang, J. Zhao and K. Han, *Chem. Commun.*, 2012, **48**, 2852–2854.
- 228 Y. Zheng, M. Zhao, Q. Qiao, H. Liu, H. Lang and Z. Xu, *Dyes Pigm.*, 2013, **98**, 367–371.
- 229 W. Sun, J. Fan, C. Hu, J. Cao, H. Zhang, X. Xiong, J. Wang, S. Cui, S. Sun and X. Peng, *Chem. Commun.*, 2013, 49, 3890–3892.
- 230 Q. Wan, Y. Song, Z. Li, X. Gao and H. Ma, *Chem. Commun.*, 2013, **49**, 502–504.
- 231 V. S. Lin, A. R. Lippert and C. J. Chang, *Proc. Natl. Acad. Sci. U. S. A.*, 2013, **110**, 7131–7135.
- 232 Q. Qiao, M. Zhao, H. Lang, D. Mao, J. Cui and Z. Xu, *RSC Adv.*, 2014, **4**, 25790.
- 233 S. Yang, Y. Qi, C. Liu, Y. Wang, Y. Zhao, L. Wang, J. Li, W. Tan and R. Yang, *Anal. Chem.*, 2014, 86, 7508–7515.
- 234 S. K. Bae, C. H. Heo, D. J. Choi, D. Sen, E. H. Joe, B. R. Cho and H. M. Kim, *J. Am. Chem. Soc.*, 2013, **135**, 9915–9923.
- 235 L. Zhang, S. Li, M. Hong, Y. Xu, S. Wang, Y. Liu, Y. Qian and J. Zhao, *Org. Biomol. Chem.*, 2014, 12, 5115–5125.
- 236 X. L. Liu, X. J. Du, C. G. Dai and Q. H. Song, *J. Org. Chem.*, 2014, **79**, 9481–9489.
- 237 R. Wang, F. Yu, L. Chen, H. Chen, L. Wang and W. Zhang, *Chem. Commun.*, 2012, **48**, 11757–11759.
- 238 H. Wu, S. Krishnakumar, J. Yu, D. Liang, H. Qi, Z. W. Lee, L. W. Deng and D. Huang, *Chem. - Asian J.*, 2014, 9, 3604–3611.
- 239 W. Sun, W. Li, J. Li, J. Zhang, L. Du and M. Li, *Tetrahedron*, 2012, **68**, 5363–5367.
- 240 W. Chen, S. Chen, B. Zhou, H. Wang, X. Song and H. Zhang, *Dyes Pigm.*, 2015, **113**, 596–601.
- 241 H. Chen, W. Lin, H. Cui and W. Jiang, *Chem. Eur. J.*, 2015, 21, 733–745.
- 242 B. Peng, W. Chen, C. Liu, E. W. Rosser, A. Pacheco, Y. Zhao, H. C. Aguilar and M. Xian, *Chem. – Eur. J.*, 2014, 20, 1010–1016.
- 243 L. Yuan and Q. P. Zuo, Chem. Asian J., 2014, 9, 1544-1549.
- 244 T. Liu, X. Zhang, Q. Qiao, C. Zou, L. Feng, J. Cui and Z. Xu, *Dyes Pigm.*, 2013, **99**, 537–542.
- 245 X. Pei, H. Tian, W. Zhang, A. M. Brouwer and J. Qian, *Analyst*, 2014, **139**, 5290–5296.
- 246 F. Zheng, M. Wen, F. Zeng and S. Wu, *Polymer*, 2013, 54, 5691–5697.
- 247 S. El Sayed, C. d. l. Torre, L. E. Santos-Figueroa, E. Pérez-Payá, R. Martínez-Máñez, F. Sancenón, A. M. Costero, M. Parra and S. Gil, RSC Adv., 2013, 3, 25690.
- 248 B. Chen, C. Lv and X. Tang, Anal. Bioanal. Chem., 2012, 404, 1919–1923.
- 249 C. S. Lim, S. K. Das, S. Y. Yang, E. S. Kim, H. J. Chun and B. R. Cho, *Anal. Chem.*, 2013, 85, 9288–9295.

Review Article

250 G. J. Mao, T. T. Wei, X. X. Wang, S. Y. Huan, D. Q. Lu, J. Zhang, X. B. Zhang, W. Tan, G. L. Shen and R. Q. Yu, *Anal. Chem.*, 2013, 85, 7875–7881.

- 251 B. Chen, W. Li, C. Lv, M. Zhao, H. Jin, H. Jin, J. Du, L. Zhang and X. Tang, *Analyst*, 2013, **138**, 946–951.
- 252 C. Yu, X. Li, F. Zeng, F. Zheng and S. Wu, *Chem. Commun.*, 2013, **49**, 403–405.
- 253 K. Zheng, W. Lin and L. Tan, *Org. Biomol. Chem.*, 2012, **10**, 9683–9688.
- 254 G. Zhou, H. Wang, Y. Ma and X. Chen, *Tetrahedron*, 2013, **69**, 867–870.
- 255 T. Chen, Y. Zheng, Z. Xu, M. Zhao, Y. Xu and J. Cui, *Tetrahedron Lett.*, 2013, 54, 2980–2982.
- 256 J. Zhang and W. Guo, *Chem. Commun.*, 2014, **50**, 4214-4217.
- 257 J. Zhou, Y. Luo, Q. Li, J. Shen, R. Wang, Y. Xu and X. Qian, New J. Chem., 2014, 38, 2770.
- 258 K. Liu and S. Zhang, Tetrahedron Lett., 2014, 55, 5566-5569.
- 259 L. E. Santos-Figueroa, C. de laTorre, S. El Sayed, F. Sancenón, R. Martínez-Máñez, A. M. Costero, S. Gil and M. Parra, Eur. J. Org. Chem., 2014, 1848–1854.
- 260 K. Wang, H. Peng, N. Ni, C. Dai and B. Wang, *J. Fluoresc.*, 2014, 24, 1–5.
- 261 K. Sun, X. Liu, Y. Wang and Z. Wu, RSC Adv., 2013, 3, 14543–14548.
- 262 S. I. Reja, N. Kumar, R. Sachdeva, V. Bhalla and M. Kumar, RSC Adv., 2013, 3, 17770–17774.
- 263 D. Zhu, L. Xue, G. Li, Y. Che and H. Jiang, *Org. Chem. Front.*, 2014, **1**, 501.
- 264 W. Xuan, R. Pan, Y. Cao, K. Liu and W. Wang, *Chem. Commun.*, 2012, **48**, 10669–10671.
- 265 Z. Wu, Y. Feng, B. Geng, J. Liua and X. Tang, RSC Adv., 2014, 4, 30398–30401.
- 266 S. Chen, P. Hou, J. W. Foley and X. Song, RSC Adv., 2013, 3, 5591.
- 267 X. Li, Y. Gong, K. Wu, S. H. Liang, J. Cao, B. Yang, Y. Hu and Y. Han, *RSC Adv.*, 2014, **4**, 36106.
- 268 Z. Dong, X. Le, P. Zhou, C. Dong and J. Ma, *New J. Chem.*, 2014, **38**, 1802–1808.
- 269 A. Zhu, Z. Luo, C. Ding, B. Li, S. Zhou, R. Wang and Y. Tian, *Analyst*, 2014, **139**, 1945–1952.
- 270 B. C. Dickinson and C. J. Chang, *Nat. Chem. Biol.*, 2011, 7, 504–511.
- 271 X. Chen, X. Tian, I. Shin and J. Yoon, *Chem. Soc. Rev.*, 2011, **40**, 4783–4804.
- 272 B. Kalyanaraman, V. Darley-Usmar, K. J. A. Davies, P. A. Dennery, H. J. Forman, M. B. Grisham, G. E. Mann, K. Moore, L. J. Roberts Ii and H. Ischiropoulos, *Free Radical Biol. Med.*, 2012, 52, 1–6.
- 273 R. Radi, J. Biol. Chem., 2013, 288, 26464-26472.
- 274 J.-H. M. Tsai, J. G. Harrison, J. C. Martin, T. P. Hamilton, M. van der Woerd, M. J. Jablonsky and J. S. Beckman, *J. Am. Chem. Soc.*, 1994, **116**, 4115–4116.
- 275 C. Szabo, H. Ischiropoulos and R. Radi, *Nat. Rev. Drug Discovery*, 2007, **6**, 662–680.
- 276 P. B. J. S. L. L. Pacher, Physiol. Rev., 2007, 87, 315-424.

- 277 M. G. Bonini, R. Radi, G. Ferrer-Sueta, A. M. D. C. Ferreira and O. Augusto, *J. Biol. Chem.*, 1999, 274, 10802–10806.
- 278 S. L. Hempel, G. R. Buettner, Y. Q. O'Malley, D. A. Wessels and D. M. Flaherty, Free Radical Biol. Med., 1999, 27, 146–159.
- 279 H. Possel, H. Noack, W. Augustin, G. Keilhoff and G. Wolf, FEBS Lett., 1997, 416, 175–178.
- 280 N. W. Kooy, J. A. Royall, H. Ischiropoulos and J. S. Beckman, *Free Radical Biol. Med.*, 1994, **16**, 149–156.
- 281 A. Negre-Salvayre, N. Augé, C. Duval, F. Robbesyn, J.-C. Thiers, D. Nazzal, H. Benoist and R. Salvayre, *Methods Enzymology*, Academic Press, 2002, pp. 62–71.
- 282 G. Ambikapathi, S. Kempahanumakkagari, B. Ramappa Lamani, D. Kuramkote Shivanna, H. Bodagur Maregowda, A. Gupta and P. Malingappa, *J. Fluoresc.*, 2013, 23, 705–712.
- 283 D. Yang, Y.-C. Tang, J. Chen, X.-C. Wang, M. D. Bartberger, K. N. Houk and L. Olson, *J. Am. Chem. Soc.*, 1999, 121, 11976–11983.
- 284 D. Yang, H.-L. Wang, Z.-N. Sun, N.-W. Chung and J.-G. Shen, *J. Am. Chem. Soc.*, 2006, **128**, 6004–6005.
- 285 Z.-N. Sun, H.-L. Wang, F.-Q. Liu, Y. Chen, P. Kwong, H. Tam and D. Yang, *Org. Lett.*, 2009, **11**, 1887–1890.
- 286 R. B. R. Muijsers, E. van den Worm, G. Folkerts, C. J. Beukelman, A. S. Koster, D. S. Postma and F. P. Nijkamp, *Br. J. Pharmacol.*, 2000, **130**, 932–936.
- 287 T. Peng, N. K. Wong, X. Chen, Y. K. Chan, D. H. Ho, Z. Sun, J. J. Hu, J. Shen, H. El-Nezami and D. Yang, *J. Am. Chem. Soc.*, 2014, 136, 11728–11734.
- 288 J. T. Hou, J. Yang, K. Li, Y. X. Liao, K. K. Yu, Y. M. Xie and X. Q. Yu, Chem. Commun., 2014, 50, 9947–9950.
- 289 X. Zhou, Y. Kwon, G. Kim, J.-H. Ryu and J. Yoon, *Biosens. Bioelectron.*, 2015, **64**, 285–291.
- 290 Q. Zhang, Z. Zhu, Y. Zheng, J. Cheng, N. Zhang, Y. T. Long, J. Zheng, X. Qian and Y. Yang, J. Am. Chem. Soc., 2012, 134, 18479–18482.
- 291 F. Martin-Romero, Y. Gutiérrez-Martin, F. Henao and C. Gutiérrez-Merino, *J. Fluoresc.*, 2004, **14**, 17–23.
- 292 J. Zielonka, A. Sikora, M. Hardy, J. Joseph, B. P. Dranka and B. Kalyanaraman, *Chem. Res. Toxicol.*, 2012, 25, 1793–1799.
- 293 A. Sikora, J. Zielonka, M. Lopez, J. Joseph and B. Kalyanaraman, *Free Radical Biol. Med.*, 2009, 47, 1401–1407.
- 294 X. Sun, Q. Xu, G. Kim, S. E. Flower, J. P. Lowe, J. Yoon, J. S. Fossey, X. Qian, S. D. Bull and T. D. James, *Chem. Sci.*, 2014, 5, 3368.
- 295 F. Yu, P. Song, P. Li, B. Wang and K. Han, *Analyst*, 2012, 137, 3740–3749.
- 296 K. Xu, H. Chen, J. Tian, B. Ding, Y. Xie, M. Qiang and B. Tang, Chem. Commun., 2011, 47, 9468–9470.
- 297 F. Yu, P. Li, G. Li, G. Zhao, T. Chu and K. Han, *J. Am. Chem. Soc.*, 2011, **133**, 11030–11033.
- 298 F. Yu, P. Li, B. Wang and K. Han, *J. Am. Chem. Soc.*, 2013, 135, 7674–7680.
- 299 B. Wang, F. Yu, P. Li, X. Sun and K. Han, *Dyes Pigm.*, 2013, 96, 383–390.
- 300 K.-K. Lin, S.-C. Wu, K.-M. Hsu, C.-H. Hung, W.-F. Liaw and Y.-M. Wang, *Org. Lett.*, 2013, **15**, 4242–4245.

301 T. Ueno, Y. Urano, H. Kojima and T. Nagano, *J. Am. Chem. Soc.*, 2006, **128**, 10640–10641.

- 302 N. A. Sieracki, B. N. Gantner, M. Mao, J. H. Horner, R. D. Ye, A. B. Malik, M. E. Newcomb and M. G. Bonini, *Free Radical Biol. Med.*, 2013, **61**, 40–50.
- 303 G. C. Van de Bittner, E. A. Dubikovskaya, C. R. Bertozzi and C. J. Chang, *Proc. Natl. Acad. Sci. U. S. A.*, 2010, **107**, 21316–21321.
- 304 J. C. Morris, J. Phys. Chem., 1966, 70, 3798-3805.

Chem Soc Rev

- 305 K. Setsukinai, Y. Urano, K. Kakinuma, H. J. Majima and T. Nagano, *J. Biol. Chem.*, 2003, **278**, 3170–3175.
- 306 J. Shepherd, S. A. Hilderbrand, P. Waterman, J. W. Heinecke, R. Weissleder and P. Libby, *Chem. Biol.*, 2007, 14, 1221–1231.
- 307 Y. Koide, Y. Urano, S. Kenmoku, H. Kojima and T. Nagano, J. Am. Chem. Soc., 2007, 129, 10324–10325.
- 308 Y. Xiao, R. Zhang, Z. Ye, Z. Dai, H. An and J. Yuan, *Anal. Chem.*, 2012, **84**, 10785–10792.
- 309 Z.-N. Sun, F.-Q. Liu, Y. Chen, P. K. H. Tam and D. Yang, Org. Lett., 2008, 10, 2171–2174.
- 310 Y. Zhou, J. Y. Li, K. H. Chu, K. Liu, C. Yao and J. Y. Li, *Chem. Commun.*, 2012, **48**, 4677–4679.
- 311 H. Zhu, J. Fan, J. Wang, H. Mu and X. Peng, *J. Am. Chem. Soc.*, 2014, **136**, 12820–12823.
- 312 X. Cheng, H. Jia, T. Long, J. Feng, J. Qin and Z. Li, *Chem. Commun.*, 2011, 47, 11978–11980.
- 313 G. Wu, F. Zeng and S. Wu, *Anal. Methods*, 2013, 5, 5589–5596.
- 314 S. I. Reja, V. Bhalla, A. Sharma, G. Kaur and M. Kumar, *Chem. Commun.*, 2014, **50**, 11911–11914.
- 315 L. Yuan, W. Lin, J. Song and Y. Yang, *Chem. Commun.*, 2011, 47, 12691–12693.
- 316 S. Kenmoku, Y. Urano, H. Kojima and T. Nagano, *J. Am. Chem. Soc.*, 2007, **129**, 7313–7318.
- 317 Y. Koide, Y. Urano, K. Hanaoka, T. Terai and T. Nagano, J. Am. Chem. Soc., 2011, 133, 5680-5682.
- 318 X. Chen, K. A. Lee, E. M. Ha, K. M. Lee, Y. Y. Seo, H. K. Choi, H. N. Kim, M. J. Kim, C. S. Cho, S. Y. Lee, W. J. Lee and J. Yoon, *Chem. Commun.*, 2011, 47, 4373–4375.
- 319 X. Chen, X. Wang, S. Wang, W. Shi, K. Wang and H. Ma, *Chem. Eur. J.*, 2008, **14**, 4719–4724.
- 320 S. Goswami, S. Das, K. Aich, P. K. Nandi, K. Ghoshal, C. K. Quah, M. Bhattacharyya, H.-K. Fun and H. A. Abdel-Aziz, *RSC Adv.*, 2014, 4, 24881–24886.

- 321 X. Jin, L. Hao, Y. Hu, M. She, Y. Shi, M. Obst, J. Li and Z. Shi, *Sens. Actuators, B*, 2013, **186**, 56–60.
- 322 Y.-K. Yang, H. J. Cho, J. Lee, I. Shin and J. Tae, *Org. Lett.*, 2009, **11**, 859–861.
- 323 S.-R. Liu and S.-P. Wu, Org. Lett., 2013, 15, 878-881.
- 324 S. T. Manjare, J. Kim, Y. Lee and D. G. Churchill, *Org. Lett.*, 2014, **16**, 520–523.
- 325 S. T. Manjare, S. Kim, W. D. Heo and D. G. Churchill, Org. Lett., 2014, 16, 410-412.
- 326 B. Wang, P. Li, F. Yu, P. Song, X. Sun, S. Yang, Z. Lou and K. Han, *Chem. Commun.*, 2013, **49**, 1014–1016.
- 327 Y. Koide, M. Kawaguchi, Y. Urano, K. Hanaoka, T. Komatsu, M. Abo, T. Terai and T. Nagano, *Chem. Commun.*, 2012, 48, 3091–3093.
- 328 Z. Lou, P. Li, Q. Pan and K. Han, *Chem. Commun.*, 2013, **49**, 2445–2447.
- 329 G. Li, D. Zhu, Q. Liu, L. Xue and H. Jiang, *Org. Lett.*, 2013, 15, 2002–2005.
- 330 F. Liu, Y. Gao, J. Wang and S. Sun, *Analyst*, 2014, **139**, 3324–3329.
- 331 F. Liu, T. Wu, J. Cao, H. Zhang, M. Hu, S. Sun, F. Song, J. Fan, J. Wang and X. Peng, *Analyst*, 2013, 138, 775–778.
- 332 L. Yuan, W. Lin, Y. Yang and H. Chen, *J. Am. Chem. Soc.*, 2012, **134**, 1200–1211.
- 333 S. Chen, J. Lu, C. Sun and H. Ma, *Analyst*, 2010, **135**, 577–582.
- 334 F. Yu, P. Song, P. Li, B. Wang and K. Han, *Chem. Commun.*, 2012, **48**, 7735–7737.
- 335 B. Wang, P. Li, F. Yu, J. Chen, Z. Qu and K. Han, *Chem. Commun.*, 2013, **49**, 5790–5792.
- 336 E. M. Stennett, M. A. Ciuba and M. Levitus, *Chem. Soc. Rev.*, 2014, 43, 1057–1075.
- 337 M. K. Kuimova, *Phys. Chem. Chem. Phys.*, 2012, **14**, 12671–12686.
- 338 A. F. Coskun and A. Ozcan, *Curr. Opin. Biotechnol.*, 2014, 25, 8–16.
- 339 X. Fan and I. M. White, Nat. Photonics, 2011, 5, 591-597.
- 340 D. A. Basiji, W. E. Ortyn, L. Liang, V. Venkatachalam and P. Morrissey, *Clin. Lab. Med.*, 2007, 27, 653–670.
- 341 A. Ozcan, Lab Chip, 2014, 14, 3187-3194.
- 342 H. Zhu, S. Mavandadi, A. F. Coskun, O. Yaglidere and A. Ozcan, *Anal. Chem.*, 2011, **83**, 6641–6647.